LBL 34259
UC-401

Chemical Sciences Divisic n

ANNUAL REPORT 1992

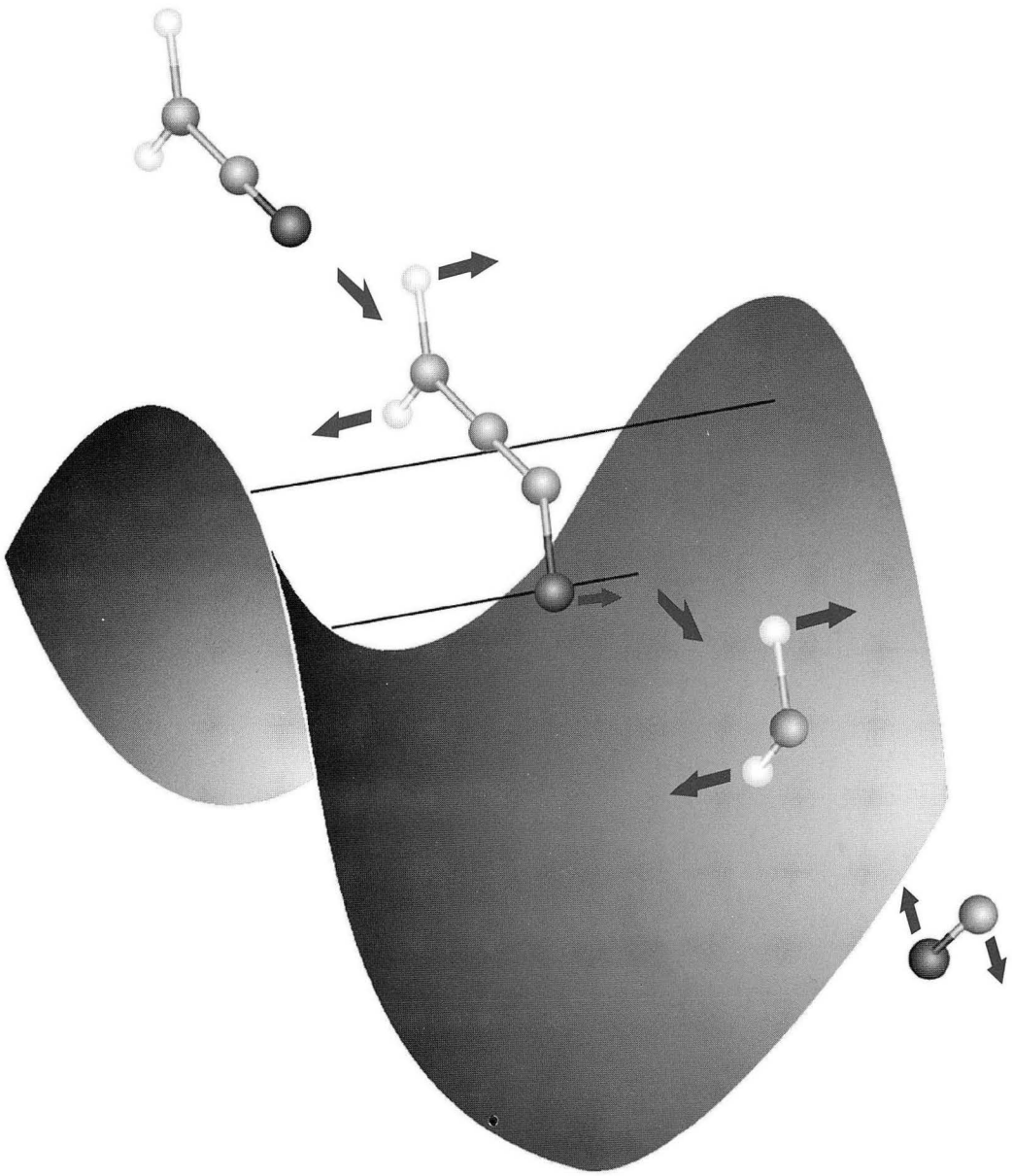

October 1993

Lawrence Berkeley Laboratory
University of California
Berkeley, California 94720

pared for the U. S. Department of Energy under Contract DE-AC03-76F00098

Cover Caption

The schematic diagram shows the unimolecular dissociation of ketene (CH_2CO). The ketene molecule is prepared in a vibrationally excited state by absorption of laser light, which is followed by a localization of energy in the C-C bond. As more energy is pumped into the molecule, vibrational excitation at the transition state (the saddle point of the energy surface) becomes possible. Stepwise increases in dissociation rate are observed as the energy increases above the threshold for each vibrational state. This confirms the fundamental assumptions of statistical theories for the rate of unimolecular reactions and demonstrates that *ab initio* calculations fo transition states can be reliable.

Available to DOE and DOE Contractors
from the Office of Scientific and Technical Information
P.O. Box 62, Oak Ridge, TN 37831
Prices available from (615) 576-8401, FTS 626-8401

Available to the public from the
National Technical Information Service
U.S. Department of Commerce
5285 Port Royal Road, Springfield, VA 22161

DISCLAIMER

LBL-34259
UC-401

CHEMICAL SCIENCES DIVISION

Annual Report 1992

September 1993

Lawrence Berkeley Laboratory
University of California
Berkeley, California 94720

Prepared for the U.S. Department of Energy under Contract No. DE-AC03-76SF00098

Contents

REMARKS BY THE DIVISION DIRECTOR

The Chemical Sciences Division (CSD) is one of twelve research Divisions of the Lawrence Berkeley Laboratory, a Department of Energy National Laboratory. The CSD is composed of individual groups and research programs that are organized into five scientific areas: Chemical Physics, Inorganic/Organometallic Chemistry, Actinide Chemistry, Atomic Physics, and Physical Chemistry. The CSD is unique in that a good deal of our Division's research activity occurs in laboratories located on the campus of the University of California at Berkeley, involving students and faculty in the Department of Chemistry. Several large programs, notably the Actinide Chemistry Program and the Atomic Physics Program, are based at the Lawrence Berkeley Laboratory (LBL) site just east of and above the University campus. The two sites, the campus and the Laboratory, are linked by an efficient minibus system that transports students, faculty, staff, and visitors between the two institutions.

The benefits of close ties with the campus are broad and numerous. One of the most important of these is the vigor, dedication, and high productivity that graduate student research assistants bring to our various research projects. In addition, the Laboratory has a staff of highly skilled engineers and crafts technicians who support the scientific mission, and it is the site of several major, world-class user facilities such as the Advanced Light Source (ALS). Combined, the two institutions represent a highly enriched research environment, attracting a large number of eminent scientists and leaders from all over the world—many of whom have close associations with the Chemical Sciences research programs.

In FY 1992 the Division continued to advance the Combustion Dynamics Initiative in support of DOE's national role in combustion research and chemical science. The intent of the initiative is to achieve fundamental advances in understanding the structure and reactivity of critical reaction intermediates and transients and the dynamics of elementary chemical reactions. The initiative envisions both experimental and theoretical efforts that would lead to accurate and reliable models for predicting combustion properties to improve the design of engines, burners, and other combustion devices.

This year, the Division also continued to place a strong emphasis on full compliance with environmental health and safety guidelines and regulations. In the coming years we will be looking at ways in which Chemical Sciences Division research can help strengthen United States' industrial competitiveness both here and abroad, and how our research can better assist our nation's environmental remediation efforts.

Awards and honors received by CSD investigators in FY 1992 include:

- Neil Bartlett received the American Chemical Society Award for Creative Work in Fluorine Chemistry and received an Honorary Doctor of Science degree from McMaster University, Hamilton, Ontario, Canada.
- Ali Belkacem received an LBL Outstanding Service Award.
- Alexis T. Bell received the 1992 R.H. Wilhelm Award in Chemical Reaction Engineering and was an Irving Langmuir Lecturer at the Division of Colloid and Surface Chemistry.
- Y.T. Lee received the Faraday Medal, Royal Society of Chemistry, Great Britain, and received an Honorary Doctor of Science degree from University of Rome, Italy; he was an Alstadt-Lord-Mark Chair Lecturer, Polytechnic University, a Gooch-Stephens Lecturer at Baylor University, and a Hill Lecturer at Duke University.
- William Lester, Jr. was elected as a Fellow of the American Association for the Advancement of Science and elected to the national board of AAAS, appointed to the Federal Networking Council Advisory Committee, and appointed to NSF's Blue Ribbon Panel on High Performance Computing.
- K.P.C. Vollhardt was selected as an Humboldt Senior Scientist Awardee.

Charles B. Harris
Division Director
Chemical Sciences Division

Chemical Sciences

FUNDAMENTAL INTERACTIONS

PHOTOCHEMICAL AND RADIATION SCIENCES

Photochemistry of Materials in the Stratosphere*

Harold S. Johnston, Investigator

INTRODUCTION

This research is concerned with global change in the chemistry of the atmosphere, including theoretical and interpretative gas-phase and heterogeneous photochemistry. Work continues on writing up former graduate student theses for publication.

The principal investigator is (1) an advisor to the Upper Atmosphere Research Program, Atmospheric Effects of Stratospheric Aircraft, of the National Aeronautics and Space Administration (NASA), (2) Trustee for the National Institute for Global Environmental Change, administered by the University of California, and (3) Member of the National Needs Task Force of the Lawrence Berkeley Laboratory.

1. Heterogeneous Chemical Reactions in the Stratosphere (Publications 3 and 4)

For a few years, it has been known that heterogeneous chemical catalysis,

$$HCl(g) + ClNO_3(g) - (cat.) \rightarrow Cl_2(g) + HNO_3(s) \quad ,$$

where the catalyst is ice or nitric acid trihydrate ice, and other heterogeneous reactions are an essential component of the Antarctic "ozone hole." In 1991, NASA scientists found that heterogeneous hydrolysis reactions on aqueous sulfuric acid aerosols

$$N_2O_5(g) + H_2O - (H_2SO_4, l) \rightarrow 2HNO_3(g)$$

$$ClNO_3(g) + H_2O - (H_2SO_4, l)) \rightarrow HOCl(g) + HNO_3(g)$$

appear to have caused global ozone reduction at mid-latitudes. These reactions convert inactive chlorine species (HCl and $ClNO_3$) to active forms (Cl, ClO) and alter the concentration of hydroxyl radicals. Work here indicates that nitrosyl sulfuric acid ($NOHSO_4$) may also convert inactive HCl to active ClNO, and nitrosyl sulfuric acid hydrolyses under certain conditions to release HONO(g), which directly leads to ozone loss.

FY 1992 PUBLICATIONS AND REPORTS

Refereed Journals

1. B. Kim, P.L. Hunter, and H.S. Johnston, "NO_3 Radical Studied by Laser Induced Fluorescence," J. Chem. Phys., **96**, 4057 (1992); LBL-30869.
2. J.D. Burley and H.S. Johnston, "Photoabsorption Cross Sections of $(FSO_3)_2$ and FSO_3," J. Photochem. Photobiol. A: Chem. **66**, 141 (1992); LBL-31547.
3. J.D. Burley and H.S. Johnston, "Ionic Mechanisms for Heterogeneous Stratospheric Reactions and Ultraviolet Photoabsorption Cross Sections for NO_2^+, HNO_3, and NO_3^- in Sulfuric Acid," Geophys. Res. Lett. **19**, 1359 (1992); LBL-31660.
4. J.D. Burley and H.S. Johnston, "Nitrosyl Sulfuric Acid and Stratospheric Aerosols," Geophys. Res. Lett. **19**, 1363 (1992); LBL-32177.

Other Publications

5. H.S. Johnston, "Atmospheric Ozone," Annual Rev. Phys. Chem. **43**, 1 (1992); LBL-33576.

Invited Talks

6. H.S. Johnston, "Stratospheric Aircraft: Impact on Ozone?" The Chemistry of the Atmosphere: Its Impact on Global Change, CHEMRAWN VII, A World Conference, Baltimore, MD, December 2–6, 1991.
7. H.S. Johnston, "Collisional Deactivation of Highly Excited Nitriogen Dioxide," Physical Chemistry Colloquium, University of Colorado, Boulder, CO, April 17, 1992.

*This work was supported by the Director, Office of Energy Research, Office of Basic Energy Sciences, Chemical Sciences Division of the U. S. Department of Energy under Contract No. DE-AC03-76SF00098.

CHEMICAL PHYSICS

Energy Transfer and Structural Studies of Molecules on Surfaces*

Charles B. Harris, Investigator

INTRODUCTION

The goal of this research is to understand the dynamics of excited electronic states on surfaces, at interfaces, and in condensed phases. The research program is both theoretical and experimental in character. It includes nonlinear optical and ultrafast laser techniques in the picosecond to femtosecond regime, in addition to more conventional surface science instruments for characterizing surfaces and adsorbate-surface interactions. Recent work has focused on the application of the new techniques that we have developed to probe the dynamics of electrons at interfaces and carrier diffusion in semiconductors. The results of this program have a direct bearing on the properties of nanoscale and quantum electronic devices, optoelectronic materials, and on other problems of general interest such as the dynamics of electrical transmission in conductors on ultrafast timescales and the optical properties of thin films.

1. Electronic Dynamics at Metal-Insulator Interfaces (Publication 1)

C.B. Harris, R.E. Jordan, R. Lingle, Jr., W.R. Merry, J. McNeill, and D.F. Padowitz

New results for electron dynamics at interfaces and in thin films are emerging from a combination of ultrafast lasers and electron spectroscopy. Time- and angle-resolved two-photon photoemission spectroscopy probes the band structure and femtosecond dynamics of *excited* electronic states at surfaces and interfaces. Electrons excited just below the photoemission threshold of a metal may remain bound at the metal surface by the *image potential*. We have found that these image potential states persist in the presence of adsorbed molecules. Electrons in the image potential states, localized in the microscopic region just outside the surface and interacting strongly with adsorbed molecules, provide a unique probe of the potential at the metal-insulator interface and of the dynamics of electrons in atomically thin films.

The new instrumental approach to two-photon photoemission developed in this group has demonstrated unprecedented energy resolution and exceptional sensitivity. We have been pursuing a systematic study of adsorbate-induced changes in the binding energies, dispersion, and linewidths of the image potential states on a metal surface. We have established that the binding energy of the electron in the image potential state is extremely sensitive to the structure of adlayers. Previously we had observed discrete steps in the image-state spectra as alkanes were deposited layer-by-layer on the metal. More recently, an order-disorder phase transition within a monolayer of n-pentane has been observed. We have mapped out phase diagrams for the series of C5-C8 alkanes and cyclohexane. Information on the growth mode and surface morphology of adsorbed films is at least as good as that obtained from low energy electron diffraction (LEED).

We are also studying the dynamics of the excited electron. We have observed localization of electrons at the surface caused by adsorbed molecules. Angle-resolved two-photon photoemission spectra reveal the dispersion of the excited electron. Also, this reveals the band structure of the normally unoccupied electronic levels and the electron's effective mass. Electrons in image states on a clean metal, though bound to the surface, have no barriers to 2-D movement parallel to the surface. They exhibit an effective mass close to the mass of a free electron. A non-dispersive peak, in which the electron's energy does not vary with angle, is characteristic of an infinite effective mass or a localized electron. A new, nondispersive peak becomes apparent for bilayers of several alkanes, shown in Figure 1-1. We attribute this feature to electrons localized by interaction with the adsorbed molecules. This is consistent with a developing picture of the spatial extent of the electron wavefunction and its overlap with the adsorbate. The nondispersive feature is very weak for monolayers. It does not appear at all for the n = 2 state, in which the electron extends much further from the surface, even with bilayer coverage. Our latest results show stronger localization by a bilayer of pentane grown on the disordered monolayer phase. This is consistent with disorder-induced localization seen in other condensed phase systems. This new technique provides unique opportunities to study this important phenomenon.

*This work was supported by the Director, Office of Energy Research, Office of Basic Energy Sciences, Chemical Sciences Division of the U. S. Department of Energy under Contract No. DE-AC03-76SF00098.

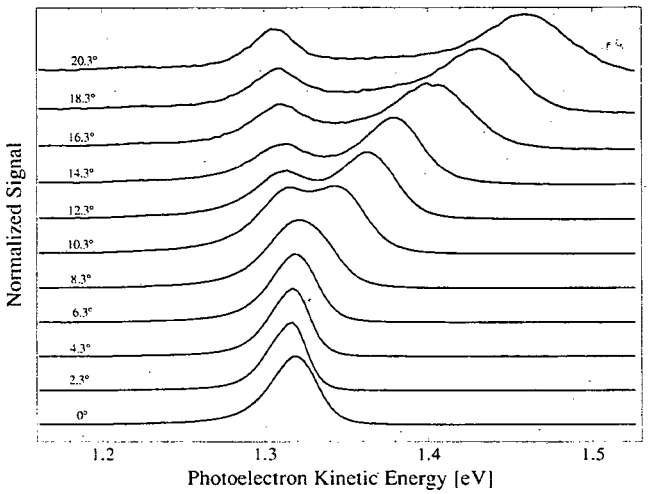

Figure 1-1. Electron localization by an adsorbate film. Angle-resolved two-photon photoemission spectra for a bilayer of n-heptane (C_7H_{16}) on Ag(111). With increasing angle a nondispersive feature separates from the free-electron peak. (XBL 937-4546)

2. Ultrafast Thermal Expansion and Diffusivity of the GaAs Surface (Publication 3)

D.M. Pennington and C.B. Harris

Two-color reflection transient grating spectroscopy was used for the first time to time resolve the ultrafast thermal expansion of a GaAs(100) surface. Understanding the dynamics of transient thermal expansion is of technological importance in fields such as heteroepitaxial semiconductor structures and optical coating design. By utilizing a 100 fsec ultraviolet probe with visible excitation beams, the electronic effects that dominate single color experiments become negligible; thus surface expansion due to heating and the subsequent contraction caused by cooling provide the dominant effect on the diffracted probe. The diffracted signal is composed of two components, heat conduction into the bulk perpendicular to the surface and heat flow parallel in the plane of the surface that fills in the nulls of the transient grating. Our initial experiments were performed using a large grating periodicity, resulting in a diffracted signal due entirely to expansion perpendicular to the surface. These results were then modeled theoretically with excellent agreement.

3. Ultrafast Dynamics in Solution (Publications 2, 4)

C.B. Harris, R.L. Hoff, J.A. King, E. Peterson, D.J. Russell, K.A. Schultz, B.J. Schwartz, and J.Z. Zhang

One of the unique aspects of liquid phase chemical reactivity is the ability of reacting species to become trapped in a "cage" of solvent molecules. This caging can qualitatively change the chemistry of a system by confining the reactive species and allowing them to interact over an extended period of time. The timescale of this process has not been well characterized and remains a central problem in liquid phase reaction dynamics. To study this process we have examined the primary geminate recombination, the nondiffusive recombination of fragments, following photodissociation. To study this we use transient absorption spectroscopy to directly follow the production and disappearance of CH_2I radical fragments produced after the photodissociation of methylene iodide (CH_2I_2) with femtosecond time resolution. These results provide the first direct observation of primary geminate recombination.

Transient absorption results for the photodissociation of CH_2I_2 in CCl_4 are shown in Fig. 3-1. The rapid

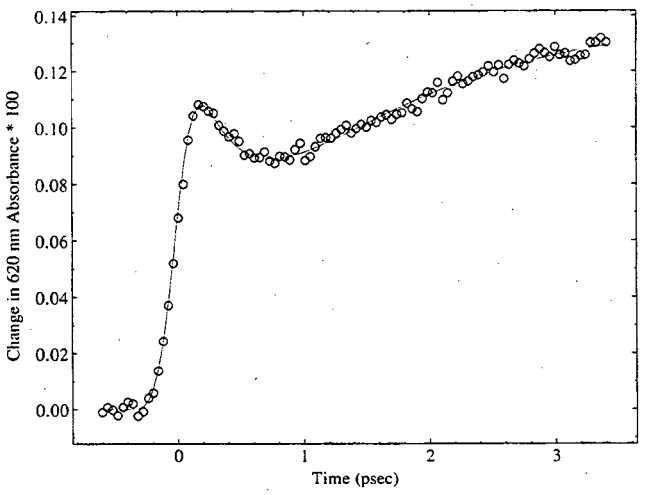

Figure 3-1. Femtosecond 620-nm transient absorption spectra of CH_2I_2 excited at 310 nm in CCl_4. Symbols are data points, the solid line is a fit to the data. The scan shows a pulse width limited rise (≤100 fs), followed by a 350 fs decay indicating disappearance of CH_2I, the absorbing species, and a slower (5–10 ps) rise due to vibrational relaxation. (XBL 937-4547)

absorption rise at 620 nm measures the presence of the CH_2I radical fragment, indicating that the direct dissociation is complete within the 120 fs instrument response. The 350 fs decay after the initial absorption rise corresponds to a disappearance of the CH_2I radicals. Since the gas phase photodissociation quantum yield is unity, the disappearance of CH_2I must be due to geminate recombination of CH_2I and I to reform the parent CH_2I_2 molecule. The 350 fs recovery time allows for only a single collision of the photofragments with the surrounding solvent cage.

In another work, the photochromic reaction dynamics of 1′,3′,3′,-trimethyl-6-hydroxyspiro[2*H*-1-benzopyran-2′,2′-indoline] (HPBS) in solution were studied with picosecond and femtosecond transient electronic spectroscopy. Photochromism is a phenomenon in which a compound changes color when exposed to light of one wavelength and reverts to its original color when irradiated with light of a different wavelength. Recently, there has been an increase in the study of photochromic materials due to their potential applications in several important areas, including high-density optical storage, optical switching, image processing, and displays. In this study the initial C-O bond dissociation was found to occur in less than 100 fs following UV excitation. A small fraction of the dissociated molecules reform the C-O bond on the timescale of 200 fs. The nascent photoproduct is found to vibrationally relax in a few picoseconds and to isomerize on the timescale of ≥100 ps.

Finally, the vibrational relaxation dynamics of large molecules undergoing photodissociation have been investigated. The vibrational relaxation dynamics following the dissociation of C ≡ O from $M(CO)_6$ (M = Cr, Mo, W) were studied with picosecond transient absorption spectroscopy. After dissociation of the C ≡ O the pentacarbonyl species forms a complex with a solvent molecule. The cooling of this solvated pentacarbonyl complex was monitored from 1 ps to 1 ns in this study. The vibrational relaxation of each of these three compounds was different. The $W(CO)_5 \cdot S$ (S = cyclohexane) vibrationally relaxed in 35 ps; whereas, $Mo(CO)_5 \cdot S$ relaxed twice as quickly, 18 ps. This is surprising because the higher density of states in $W(CO)_5 \cdot S$ would be expected to lead to faster cooling of the hot solvated complex. The primary cooling of $Cr(CO)_5 \cdot S$ is completed in 18 ps just as in $Mo(CO)_5 \cdot S$, but a slower component in the relaxation, approximately 150 ps is also present. This component is assigned to vibrational relaxation of the C ≡ O stretching mode. From comparisons with other studies, it appears that the existence of this slower cooling component is only present in first row transition metal carbonyls.

4. Work in Progress

The dynamics of $e^- - h^+$ pairs in graded and alloy semiconductors, i.e., CdS_xSe_{1-x}, are under continuing investigation. Photoluminescence spectra show the effects of disorder and band-gap gradients on carrier diffusion and relaxation dynamics. A fluorescence upconversion spectrometer using a synchronously pumped dye laser, computer-controlled optical delay and data collection, and single-photon counting methods has just been completed. The 1 ps resolution of this system will permit analysis of the fast risetimes of photoluminescence spectra. This will give the most direct information on intraband carrier relaxation and carrier diffusion through inhomogeneous graded samples. These studies probe the effects of a macroscopic potential gradient, as well as local potential fluctuations, on the carrier dynamics.

The work on electron dynamics continues in several directions. Experiments to explore the mechanism of electron localization are in progress. Chemical interactions between excited electrons and adsorbates will be examined in molecules having low-lying electronic levels which may couple to the image states. An alkali metal doser is being built in order to study electron dynamics at metal/metal junctions. Results from two-photon photoemission experiments on alkali metal covered surfaces will yield precise, detailed information about changes electronic structure due to the presence of an alkali layer. Such information is a useful test of current theories about excess electronic states at surfaces.

FY 1992 PUBLICATIONS AND REPORTS

Refereed Journals

1. D.F. Padowitz, W.R. Merry, R.E. Jordan, and C.B. Harris, "Two-Photon Photoemission as a Probe of Electron Interaction with Adsorbates and Thin Dielectric Films on Metal Surfaces," Phys. Rev. Lett. **69**, 3583 (1992); LBL-31906.
2. K.E. Schultz, D.J. Russell, and C.B. Harris, "The Applicability of Binary Collision Theories to Complex Molecules in Simple Liquids," J. Chem. Phys. **97**, 5431 (1992); LBL-30636.†‡
3. D.M. Pennington and C.B. Harris, "Dynamics of Photothermal Surface Expansion Using Laser-Induced Holographic Gratings," IEEE Quantum Electronics (Special Issue) **28**, 2523 (1992); LBL-31946.§
4. J.Z. Zhang, B.J. Schwartz, J.C. King, and C.B. Harris, "Ultrafast Studies of Photochromic Spiropyrans in Solution," J. Am. Chem. Soc. **114**, 10922 (1992); LBL-32768.†

LBL Reports

5. K.E. Schultz, (Ph.D. Thesis), "The Dynamics of Azulene in Liquids and Compressed Gases on Ultrafast Timescales" (1992); LBL-31926.
6. E.S. Peterson (Ph.D. Thesis), "Electronic Excited States as a Probe of Surface Adsorbate Structure and Dynamics in Liquid Xenon" (1992); LBL-32841.
7. B.J. Schwartz (Ph.D. Thesis), "Femtosecond Dynamics of Fundamental Reaction Processes in Liquids: Proton Transfer, Geminate Recombination, Isomerization and Vibrational Relaxation" (1992); LBL-33205.
8. D.M. Pennington (Ph.D. Thesis), "Investigation of Ultrafast Photothermal Surface Expansion and Diffusivity in GaAs Via Laser-Induced Dynamic Grating" (1992); LBL-32383.
9. W.R. Merry (Ph.D. Thesis), "Image Potential States at Metal-Dielectric Interfaces" (1992); LBL-32352.

Invited Talks

10. C.B. Harris, "Dynamics of Electrons at Metal and Semiconductor Interfaces on Ultrafast Timescales," Physical Chemistry Seminar at the University of California, San Diego, CA, October 15, 1991.
11. C.B. Harris, "Energy Redistribution in Molecules on the Femtosecond Timescale," Symposium on the Transient Processes in Liquids and Molecules, Optical Society of America Annual Meeting, San Jose, CA, November 3, 1991.
12. C.B. Harris, "Dynamic of Electrons at Interfaces," Physical Chemistry Seminar at the University of Texas at Austin, November 12, 1991.
13. C.B. Harris, "The Dynamics and Spectroscopy of Electrons at Metal Interfaces," Western Spectroscopy Association Conference, Asilomar, CA, January 29–31, 1992.
14. C.B. Harris, "The Dynamics and Spectroscopy of Electrons at Metal Interfaces," Seminar at Cal. Tech., Pasadena, CA, February 11, 1992.
15. C.B. Harris, "The Dynamics of Electrons at Metal-Insulator and Metal-Semiconductor Interfaces," Condensed Matter Physics Seminar at the University of California, Berkeley, April 1, 1992.
16. C.B. Harris, "Dynamics of Electrons at Interfaces," Scientific and Educational Advisory Committee, Lawrence Berkeley Laboratory, April 3, 1992.
17. C.B. Harris, "Ultrafast Time-Resolved Luminescence of CdS_xSe_{1-x} Alloy Semiconductors," Office of Naval Research Site Review, University of California, Berkeley, April 6, 1992.
18. C.B. Harris, "A New Method of Q-Switching Carbon Monoxide Lasers, Office of Naval Research Site Review, University of California, Berkeley, April 6, 1992.
19. C.B. Harris, "Dynamics of Photothermal Surface Expansion and Diffusivity in GaAs Using Transient Gratings," Office of Naval Research Site Review, University of California, Berkeley, April 6, 1992.
20. C.B. Harris, "The Dynamics of Electrons at Interfaces," Chemistry Department Seminar, UCLA, April 13, 1992.
21. C.B. Harris, "Energy Redistribution in Large Molecules on Ultrafast Timescales," International Conference, Ultrafast Phenomena VIII, Antibes-Juan les Pins, France, June 8–12, 1992.
22. C.B. Harris, "Energy Redistribution in Large Molecules on Ultrafast Timescales," ACS Meeting, Washington, D.C., Aug. 24–28, 1992.
23. C.B. Harris, "Dynamics of Electrons at Interface," Physical Chemistry Seminar, Chemistry Department, University of California, Berkeley, September 1, 1992.
24. C.B. Harris, "Dynamics of Electrons at Interfaces," Physical Chemistry Seminar, Department of Chemistry, University of Michigan, September 24, 1992.
25. D.F. Padowitz, "Electrons at Metal-Insulator Interfaces," Physical Electronics Conference, Irvine, CA, June, 1992.
26. D.F. Padowitz, "Electrons at Interfaces," University of Illinois, Champaign-Urbana, April, 1992.

---

†National Science Foundation Program using DOE equipment.

‡Calculations performed at the San Diego Supercomputer Center Current and Pending Support—Prof. C.B. Harris.

§Office of Naval Research Program using DOE equipment.

Laser Sources and Techniques*

Andrew H. Kung, Investigator

INTRODUCTION

This new program focuses on the development of novel laser and spectroscopic techniques in the IR, UV, and VUV regions for studying combustion-related molecular dynamics at the microscopic level. Laser spectroscopic techniques have proven to be extremely powerful in the investigation of molecular processes that require very high sensitivity and selectivity. Our approach is to use quantum electronic and nonlinear optical techniques to extend the spectral coverage and to enhance the optical power of ultrahigh resolution laser sources so as to obtain and analyze photoionization, fluorescence, and photoelectron spectra of jet-cooled free radicals and of reaction products resulting from unimolecular and bimolecular dissociations. New spectroscopic techniques are developed with these sources for the detection of optically thin and often short-lived species. Recent activities center on regenerative amplification of high-resolution solid-state lasers, development of tunable high-power mid-IR lasers, and short-pulse UV/VUV tunable lasers, and development of a multipurpose high-order suppressor crossed molecular beam apparatus for use with synchrotron radiation sources. This program also provides scientific and technical support within the Chemical Sciences Division to the development of LBL's Combustion Dynamics Initiative.

1. Regenerative Amplification of Single-Frequency Optical Parametric Oscillators

A.H. Kung

We have demonstrated for the first time an extremely broadly tunable all solid-state single-frequency source based on an optical parametric oscillator (OPO) regenerative amplifier arrangement. The source combines the virtues of an OPO with those of a solid-state laser amplifier to provide high-power jitter-free pulsed radiation that is near-diffraction limited, rapidly and broadly tunable, and very narrowband. The work is motivated by the desire to have a solid-state device that would have excellent frequency control and can easily be time-synchronized to other laser pulses. To achieve this, we started with a commercial single-frequency OPO that is tunable from 700 nm to 1000 nm and injected its 2-nsec long pulses into a Ti:Al_2O_3 ring cavity. Optics in the cavity were arranged to operate in the regenerative amplifier mode. Pulse injection and extraction were achieved by polarization coupling using two Pockels cells and a polarizer. A half-wave Fresnel Rhomb served to spoil lasing in the absence of an injected pulse. This regenerative arrangement has the advantage of being extremely broadband. It relaxes the need for longitudinal and transverse mode-matching. Timing and frequency are controlled by the OPO, while output power and spatial filtering are provided by the Ti:Al_2O_3 resonator. The amplifier output is nearly TEM_{00}. Pulse energy is measured from 840 nm to 910 nm. With injection of a 0.5 mJ pulse from the OPO, the output energy ranges from 40 mJ at 840 nm to 28 mJ at 910 nm. The slow fall-off in wavelength dependence is significant because stand-alone Ti:Al_2O_3 lasers and linear amplifiers become inefficient at 910–920 nm and beyond. This device thus results in a much broader tuning range. The output photon efficiency is 20%. Improvements to the cavity should increase this efficiency since depletion of the Ti:Al_2O_3 fluorescence is observed to reach 60%. Addition of a power amplifier will boost the output energy to more than 100 mJ.

2. Tunable High Power IR Laser Development

J. Xie and A.H. Kung

The purpose of this task is to develop a high-resolution, high-power, mid-infrared laser source. The goal is to make available a tunable infrared laser that is suitable to use in research on multiphoton excitation and dissociation experiments. It has been commonly recognized that understanding the photodissociation dynamics and reactivity of hydrocarbon free radicals are essential for understanding the combustion processes of fossil fuels. Infrared multiple-photon absorption will imitate the combustion process in the excitation of reactive species. IR-UV pump and probe will allow the study of mode selectivity in photodissociation. In both cases, an intense IR laser is required. The preliminary specifications of the IR laser are as follows: tuning range, 3 to 10 μm, pulse energy 10 to 100 mJ, wavelength stability 1 in 10^4, and transform-limited resolution.

*This work is supported by the Director, Office of Energy Research, Office of Basic Energy Sciences, Chemical Sciences Division of the U.S. Department of Energy under Contract No. DE-AC03-76SF00098.

Three approaches were evaluated for this development, all involving nonlinear optical techniques to convert fixed frequency or tunable high-power visible or near-IR lasers to the mid-IR: difference frequency mixing, OPO, and Raman shifting. It was clear that a fourth approach, direct lasing, is not feasible because no suitable material is available.

Crystal materials that are transparent in the mid-IR generally have low optical damage thresholds. This investigation therefore focuses on using Raman shifting in gases as the wavelength conversion stage. Gases can be replenished easily if needed. Previous studies have shown that good conversion can be achieved in a multipass Raman cell of H_2 and its isomers. Furthermore, the monochromaticity and spatial quality of the input can be preserved. Our calculation shows that a 20 pass Raman cell operating with 10 atm of H_2 will be required to obtain powerful IR radiation down to 8 μm. Generation at 10 μm becomes problematic due to decreasing Raman gain and inception of H_2 dimer absorption.

For a preliminary study, we have constructed a high pressure Raman cell using second order Stokes in H_2 to produce IR in the region of 2 to 4 μm. The cell was tested for 600 psia operation. It was placed in a cavity of two 1 in. diameter concave copper mirrors that are separated by ~2 m to effect multiple passing of a pump laser beam. We have chosen an external mirror arrangement because it simplifies the initial multipass alignment procedure. Successful second Stokes generation has been obtained with this cell using a Ti:sapphire based pump laser. In this preliminary study, 0.5 mJ of 3 μm radiation has been produced using 10 mJ of incident pump energy. With optimization of the Raman process and use of full power from the OPO regenerative amplifier system that is being developed for this project, we should meet the goal of obtaining >10 mJ in the 3 μm region.

3. Multipurpose High Order Suppressor and Crossed Molecular Beam Apparatus

T.T. Miau, J. Xie, and Y.T. Lee

Studies on high-order suppression of undulator light have shown that a combination of reflection filtering and rare gas filtering will provide a spectral purity of better than 1/100,000 for the energy range of 5–30 eV. The reflection filters cut off photons with energy higher than 30 eV and the rare gas filter then serves to absorb unwanted orders from the undulator emission. We have finished the engineering design of a gas filter. The filter employs an active length of 10 cm and is for use with a maximum gas pressure of 30 Torr. It is embedded in a multipurpose triply differentially pumped chamber that features a flexible design. By placing a rare gas tube in the center of the chamber the machine will serve as a high-order suppressor. Alternatively, when a rotating pulsed molecular beam source is placed in the center of the chamber, it can be used as a photodissociation apparatus.

4. Work in Progress

Development of the regenerative amplifier continues with measurements to determine the full tuning range of the device. A booster amplifier is being incorporated to increase the device output energy by a factor of ten. With this pulse energy, the device will be suitable for use as the front-end of the tunable IR system.

Investigation in using high-order Raman shifting to generate high-power tunable IR is in progress. We are optimizing the use of the external cavity multipass cell to generate 2 to 4 μm radiation. This will provide us with a preliminary IR source to study the spectroscopy and mode-selective dissociation dynamics of hydrocarbon free radicals. In order to reach the ultimate goal of making 5–8 μm mid-IR radiation, we are designing a 39-pass cell with internal mirrors for third order Raman shifting. A large number of passes are necessary to reach threshold for Raman conversion since the Raman gain falls off significantly as the IR wavelength gets longer. In addition to H_2, we are also investigating using HD and D_2 as the medium for efficient conversion.

Development of the multipurpose chamber is proceeding with the design of a versatile rotating source chamber that fits into the main chamber of the high-order suppressor. When mounted at the top of the main chamber, the source chamber supplies rare gases for high-order suppression of undulator radiation. This source chamber can also be utilized to produce free radicals by photolysis in front of a pulsed nozzle or by pyrolysis in a nozzle attached to the chamber. As another option, two such chambers can be fitted to the main chamber to form a crossed-beam machine for studying scattering experiments.

Crossed Molecular Beams*

Yuan T. Lee, Investigator

INTRODUCTION

The major thrust of this research project is to elucidate detailed dynamics of simple elementary reactions that are theoretically important and to unravel the mechanism of complex chemical reactions or photochemical processes that play important roles in many macroscopic processes. Molecular beams of reactants are used to study individual reactive encounters between molecules or to monitor photodissociation events in a collision-free environment. Most of the information is derived from measurement of the product fragment energy and angular and state distributions. Recent activities are centered on the mechanisms of elementary chemical reactions involving oxygen atoms with unsaturated hydrocarbons, the dynamics of endothermic substitution reactions, the dependence of the chemical reactivity of electronically excited atoms on the alignment of excited orbitals, the primary photochemical processes of polyatomic molecules, intramolecular energy transfer of chemically activated and locally excited molecules, the energetics of free radicals that are important to combustion processes, the infrared-absorption spectra of carbonium ions and hydrated hydronium ions, and bond-selective photodissociation through electronic excitation.

1. Reactions of Barium Atoms with Triatomic Oxidants. I. Ba + NO_2 (Publication 5)

H.F. Davis, A.G. Suits, and Y.T. Lee

Angular and velocity distributions of the neutral products resulting from the reaction Ba + NO_2 were measured using the crossed molecular beams method. Despite a large reaction exoergicity (ΔH = –61 kcal/mol), formation of the dominant ground state $BaO(^1\Sigma)$ + NO products results primarily from decay of long-lived $Ba^+NO_2^-$ collision complexes, even at incident collision energies as high as 59 kcal/mol or with electronic excitation of the Ba atom. A large fraction of the reaction exoergicity is channeled into product translational energy. This rather unusual behavior results from a large exit potential energy barrier for decay of the initially formed singly ionic $Ba^+NO_2^-$ intermediate to ground state doubly ionic $Ba^{2+}O_2^-$. A secondary source of forward scattered, internally excited BaO results from a direct reaction without the involvement of long-lived intermediates. An additional minor channel, formation of BaNO + O is observed from ground state Ba + NO_2 at high collision energies by a direct reaction mechanism. Unlike the dominant BaO + NO channel, which involves harpooning at the first ionic-covalent curve crossing, formation of BaNO from reaction of ground state Ba likely results from the small range of collision geometries that are able to avoid long-range electron transfer. The BaNO + O channel was enhanced substantially by electronic excitation of the incident barium atom. However, BaNO from reactions of electronically excited Ba primarily resulted from decay of collision complexes, rather than from a direct mechanism.

2. Photodissociation of Ethylene at 193 nm (Publication 8)

B.A. Balko, J. Zhang, and Y.T. Lee

The photodissociation of ethylene at 193 nm was studied by measuring the product translational energy distributions for the H + C_2H_3 and H_2 + C_2H_2 channels. In agreement with previous workers, it was determined that atomic and molecular elimination occur in roughly equal amounts. Using 1,1 D_2CCH_2 and 1,2 cis HDCCDH, it was shown that both acetylene and vinylidene are formed and that the acetylene/vinylidene ratio is approximately 2/3 in the molecular elimination. This H_2 elimination channel has a translational energy distribution peaked at around 20 kcal/mol, indicating that it is a concerted process with a substantial exit barrier. It was found that the H atom elimination channel is best described as a simple bond rupture occurring after internal conversion of the electronically excited molecule to the vibrationally excited ground state ethylene. Some of the primary C_2H_3 product has sufficient internal energy to spontaneously decompose to H + HC ≡ CH. At higher laser intensity a large fraction of the C_2H_3, however, absorbs another photon and fragments to H + H_2C = C: ($^1A_1$ and $^3B_2$).

*This work was supported by the Director, Office of Energy Research, Office of Basic Energy Sciences, Chemical Sciences Division of the U.S. Department of Energy under Contract No. DE-AC03-76SF00098.

3. Dynamics and Mode Specificity in OClO Photodissociation (Publication 9)

H.F. Davis and Y.T. Lee

The photodissociation of OClO in a molecular beam was studied using photofragment translational energy spectroscopy at wavelengths between 350 and 475 nm. Although the dominant products are $ClO(X^2\Pi) + O(^3P)$, we observe formation of $Cl(^2P) + O_2(^3\Sigma_g^-)$ and find strong evidence for a substantial yield of $Cl(^2P) + O_2(^1\Delta_g)$. The total yield reaches a maximum of $3.9 \pm 0.8\%$ near 404 nm and decreases to <0.2% under the absorption peaks in the wavelength range 350–370 nm. The branching ratios display mode specificity: the yield of $Cl + O_2$ from OClO with symmetric stretching excitation or symmetric stretching + bending is ~10 times greater than from states at nearly the same energy with asymmetric stretching excitation. The $Cl + O_2$ results from concerted unimolecular decomposition with release of up to ~68 kcal/mol in relative translational energy.

4. Dynamics of Ethylene Photodissociation from Rovibrational and Translational Energy Distributions of H_2 Products (Publication 10)

E.F. Cromwell, A. Stolow, M.J.J. Vrakking, and Y.T. Lee

The dynamics of H_2 elimination from ethylene was studied via a pump and probe technique utilizing an ultrahigh resolution vacuum ultraviolet laser system. H_2 product internal and translational energy distributions were obtained for the photodissociation at 193 nm. The distribution of energy in H_2 product from the dissociation of (1,1)-dideuteroethylene is also presented. Two separate H_2 elimination channels are inferred: a 1,1 elimination producing the vinylidene radical and a 1,2 elimination producing the acetylene molecule. Differences between the vibrational, rotational, and translational energy distributions for these two channels are discussed and correlations between product internal and translational energy are presented. A comparison with *ab initio* calculations of the transition state configurations for these processes is made. We suggest that the H_2 elimination process may be nonstatistical in nature. The D atom elimination from C_2D_4 was examined and kinetic energy distribution for this product measured.

5. The Dynamics of Electronic to Vibrational, Rotational, and Translational Energy Transfer in Collision of $Ba(^1P_1)$ with Diatomic Molecules (Publication 11)

A.G. Suits, P. de Pujo, O. Sublemontier, J.-P. Visticot, J. Berlande, J. Cuvellier, T. Gustavsson, J.-M. Mestdagh, P. Meynadier, and Y.T. Lee

Doppler measurements taken over a range of probe-laser angles in a crossed-beam experiment were used, in conjunction with forward convolution analysis, to obtain flux-velocity contour maps for $Ba(^3P_2)$ produced in a collision of $Ba(^1P_1)$ with H_2, N_2, O_2, and NO. The contour maps suggest a general model for dynamics of this process in which large impact parameter collisions result in a near-resonant transfer of initial electronic energy into final vibrational energy, while close collisions produce sideways scattering and effectively couple electronic energy to translation. The molecular collision partners fall into two categories: for one group, comprising O_2 and NO, the existence of a well-defined molecular anion with favorable Franck-Condon factors linking excited vibrational levels to the ground vibrational state of the neutral results in greatly enhanced coupling for near-resonant process. Molecules for which there exist no stable anions, such as N_2 and H_2, represent a second category. The electronically inelastic collision for this group is instead dominated by the nonresonant process yielding the ground vibrational state and large translational energy release.

6. Reaction Dynamics of Ground State and Electronically Excited Barium Atoms (Publication 12)

H.F. Davis, A.G. Suits, and Y.T. Lee

The two general classes of chemical reactions observed for ground state and electronically excited Ba atoms are illustrated. As in the case of monovalent alkali atoms, reactions of Ba with NO_2, O_3, and ClO_2 are initiated by long-range electron transfer. However, the ensuing dynamics are considerably richer than for alkali atoms due to the need for second electron transfer for formation of the dominant ground state products. Measurements of angular and velocity distributions of the products under well-defined single-collision conditions provide insight into this process. Reactions of Ba with water and its methyl

derivatives, on the other hand, can only result from close collisions since long-ranged electron transfer is not thermodynamically possible. Several competing channels were observed. Reactions of ground state Ba(^{1}S) with H_2O led primarily to formation of BaO + H_2. Upon electronic excitation of the incident Ba atom to the ^{1}D state, a large increase in reaction cross section was observed; however, the chemical product was primarily BaOH + H. Reaction of ground state and electronically excited Ba with CH_3OH led to dominant formation of $BaOCH_3$ + H, and CH_3OCH_3 was found to be unreactive. This behavior suggests that the radical channels occur by H-atom migration.

7. Crossed Molecular Beam Study of the Reaction of O(^{3}P) + Allene (Publication 13)

A.M. Schmoltner, S.Y. Huang, R.J. Brudzynski, P.M. Chu, and Y.T. Lee

The reaction between ground state (^{3}P) oxygen atoms and allene was studied under single-collision conditions using the crossed molecular beams method. Product angular distributions and time-of-flight spectra were measured, and for each channel the translational energy distribution was determined. Two major reaction channels could be identified unambiguously: the formation of carbon monoxide and ethylene following oxygen atom attack on the central carbon atom, and the formation of hydrogen atom and allenyloxy (formyl-vinyl) radical following oxygen atom attack on the terminal carbon atom. In addition, at least one other reaction channel occurs, which could be identified as the production of vinyl and formyl radicals. This channel involves the decomposition of acrolein that is formed by the addition of oxygen to the terminal carbon atom, followed by 1,2-hydrogen migration.

8. Infrared Spectroscopy of $CH_5^+(H_2)$ (Publication 14)

D.W. Boo, J.M. Price, and Y.T. Lee

The infrared spectrum of $CH_5^+(H_2)$ has been obtained from 2650 cm^{-1} to 4200 cm^{-1} with 0.2 cm^{-1} resolution. In the spectrum two peaks were found: one broad and asymmetric band in the 2800–3150 cm^{-1} region and one rotationally resolved band in the 4050–4120 cm^{-1} region. They were assigned as the C-H and H-H stretching bands of the CH_5^+ moiety of $CH_5^+(H_2)$ and as the H-H stretching band of the H_2 moiety, respectively. The observed frequency range of the C-H and H-H stretching modes agree well with *ab initio* predictions on CH_5^+. The broad and asymmetric band features would be attributed to the contribution from spectral congestion and hot band transitions, respectively. In this work we modeled the structure of $CH_5^+(H_2)$ based upon the results of this work and other works on related cluster ions. Using the model structure of $CH_5^+(H_2)$ we were able to find the best-fit simulated spectrum to the observed H-H stretching band of the H_2 moiety, thus improving the model structure. In the spectrum of the H-H stretching band of the H_2 moiety, evidence of tunneling splittings and hot band transitions was also found.

9. Resonance-Enhanced One- and Two-Photon Ionization of Water Molecule: Preliminary Analysis by Multichannel Quantum Defect Theory (Publication 15)

M.J.J. Vrakking, Y.T. Lee, R.D. Gilbert, and M.S. Child

Experimental results are presented for one- and two-photon ionization of the water molecule, obtained by using a near transform-limited XUV laser. The single-photon ionization results show rotationally resolved auto-ionizing resonances corresponding to members of Rydberg series ($nd \leftarrow 1b_1$; $n = 6–11$) converging on the $H_2O^+(100)$ vibrational state. The (1+1) multi-photon ionization results show rotationally resolved structure corresponding to Rydberg series ($nd \leftarrow 1b_1$; $n \geq 6$) converging on the $H_2O^+(000)$ vibrational state. Typical linewidths below and above the $H_2O^+(000)$ ionization threshold are 1 cm^{-1} and 2 cm^{-1}, respectively.

The experimental results are simulated by multichannel quantum defect theory (MQDT). The main features in the spectrum are reproduced in a treatment of the rotational channel interactions with partial *l* mixing. It is argued that remaining discrepancies between experiment and theory arise from perturbative interactions between the ($nd \leftarrow 1b_1$) levels and members of the ($nd \leftarrow 3a_1$) Rydberg series. Also, it is argued that in the (1+1) multiphoton ionization spectra lines may be missing due to selective predissociation.

10. Photodissociation Dynamics of CO_2 at 157.6 nm by Photofragment-Translational Spectroscopy (Publication 17)

A. Stolow and Y.T. Lee

The photodissociation of CO_2 at 157 nm was studied by the photofragment-translational spectroscopy technique. Product time-of-flight spectra were recorded and center-of-mass translational energy distributions were determined. Two electronic channels were observed — one forming

$O(^1D)$ and the other $O(^3P)$. With previously determined anisotropy parameters of $\beta = 2$ for the $O(^3P)$ channel and $\beta = 0$ for the $O(^1D)$ channel, an electronic branching ratio of 6% ± 2% $O(^3P)$ was obtained, consistent with previous results. The translational energy distribution for the CO(v) + $O(^3P)$ channel was very broad (over 30 kcal/mol) and appeared to peak near CO(v = 0). The value of $\beta = 2$ for the $O(^3P)$ channel was confirmed by comparing Doppler profiles, derived from our measured translational energy distribution, with previously measured Doppler profiles. This suggests that the O(3P) channel arises from a direct transition to an excited triplet state. The $O(^1D)$ channel had a structured time-of-flight that related to rovibrational distributions of the CO product. The influence of the excitation of the $CO_2(v_2)$ bending mode was investigated and shown to have a small but not negligible contribution. Based upon a comparison of our data with a previous VUV laser induced fluorescence study, we obtain as our best estimate of the vibrational branching ratio, CO(v=0)/CO(v=1) = 1.9, for the CO(v) + $O(^1D)$ channel.

11. Ultra-Sensitive Detection of Hydrogen Molecules by (2+1) REMPI (Publication 18)

M.J.J. Vrakking, A.S. Bracker, T. Suzuki, and Y.T. Lee

Ultrasensitive detection of molecular hydrogen is reported by using Doppler-free (2+1) REMPI through the E,F $^1\Sigma_g^+$ state. By using an arrangement with two near transform-limited counterpropagating laser beams, a *single shot* detection efficiency of 6.8 10^3 molecules/cm^3 has been demonstrated. Frequency scans of the two-photon transitions show that the detection efficiency is limited by AC Stark effects.

12. The Dissociation Energy and Photochemistry of NO_3 (Publication 19)

H.F. Davis, B. Kim, H.S. Johnston, and Y.T. Lee

The photodissociation of NO_3 was studied using the method of molecular beam photofragmentation translational spectroscopy. The existence of two photodissociation channels was confirmed under collision free conditions. At excitation energies below $D_0(O\text{-}NO_2)$ for internally cold NO_3, we observe a large quantum yield (0.7±0.1 at 588 nm) for a concerted 3-center rearrangement resulting in $NO(^2\Pi) + O_2(^3\Sigma_g^-, ^1\Delta)$. The quantum yield for the NO + O_2 channel decreased sharply at wavelengths shorter than 587 nm, falling to <0.01 at 583 nm, while the $NO_2 + O(^3P)$ quantum yield increased to >0.99. Based on this wavelength dependence and the product translational energy distributions, we conclude that the wavelength threshold for NO_3 (0,0,0,0) → NO_2(0,0,0) + $O(^3P)$ is 587 ± 3 nm, i.e., $D_0(O\text{-}NO_2) = 48.69 \pm 0.25$ kcal/mole. From the enthalpies of formation of $O(^3P)$ and $NO_2(^2A_1)$, we calculate $\Delta H_f^o(NO_3) = 18.87 \pm 0.33$ kcal/mole at 0 K, and $\Delta H_f^o(NO_3) = 17.62 \pm 0.33$ kcal/mole (298 K). This is 2.23 kcal/mole higher than the most recent thermochemical value but is consistent with a value calculated indirectly using the most recent values for the electron affinity (EA) distributions and $\Delta H_f^o(NO_3^-)$. Based on the wavelength dependence and translational energy distributions for NO_3 → NO + O_2, the potential energy barrier for $NO_3(^2A') \rightarrow NO(^2\Pi) + O_2(^3\Sigma_g^-)$ was found to be 47.3 ± 0.8 kcal/mole.

13. Work in Progress

The investigation of the dissociation dynamics of $CH_3 = NCH_3$ revealed that these molecules dissociate in a concerted yet asymmetric manner. Stretching of one of the C-N bonds triggers the rearrangement of electrons to form $CH_3\text{---}N_2{\bullet}CH_3$, from which the two CH_3 radicals recoil with different kinetic energies. Further detailed investigations of asymmetric concerted decomposition are now under way.

The equipment specially designed to search for dynamic resonances in $D + H_2 \rightarrow DH(v,J) + H$, by measuring angular distributions of state resolved products using position sensitive detection, has now been completed and experimental studies initiated.

A substantial effort is currently focused on the investigation of the dissociation dynamics of polyatomic radicals energized by various means. IR multiphoton dissociation through selective excitation of various vibrational degrees of freedom using a newly developed high power tunable IR laser is expected to reveal some interesting results.

IR spectroscopy of carbonium ions and their solvated complexes are under investigation.

FY 1992 PUBLICATIONS AND REPORTS

Refereed Journals

1. A.G. Suits, P. de Pujo, O. Sublemontier, J.-P. Visticot, J. Berlande, T. Gustravsson, J.-M. Mestdagh, P. Meynadier, and Y.T. Lee, "The Dynamics of Electronically Inelastic Collisions from 3-Dimensional Doppler Measurements," Phys. Rev. Lett. **67**, 3070 (1991); LBL-30900.

2. A. Stolow, B.A. Balko, E.F. Cromwell, J. Zhang, and Y.T. Lee, "The Dynamics of H_2 Elimination from Ethylene," J. Photochem. Photobiol. **62**, 285 (1992); LBL-31009.
3. A.G. Suits, H. Hou, H.F. Davis, and Y.T. Lee, "Reaction Dynamics from Orbital Alignment Dependence and Angular Distributions of Ions Produced in Collision of Ba(^{1}P) with NO_2 and O_3," J. Chem. Phys. **96**, 2777 (1992); LBL-31260.
4. A. Schmoltner, D.S. Anex, and Y.T. Lee, "IR Multiphoton Dissociation of Anisole: Production and Dissociation of Phenoxy Radical," J. Phys. Chem. **96**, 1236 (1992); LBL-30788.
5. H.F. Davis, A.G. Suits, and Y.T. Lee, "Reactions of Barium Atoms with Triatomic Oxidants. 1: Ba + NO_2," J. Chem. Phys. **96**, 6710 (1992); LBL-31492.
6. M.J.J. Vrakking, A. Bracker, and Y.T. Lee, "Comment on Two-Photon Spectroscopy of N_2: Multiphoton Ionization, Laser-Induced Fluorescence, and Direct Absorption via the $a''^1\Sigma_{g+}$ State," J. Chem. Phys. **96**, 7195 (1992); LBL-31486.
7. B.A. Balko, J. Zhang, and Y.T. Lee, "Photodissociation of Ethylene at 193 nm," J. Chem. Phys. **97**, 935 (1992); LBL-31102.
8. M.H. Covinsky, A.G. Suits, H.F. Davis, and Y.T. Lee, "The Reaction Dynamics of Sodium with Ozone," J. Chem. Phys. **97**, 2515 (1992); LBL-30555.
9. H.F. Davis and Y.T. Lee, "Dynamics and Mode Specificity in OClO Photodissociation," J. Phys. Chem. **96**, 5681 (1992); LBL-32189.
10. E.F. Cromwell, A. Stolow, M.J.J. Vrakking, and Y.T. Lee, "Dynamics of Ethylene Photodissociation from Ro-Vibrational and Translational Energy Distributions of H_2 Products," J. Chem. Phys. **97**, 4029 (1992); LBL-32292.
11. A.G. Suits, P. de Pujo, O. Sublemontier, J.-P. Visticot, J. Berlande, T. Gustravsson, J.-M. Mestdagh, P. Meynadier, and Y.T. Lee, "The Dynamics of Electronic to Vibrational, Rotational and Translational Energy Transfer in Collision of Ba($^1P_1$) with Diatomic Molecules," J. Chem. Phys. **97**, 4094 (1992); LBL-32441.

Other Publications

12. H.F. Davis, A.G. Suits, and Y.T. Lee, "Reaction Dynamics of Ground State and Electronically Excited Barium Atoms, in *Gas Phase Metal Reactions*, A. Fontijn, ed., Elsevier (1992), p. 319; LBL-32009.

LBL Reports

13. A.M. Schmoltner, S.Y. Huang, R.J. Brudzynski, P.M. Chu, and Y.T. Lee, "Crossed Molecular Beam Study of the Reaction of O(^{3}P) + Allene," J. Chem. Phys. (submitted) (1992); LBL- 27917.
14. D.W. Boo, J.M. Price, and Y.T. Lee, "Infrared Spectroscopy of $CH_{5+}(H_2)$," J. Chem. Phys. (submitted) (1992); LBL-32503.
15. M.J.J. Vrakking, Y.T. Lee, R.D. Gilbert, and M.S. Child, "Resonance-Enhanced One- and Two-Photon Ionization of Water Molecule: Preliminary Analysis by Multichannel Quantum Defect Theory," J. Chem. Phys. (submitted) (1992); LBL-32590.
16. L.I. Yeh, Y.T. Lee, and J.T. Hougen, "Vibration-Rotation Spectroscopy of the Hydrated Hydronium Ions $H_5O_2^+$ and $H_9O_4^+$, J. Chem. Phys. (submitted) (1992); LBL-32591.
17. A. Stolow and Y.T. Lee, "Photodissociation Dynamics of CO_2 at 157.6 nm by Photofragment-Translational Spectroscopy," J. Chem. Phys. (submitted) (1992); LBL-32651.
18. M.J.J. Vrakking, A.S. Bracker, T. Suzuki, and Y.T. Lee, "Ultra-Sensitive Detection of Hydrogen Molecules by (2+1) REMPI," Rev. Sci. Instrum. (in press) (1993); LBL-32881.
19. H.F. Davis, B. Kim, H.S. Johnston, and Y.T. Lee, "The Dissociation Energy and Photochemistry of NO_3," J. Phys. Chem. (in press) (1993).
20. P. Chu (Ph.D. Thesis), "Collision Dynamics of Methyl Radicals and Highly Vibrationally Excited Molecules Using Crossed Molecular Beams," LBL-32440.
21. H.F. Davis (Ph.D. Thesis), "Reaction Dynamics and Photochemistry of Divalent Systems," LBL-32515.
22. M.J.J. Vrakking (Ph.D. Thesis), "Towards Rotationally State-Resolved Differential Cross Sections for the Hydrogen Exchange Reaction," LBL-33219.

Invited Talks

23. Y.T. Lee, "Molecular Beam Studies of Chemical Reaction Dynamics," Department of Chemistry, Brooklyn Polytechnic University, Brookhaven, NY, October 21, 1991.
24. Y.T. Lee, "Crossed Molecular Beams Studies on Chemical Reaction Dynamics," Department of Chemistry, Baylor University, Waco, TX, October 31, 1991.
25. Y.T. Lee, "3 & 4-Centered Elimination of H_2 in the Photodissociation of Ethylene," Department of Chemistry, University of Stockholm, Sweden, December 6, 1991.
26. Y.T. Lee, "Crossed Molecular Beams Studies on Elementary Chemical Reactions Involved in Combustion," Symposium on Elementary Reactions to Combustion, University of Trieste, Italy, December 16, 1991.
27. Y.T. Lee, "Diamond Film Synthesis by Molecular Beam Technique," Institute of Chemistry, Chinese Academy of Sciences, Beijing, China, January 3, 1992.
28. Y.T. Lee, "Molecular Beam Studies of Chemical Reaction Dynamics," 1992 Hill Memorial Lecture, Department of Chemistry, Duke University, Durham, NC, March 24, 1992.
29. Y.T. Lee, "Mode Specific Photodissociation of ClO_2," 203rd American Chemical Society National Meeting, Symposium on Reactions on Multiple Potential Energy Surfaces, San Francisco, CA, April 10, 1992.
30. Y.T. Lee, "Molecular Beam Chemical Kinetics," Department of Chemistry, University of Michigan, Ann Arbor, MI, April 28, 1992.
31. Y.T. Lee, "Photodissociation Dynamics of NO_3 and ClO_2," XXth Informal Conference on Photochemistry, Atlanta, GA, April 30, 1992.
32. Y.T. Lee, "Vibrational-Rotational Spectroscopy of Solvated Ions," Department of Chemistry, University of Southampton, Great Britain, May 12, 1992.

33. Y.T. Lee, "Molecular Beams in the Chemical Era," 1992 Faraday Lecture, London, Great Britain, May 13, 1992..
34. Y.T. Lee, "Infrared Absorption Spectroscopy of Hydrated Hydronium Ions and Ammoniated Ammonium Ions," University of Essex, Colchester, Great Britain, May 15, 1992.
35. Y.T. Lee, "Electron Transfers in Chemical Reactions," Department of Chemistry, University of New Castle, Great Britain, May 18, 1992.
36. Y.T. Lee, "One and Two Electron Transfer in the Reaction of Ba with Simple Molecules," Department of Chemistry, University of Edinburgh, Scotland, May 20, 1992.
37. Y.T. Lee, "Dynamics of Chemical Reactions by Crossed Molecular Beams Technique," Department of Chemistry, University of Manchester, Great Britain, May 21, 1992.
38. Y.T. Lee, "Recent Advances in Molecular Beam Chemical Kinetics," IBM Research Center, Yorktown Heights, NY, June 1, 1992..
39. Y.T. Lee, "Thirty Years of Reaction Dynamics by Mass Spectrometry," Plenary Lecture, Annual Meeting of American Society for Mass Spectrometry, Washington, DC, June 4, 1992.
40. Y.T. Lee, "Molecular Beam Chemistry," 1992 Combustion Contractors' Meeting, Granlibakken Conference Center, Tahoe City, CA, June 17, 1992.
41. Y.T. Lee, "Recent Advances in Molecular Beam Studies of Chemical Reaction Dynamics and Photochemical Dynamics and Photochemical Processes,' Department of Chemistry, University of Rome, Italy, June 23, 1992.
42. Y.T. Lee, "Molecular Beam Studies of Atmospheric and Combustion Chemistry," Dudley Herschbach Birthday Symposium, Harvard University, Cambridge, MA, July 16, 1992.

Molecular Interactions*

William A. Lester, Jr., Investigator

INTRODUCTION

This research program is directed at extending fundamental knowledge of atoms and molecules including their electronic structure, mutual interaction, collision dynamics, and interaction with radiation. The approach combines the use of *ab initio* methods—Hartree-Fock (HF), multiconfiguration-HF, configuration interaction, and the recently developed quantum Monte Carlo (QMC)—to describe electronic structure, intermolecular interactions, and other properties, with various methods for characterizing inelastic and reactive collision processes, and photodissociation dynamics. Present activity is focused on the development and application of the QMC method.

1. Optimization of a Multideterminant Wavefunction for Quantum Monte Carlo (Publication 1)

Z. Sun,† R.N. Barnett,‡ and W.A. Lester, Jr.

A wavefunction constructed as a product of a four-determinant function and a symmetric correlation function is employed in Monte Carlo computations of the ground-state energy of Li_2 at R_e = 5.05 Bohrs. Wavefunction parameters are determined by a fixed-sample minimization of deviations of the local energy. Although the variational Monte Carlo energy for this function lies, as expected, below that of a similar wavefunction constructed with a single determinant, the four-determinant/correlation function wavefunction gives no improvement in quantum Monte Carlo energy. However, the unoptimized four-determinant/correlation function wavefunction does yield an energy in excellent agreement with the estimated exact result. The poorer energy of the optimized function is caused by degradation of the nodal structure during parameter optimization.

†Permanent address: Institute of Mechanics, Chinese Academy of Sciences, People's Republic of China.
‡Present address: Department of Chemistry, University of California, Berkeley.

*This work was supported by the Director, Office of Energy Research, Office of Basic Energy Sciences, Chemical Sciences Division of the U. S. Department of Energy under Contract No. DE-AC03-76SF00098.

2. Monte Carlo Determination of the Oscillator Strength and Excited State Lifetime for the Li $2^2S \rightarrow 2^2P$ Transition (Publication 2)

R.N. Barnett,† P.J. Reynolds,‡ and W.A. Lester, Jr.

A recently developed Monte Carlo method is used to compute the 2^2S 2^2P transition dipole moment of Li. This approach employs a guided Metropolis random walk with quantum Monte Carlo "side" walks to sample the required probability distributions. The transition dipole moment is employed to obtain the oscillator strength and excited-state lifetime. Our most accurately converged calculations yield an oscillator strength of 0.742(7) and excited-state lifetime of 27.41(35) ns. These results are in excellent agreement with precise experimental measurements of 0.742(1) and 27.29(4) ns, respectively. In addition, single-state expectation values are computed for both states. Monte Carlo parameters, such as the time step size and the convergence time, are varied in order to study their effect on computed results.

†Present address: Department of Chemistry, University of California, Berkeley.
‡Present address: Physics Division, Office of Naval Research, Arlington, Virginia.

3. Quantum and Variational Monte Carlo Interaction Potentials for $Li_2(X\ ^1\Sigma_g^+)$ (Publication 3)

Z. Sun,†R.N. Barnett,‡ and W.A. Lester, Jr.

Optimized trial functions are used in quantum Monte Carlo and variational Monte Carlo calculations of the Li_2 $(X^1\Sigma_g^+)$ potential curve. The trial functions used are a product of a Slater determinant of molecular orbitals multiplied by correlation functions of electron-nuclear and electron-electron separation. The parameters of the determinant and correlation functions are optimized simultaneously by reducing the deviations of the local energy E_L ($E_L = \Psi_T^{-1} H\Psi_T$, where Ψ_T denotes a trial function) over a fixed sample. At the equilibrium separation, the variational Monte Carlo and quantum Monte Carlo methods recover 68% and 98% of the correlation energy, respectively. At other points on the curves, these methods yield similar accuracies.

†Permanent address: Institute of Mechanics, Chinese Academy of Sciences, People's Republic of China.
‡Present address: Department of Chemistry, University of California, Berkeley.

4. Correlated Sampling of Monte Carlo Derivatives with Iterative-Fixed Sampling (Publication 4)

Z. Sun,[†] W.A. Lester, Jr., and B.L. Hammond[‡]

A correlated sampling method for determining energy and other property derivatives by finite difference is implemented within variational Monte Carlo. Determination of derivatives takes place over a fixed sample of electronic coordinates, so it is possible to distinguish small energy or other property differences accurately. Using finite differences avoids the evaluation of complicated derivative expressions and can be directly applied to Green's function Monte Carlo methods without the need for derivatives of the Green's function. The algorithm can be used to evaluate derivatives with respect to any parameters in the Hamiltonian or in the trial function. It is applied to H_2 and Li_2 for their energy derivatives with respect to nuclear coordinates. Results are in agreement with experimental data.

[†]Permanent address: Institute of Mechanics, Chinese Academy of Sciences, People's Republic of China.
[‡]Present address: Fujitsu America, Inc., Computational Research Division, San Jose, California.

5. Theoretical Studies of the Structure and Thermochemistry of FO_2 Radical: Comparison of Moller-Plesset Perturbation, Complete-Active-Space Self-Consistent-Field, and Quadratic Configuration Interaction Methods (Publication 5)

J.S. Francisco,[†] Y. Zhao,[†] W.A. Lester, Jr., and I.H. Williams[‡]

The structure of FO_2 has been calculated for the X^2A'' ground state using Moller-Plesset (MP) perturbation, complete-active-space self-consistent field (CASSCF), and quadratic configuration interaction (QCI) *ab initio* molecular orbital methods. Basis sets with polarization and diffuse functions were used. Compared with the experimental structure, bond lengths obtained with MP perturbation methods are found to be consistently too short. CASSCF calculations yield a structure that varies considerably with the size of the active space and basis set used. Calculations using the single-configuration-based QCI in the single and double-space with perturbative inclusion of triple substitutions, denoted by QCISD (T), yield structures very close to the experimental structure of FO_2. The thermochemistry of FO_2 radical has been calculated using the MP, QCI, and GAUSSIAN-1 (G1) methods. The QCI method isodesmic and isogyric schemes has predicted the heat of formation for FO_2 at 0 K to be 8.9 $\pm$ 3 kcal mol^{-1}.

[†]Permanent address: Department of Chemistry, Wayne State University, Detroit, Michigan.
[‡]Permanent address: Department of Chemistry, University of Bath, Bath, United Kingdom.

6. A Quantum-Mechanical Model of Heterogeneous Catalysis (Publication 6)

V.Z. Kresin and W.A. Lester, Jr.

A quantum-mechanical model for heterogeneous catalytic reactions has been developed based on the reaction Hamiltonian method developed by the authors. It is shown that the presence of the surface leads to additional channels of reaction. These are found to dominate the exponential smallness of the reaction probability of the direct channel producing large reaction probabilities for surface-catalyzed reactions. The dependence of catalytic reaction probability on reactant dissociation energy and vibrational frequencies, and the leakage of the electronic wavefunction out of the surface is discussed.

7. Work in Progress

Our quantum Monte Carlo approach for the calculation of vibrational eigenvalues of polyatomic molecules, with particular attention to floppy molecules, and applicable to systems with an arbitrary number of nuclei, in all cases given a potential energy surface, is being coded to run efficiently on massively parallel computers. This effort, a collaboration with workers at the National Energy Research Supercomputer Center and initiated with colleagues at Sandia Livermore Laboratory, is directed initially at treating the C_3 system.

A manuscript describing our computational study of reorientation cross section of $H_2(B\ ^1\Sigma_u^+)$ scattered by helium is nearing completion. Calculations have begun for $D_2(B)$ and HD(B). This effort will complement experiments of C.B. Moore and collaborators.

FY 1992 PUBLICATIONS AND REPORTS

Refereed Journals

1. Z. Sun, R.N. Barnett, and W.A. Lester, Jr., "Optimization of a Multideterminant Wave Function for Quantum Monte Carlo," J. Chem. Phys. **96**, 2422 (1992); LBL-31429.

2. R.N. Barnett, P.J. Reynolds, and W.A. Lester, Jr., "Monte Carlo Determination of the Oscillator Strength and Excited State Lifetime for the Li 2^2S 2^2P Transition," Int. J. Quan. Chem. **42**, 837 (1992); LBL-30152.
3. Z. Sun, R.N. Barnett, and W.A. Lester, Jr., "Quantum and Variational Monte Carlo Interaction Potentials for Li_2 ($X\ ^1\Sigma_g^+$)," Chem. Phys. Letts. **195**, 365 (1992); LBL-32366.
4. Z. Sun, W.A. Lester, Jr., and B.L. Hammond, "Correlated Sampling of Monte Carlo Derivatives with Iterative-Fixed Sampling," J. Chem. Phys. **97**, 7585 (1992); LBL-32747.
5. J.S. Francisco, Y. Zhao, W.A. Lester, Jr., and I.H. Williams, "Theoretical Studies of the Structure and Thermochemistry FO_2 Radical: Comparison of Moller-Plesset Perturbation, Complete-Active-Space Self-Consistent-Field, and Quadratic Configuration Interaction Methods," J. Chem. Phys. **96**, 2861 (1992); LBL-32800.
6. V.Z. Kresin and W.A. Lester, Jr., "A Quantum-Mechanical Model of Heterogeneous Catalysis," Chem. Phys. Letts. **197**, 1 (1992); LBL-32344.

Invited Talks

7. W.A. Lester, Jr., "Theoretical Studies of Molecular Interactions," DOE Office of Basic Energy Sciences Combustion Research Meeting, Granlibakken Conference Center, Tahoe City, CA, June 15–17, 1992; LBL-33323 Abs.
8. W.A. Lester, Jr., "Quantum Monte Carlo for Molecules: Methodology, Applications, and Future Prospects," 19th Annual National Organization of Black Chemists and Chemical Engineers National Conference, New Orleans, LA, April 20–24, 1992.
9. W.A. Lester, Jr., "Monte Carlo Computation of Expectation Values of Coordinate Operators and Transition Dipole Moments," Centre Europeen de Calcul Atomique et Moleculaire Workshop on Quantum Monte Carlo, Orsay, France, July 1, 1992.
10. W.A. Lester, Jr., "Quantum Monte Carlo for Molecules," Department of Chemistry, University of Bilkent, Ankara, Turkey, July 9, 1992.
11. J.C. Andrews (Presenter), V.Z. Kresin, and W.A. Lester, Jr., "Chemical Reaction as a Quantum Transition: Product Energy Distributions for the Hydrogen Exchange Reaction," American Chemical Society National Meeting, San Francisco, CA, April 5–10, 1992; LBL-32626.
12. W.R. Brown (Presenter), W.A. Glauser, and W.A. Lester, Jr., "Correlation Function Quantum Monte Carlo," American Chemical Society National Meeting, San Francisco, CA, April 5–10, 1992; LBL-32627.
13. E.M. Johnson (Presenter), R.N. Barnett, and W.A. Lester, Jr., "Computation of Transition Dipole Moments by Quantum Monte Carlo: Higher Accuracy," American Chemical Society National Meeting, San Francisco, CA, April 5–10, 1992; LBL-32628.
14. V.Z. Kresin (Presenter), and W.A. Lester, Jr., "Heterogeneous Catalysis from the Perspective of Quantum Transition Theory," American Chemical Society National Meeting, San Francisco, CA, April 5–10, 1992; LBL-32629.
15. J.A. Odutola (Presenter), R.M. Grimes, and W.A. Lester, Jr., "Reorientation Cross Sections in Collisions of He (^1S) + $H_2(B\ ^1\Sigma_u^1)$," American Chemical Society National Meeting, San Francisco, CA, April 5–10, 1992; LBL-32630.
16. M.M. Soto (Presenter), A.D. McLean, and W.A. Lester, Jr., "Quantum Monte Carlo for Electronic Structure," American Chemical Society National Meeting, San Francisco, CA, April 5–10, 1992; LBL-32631.
17. Z. Sun (Presenter) and W.A. Lester, Jr., "Quantum Monte Carlo on the $1^1A'$ and $2^1A'$ Potential Energy Surface of He + H_2 System," American Chemical Society National Meeting, San Francisco, CA, April 5–10, 1992; LBL-32632.
18. J.Y. Yu (Presenter) and W.A. Lester, Jr., "Time-Dependent Wave Packet Study in the Interaction Representation of Rotational Excitation and Reorientation in Atom-Molecule Collisions," American Chemical Society National Meeting, San Francisco, CA, April 5–10, 1992; LBL-32633.

LBL Reports

19. W.A. Glauser, W.R. Brown, W.A. Lester, Jr., D. Bressanini, B.L. Hammond, and M.L. Koszykowski, "Random Walk Approach to Mapping Nodal Regions of N-Body Wavefunctions. Ground State Hartree-Fock Wavefunctions for Li-C," accepted by J. Chem. Phys.; LBL-32885.
20. J.W. De M. Carneiro, P.R. Seidl, J.G.R. Tostes, C.A. Taft, B.L. Hammond, M.M. Soto, and W.A. Lester, Jr., "The Effects of Lone Pairs on Charge Distribution in the Tetracyclic Norbornyl Derivatives," accepted by Chem. Phys. Letts.; LBL-33127.

Theory of Atomic and Molecular Collision Processes*

William H. Miller, Investigator

INTRODUCTION

This research is primarily involved with the development and application of theoretical methods and models for describing atomic and molecular collision processes and chemical reaction dynamics. Specific topics of interest have included the theory of inelastic and reactive scattering, collision processes involving electronically excited atoms or molecules, collisional ionization phenomena, statistical theories of chemical reactions, scattering of atoms and molecules from surfaces, and the interactions of molecular systems with high-power laser radiation.

Research deals with both the development of rigorous theoretical approaches that are applicable to simple chemical systems, and also more approximate methods that are applicable to *complex* chemical systems, e.g., polyatomic molecules and their reactions. Even in the latter area, though, the goal is to develop approaches that can utilize *ab initio* quantum chemical calculations of the potential energy surface (in the Born-Oppenheimer approximation) as direct input into the dynamical treatment, and thus, to as great an extent as possible, have a truly predictive theory.

1. Classical Trajectory Studies of the Molecular Dissociation Dynamics of Formaldehyde: $H_2CO \rightarrow H_2 + CO$ (Publication 1)

Y.-T. Chang,† C. Minichino,‡ and W.H. Miller

Classical trajectory calculations have been carried out to simulate the unimolecular decomposition of formaldehyde in the ground electronic state (S_0). Global potential energy surfaces were constructed using the empirical valence bond (EVB) approach. Two sets of *ab initio* input were used to characterize two different EVB potential energy surfaces, and trajectory calculations using one of these gives excellent agreement with experimental data for the product state distributions of H_2 and CO. The trajectory study of vector correlations with prompt dissociation of the parent molecule provides understanding of the dissociation dynamics in the molecular frame. From comparison with some of the experimental results and information from a few *ab initio* calculations, some improvements for the current potential surfaces are suggested.

*This work was supported by the Director, Office of Energy Research, Office of Basic Energy Sciences, Chemical Sciences Division of the U.S. Department of Energy under Contract No. DE-AC03-76SF00098.

†Molecular Research Institute, Palo Alto, CA 94304.
‡Dipartimento di Chimica, Universita' della Basilicata via Nazario Sauro 85, I-85100 Potenza, Italy.

2. Calculation of the Cumulative Reaction Probability via a Discrete Variable Representation with Absorbing Boundary Conditions (Publication 3)†

Tamar Seideman‡ and W.H. Miller

A new method is suggested for the calculation of the microcanonical cumulative reaction probability via flux autocorrelation relations. The Hamiltonian and the flux operators are computed in a discrete variable representation (DVR) and a well-behaved representation for the Green's operator, $G(E^+)$, obtained by imposing absorbing boundary conditions (ABC). Applications to a one-dimensional-model problem and to the collinear $H + H^2$ reaction show that the DVR-ABC scheme provides a very efficient method for the direct calculation of the microcanonical probability, circumventing the need to compute the state-to-state dynamics. Our results indicate that the cumulative reaction probability can be calculated to a high accuracy using a rather small number of DVR points, confined to the vicinity of the transition state. Only limited information regarding the potential-energy surface is therefore required, suggesting that this method would be applicable also to higher dimensionality problems, for which the complete potential surface is often unknown.

†This work is also supported in part by the National Science Foundation, Grant CHE-8920690.

‡NASA Ames Research Center, Moffett Field, CA 94035.

3. Quantum Mechanical Reaction Probabilities via a Discrete Variable Representation-Absorbing Boundary Condition Green's Function (Publication 6)†

T. Seideman‡ and W.H. Miller

The use of a discrete variable representation (DVR) and absorbing boundary conditions (ABC) to construct outgoing Green's function $G(E^+) \equiv \lim_{\varepsilon \to 0} (E + i\varepsilon - H)^{-1}$,

and its subsequent use to determine the cumulative reaction probability for a chemical reaction, has been extended beyond our previous work in several significant ways. In particular, the present paper gives a more thorough derivation and analysis of the DVR-ABC approach, shows how the same DVR-ABC Green's function can be used to obtain state-to-state (as well as cumulative) reaction probabilities, derives a DVR for the exact, multidimensional Watson Hamiltonian (referenced to a transition state), and presents illustrative calculations for the three-dimensional H + H_2 reaction with zero total angular momentum.

†This work is also supported in part by the National Science Foundation, Grant CHE-8920690.
‡NASA Ames Research Center, Moffett Field, CA 94035.

4. Quantum Mechanical Reaction Probabilities with a Power Series Green's Function (Publication 12)

S.M. Auerbach and W.H. Miller

We present a new method to compute Green's function with absorbing boundary conditions for use in the calculation of quantum mechanical reaction probabilities. This is an iterative technique to compute the inverse of a complex matrix that is based on Fourier transforming time-dependent dynamics. The Hamiltonian is evaluated in a sinc-function based discrete variable representation, which we argue may often be superior to the FFT method for reactive scattering. We apply the resulting power series Green's function to the calculation of the cumulative reaction probability for the benchmark collinear H + H_2 system over the energy range 0.37 to 1.27 eV. The convergence of the power series is found to be stable at all energies, and accelerated by the use of a stronger absorbing potential.

5. A Semiclassical Model to Incorporate Multidimensional Tunneling in Classical Trajectory Simulations Using Locally Conserved Actions (Publication 11)

S. Keshavamurthy and W.H. Miller

Earlier work, within the context of transition state theory, has shown that tunneling through the saddle point region of a potential energy surface can be characterized by locally conserved action variables associated with the saddle point (transition state). The present paper shows how this idea can be combined with classical trajectory simulation methods and thus allow tunneling effects to be incorporated into a much wider class of dynamical processes. Application of this approach to a two-dimensional model unimolecular decay potential gives good results over a wide range of system parameters.

6. Cumulative Reaction Probabilities for H + H_2 → H_2 + H from a Knowledge of the Anharmonic Force Field (Publication 4)

M.J. Cohen,† N.C. Handy,† R. Hernandez, and W.H. Miller

In an earlier publication, the authors showed how knowledge of a quartic force field expanded about a transition state can be used to obtain transition state theory tunneling probabilities. Thus coupling between the reaction mode and other modes is included in this second-order perturbation theory approach. Here we study the very anharmonic reaction H + H_2 → H_2 + H and show that even in this extreme case, there is reasonable agreement between the cumulative reaction probabilities calculated by this semiclassical approach, and full quantum calculations.

†University Chemical Laboratory, Lensfield Road, Cambridge, CB2 1EW, UK.

7. Work in Progress

The new ways developed for computing the cumulative reaction probability in a direct (yet rigorous) fashion is being applied to the reactions

$$H + H_2O \rightarrow H_2 + OH$$

$$H + O_2 \rightarrow OH + H \quad .$$

This methodology will allow absolutely rigorous calculations of the rates of simple reactions (given a potential energy surface).

FY 1992 PUBLICATIONS AND REPORTS

Refereed Journals

1. Y.T. Chang, C. Minichino, and W.H. Miller, "Classical Trajectory Studies of the Molecular Dissociation Dynamics of Formaldehyde: $H_2CO \rightarrow H_2 + CO$," J. Chem. Phys. **96**, 4341 (1992); LBL-31623.
2. D.T. Colbert and W.H. Miller, "A Novel Discrete Variable Representation (DVR) for Quantum Mechanical Reactive Scattering via the S-Matrix Kohn Method," J. Chem. Phys. **96**, 1982 (1992).
3. T. Seideman and W.H. Miller, "Calculation of the Cumulative Reaction Probability Via a Discrete Variable Representation with Absorbing Boundary Conditions," J. Chem. Phys. **96**, 4412 (1992); LBL-31624.

4. M.J. Cohen, N.C. Handy, R. Hernandez, and W. H. Miller, "Cumulative Reaction Probabilities for H + H_2 → H_2+H from a Knowledge of the Anharmonic Force Field," Chem. Phys. Lett. **192**, 407 (1992).
5. T.D. Sewell, D.L. Thompson, D. Gezelter, and W. H. Miller, "Some Problems of Correcting the Zero-Point Energy Problem in Classical Trajectories," Chem. Phys. Lett. **193**, 512 (1992).
6. T. Seideman and W.H. Miller, "Quantum Mechanical Reaction Probabilities via a Discrete Variable Representation-Absorbing Boundary Condition Green's Function," J. Chem. Phys. **97**, 2499 (1992); LBL-32180.
7. G. Stock and W.H. Miller, "A Classical Model for Time- and Frequency-Resolved Spectroscopy of Nonadiabatic Excited State Dynamics," Chem. Phys. Lett. **197**, 396 (1992).

LBL Reports

8. W.H. Miller, "Reaction Dynamics in Polyatomic Molecular Systems: Some Approaches for Constructing Potential Energy Surfaces and Incorporating Quantum Effects in Classical Trajectory Simulations," in *Molecular Aspects of Biotechnology: Computational Models and Theories*, ed. J. Bertran, Kluwer Academic, p. 193 (1992); LBL-31626.
9. W.H. Miller and T. Seideman, "Cumulative and State-to-State Reaction Probabilities via a Discrete Variable Representation—Absorbing Boundary Condition Green's Function," in *Time Dependent Quantum Molecular Dynamics: Experiments and Theory*, ed. J. Broeckhove and L. Lathouwers, Plenum, NY, 1992, p. 267; LBL-32181.
10. W.H. Miller, "Beyond Transition State Theory—A Rigorous Quantum Theory of Chemical Reaction Rates," Accts. Chem. Res. (in press); LBL- 33326.
11. S. Keshavamurthy and W.H. Miller, "A Semiclassical Model to Incorporate Multidimensional Tunneling in Classical Trajectory Simulations Using Locally Conserved Actions," Chem. Phys. Lett. (in press); LBL-33344.
12. S.M. Auerbach and W.H. Miller, Quantum Mechanical Reaction Probabilities with a Power Series Green's Function, J. Chem. Phys. (in press); LBL-33325.

Invited Talks

13. W.H. Miller, "Recent Developments and Future Prospects in Rigorous Quantum Mechanical Descriptions of Chemical Reactions," Molecular Science: Current Status and Future Prospects, January 7–9, 1992, Okazaki, Japan.
14. W.H. Miller, "A Discrete Variable Representation for Quantum Reactive Scattering via the S-Matrix Kohn Method," Joint US-Israel Workshop on Computational Chemistry, January 28–30, 1992, Berkeley, CA.
15. W.H. Miller, "Quantum Mechanical Reactive Flux Correlation Functions," NATO Advanced Research Workshop on Time-Dependent Quantum Molecular Dynamics: Experiments and Theory, March 30–April 3, Snowbird, UT.
16. W.H. Miller, "Direct Calculation of the Cumulative Reactive Probability," Symposium of Frontiers of Molecular Simulations, ACS National Meeting, August 24–28, 1992, Washington, DC.
17. W.H. Miller, "Use of Discrete Variable Representative and Absorbing Boundary Conditions to Calculate State-to-State and Cumulative Reaction Probabilities," NATO Advanced Research Workshop on Grid Methods in Atomic and Molecular Quantum Calculations, September 27–October 3, 1992, Corsica, France.

Selective Photochemistry*

C. Bradley Moore, Investigator

INTRODUCTION

The fundamental goals of this work are to elucidate the molecular dynamics of energy transfer and chemical reaction processes and to assess the opportunities for selecting reaction products through selective excitation of reactants. Lasers are used to prepare molecules in selected excited states, and a variety of spectroscopic probes are used to follow energy transfers and chemical reactions with quantum-state, resolution. Ideally all quantum numbers are resolved in the initial excitation and for each of the product states. By exploring the dependence of processes on quantum state and other experimentally controllable parameters, it is usually possible to establish a physical model for the process. Optimally accurate benchmarks are established for the quantitative test of first principles theory.

Chemical reactions usually require excitations corresponding to ultraviolet photon energies, and hence the initial state is usually an electronically excited one. The first step is then to understand the transfer of electronic (and perhaps vibrational and even rotational) energy to different electronic states and to vibrational, rotational, and translational degrees of freedom. These processes occur both unimolecularly and in collisions. To the extent that initial excitation is randomized, among the available degrees of freedom opportunities for selectivity may be lost. The simplest stable molecular electronic state is B-state H_2. In the absence of collisions, the molecule simply radiates. Collisions cause electronic energy transfer to a repulsive potential surface depositing the energy into translation of the product H-atom fragments. Collisions also cause changes in vibrational and rotational quantum numbers. The dynamics of these processes and the relationship between them is under study.

When the ketene molecule is placed into its first excited electronic state, strong electronic-vibrational and spin-orbit couplings produce a statistical mixture of excited singlet, triplet, and ground singlet states. The lower the electronic energy, the greater the vibrational energy and the greater the corresponding statistical weight. The lowest threshold for dissociation to CH_2 + CO is on the triplet surface. The total energy and angular momentum can be finely controlled. The microcanonical reaction rate, k(E,J), and reaction product attributes can be studied to reveal the dynamics of the reaction in the transition state region. In this same energy region unimolecular exchange of the carbon atoms occurs and, thus excitation of $^{13}CH_2CO$ can yield ^{13}CO product. This reaction permits the first study of reaction rate resonances due to vibrational resonances in the reaction coordinate degree of freedom. These studies are providing an increasingly sharp picture of molecular dynamics in the region of a unimolecular transition state.

Lasers are particularly useful in studying the highly reactive species important in combustion and homogenous catalysis. Flash photolysis with a laser provides a controlled source of these species for study in gases or liquids. Laser spectroscopy provides excellent wavelength and time resolution for observation of the spectrum and study of the reaction kinetics of reactive species. Studies here concentrate on infrared absorption spectroscopic studies of hydrocarbon radicals important in combustion and, in collaboration with Robert Bergman, coordinatively unsaturated organometallics important in CH activation chemistry.

1. Observation of Transition-State Vibrational Thresholds in the Rate of Dissociation of Ketene (Publication 1)

E.R. Lovejoy, S.K. Kim, and C.B. Moore

The elementary chemical reaction is one of the most fundamental processes in nature, and the theoretical and experimental study of the transformation of reactants into products has been an important area of research for many decades. Experimental studies of unimolecular reactions of highly energized molecules provide strong tests of the theories developed to describe chemical reactivity. The unimolecular rate theory of Rice, Ramsperger, Kassel, and Marcus (RRKM) is based on the assumptions that (i) the vibrational energy in the excited molecule is distributed statistically among all the vibrational degrees of freedom, (ii) the energy flows freely among the different degrees of freedom at a rate much faster than the reaction rate, and (iii) the rate of reaction is controlled by the passage through a transition state located at the dynamical bottleneck separating the reactant from products on the potential energy surface for the reaction. In the region of the transition state, the bound vibrational motions of the molecule are not coupled to the reaction coordinate, and passage through the transition state is vibrationally adiabatic. In this sense, the vibrational levels of the transition state represent reaction thresholds, that is, quantized channels connecting the reactant to products.

*This work was supported by the Director, Office of Energy Research, Office of Basic Energy Sciences, Chemical Sciences Division of the U. S. Department of Energy under Contract No. DE-AC03-76SF00098.

The energy dependence of the RRKM rate constant for a molecule with a fixed energy (E) and total angular momentum (J) is given by

$$k(E,J) = W^{\ddagger}(E,J)/[h\rho(E,J)] \quad (1)$$

where $W^{\ddagger}(E,J)$ is the number of vibrational levels of the transition state with energy less than E, $\rho(E,J)$ is the density of vibrational states of the reactant (number of states per unit energy), and h is Planck's constant.

Definitive tests of RRKM theory are hampered by the difficulty in evaluating the individual terms in Eq. 1. Historically, the density of reactant states [$\rho(E,J)$] has been estimated by extrapolating a normal mode treatment of the molecular vibrations to higher energies. However, recent spectroscopic studies show that the actual densities of states for a number of molecules are significantly higher (five to ten times for 10,000 cm^{-1} < E < 30,000 cm^{-1}) than predicted by the normal mode picture. The number of accessible reaction channels at the transition state [$W^{\ddagger}(E,J)$] is even more difficult to evaluate because of the lack of knowledge of the properties of the short-lived transition state. Generally, the vibrational frequencies of the transition state are estimated by extrapolating from the properties of the stable molecule. However, high-level quantum mechanical calculations now provide quantitative predictions for the properties of transition states of small molecules.

RRKM theory predicts that the rate constant increases by steps with an amplitude equal to $1/[h\rho(E,J)]$ as the energy of the reactant are increased through each vibrational state of the transition state. In the past, experiments have lacked the energy resolution and control of the angular momentum needed to resolve possible transition-state structure in the energy dependence of a rate constant. In this work, rate constants for the unimolecular dissociation of ketene were measured with an energy resolution much finer than the expected vibrational energy spacing at the transition state. The energy dependence of the rate constant exhibits clear steplike structures, Figure 1-1. Analysis of these structures provides a strong test of the basic tenets of unimolecular reaction theory.

A significant fraction (0.22) of the potential energy released as the CH_2 and CO fragments repel each other appears as rotational energy of the CO fragment, consistent with the strongly bent C-C-O geometry of the transition state and rapid release of the energy along the C-C bond. The angular momentum imparted to the CO, J_p, is reproduced very well by a simple classical model that assumes that the available energy is released impulsively along the C-C bond at the transition state. This model predicts only the fraction of energy released to rotation (that is, only one J_p value for CO) and not the distribution of angular momentum. The shapes of the CO rotational distributions are derived from the vibrational motion of the

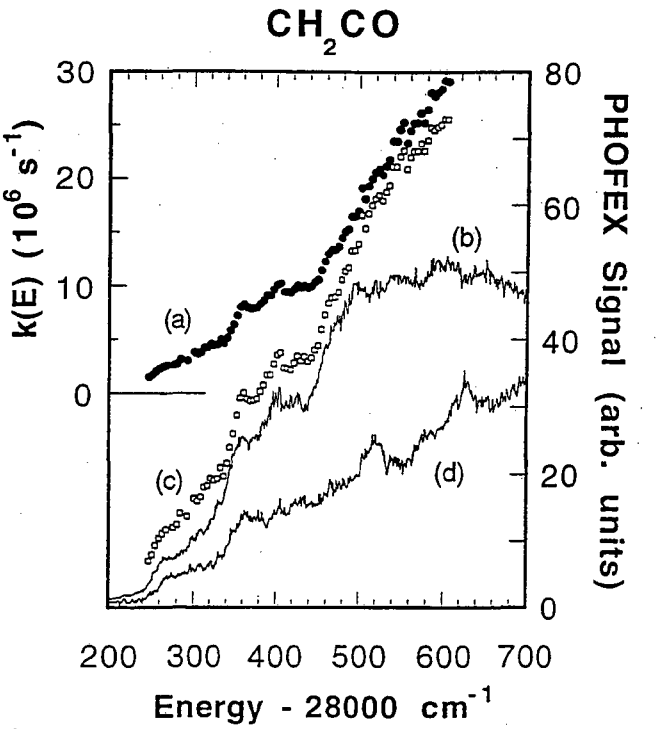

Figure 1-1. CH_2CO dissociation rate constant and PHOFEX data. Curve a, experimental rate constants for the unimolecular decay of ketene. Curve b, CO($v = 0,J_p = 12$) PHOFEX signal. The photofragment excitation spectrum (PHOFEX) is obtained by scanning the excitation laser while monitoring the CO(v,J_p)signal at a time short compared to the inverse reaction rate. Curve c, PHOFEX spectrum calculated from the experimental rate constant data. Curve d, CO($v = 0,J_p = 2$) PHOFEX signal. The actual ratio of the yields of CO($v = 0,J_p = 12$) to CO($v = 0,J_p = 2$) is about 10:1 at 28,500 cm^{-1} for CH_2 CO. (XBL 937-5143)

molecule when the C-C bond breaks. This dynamical model predicts that each vibrational state of the transition state, with its characteristic motion, gives a unique distribution of angular momentum in the products. The variation in the CO(v,J_p) yield with energy is reflected in the PHOFEX spectra. Therefore, these spectra contain detailed information about the vibrational character of the transition-state thresholds.

For example, the CO($v = 0,J_p = 2$) PHOFEX spectrum exhibits two sharp features at about 28,500 and 28,600 cm^{-1} that are absent from the CO($v = 0,J_p = 12$) spectrum but which correlate with the sudden change in slope in the CO($v = 0,J_p = 12$) spectrum. The prominence of these features in the low J_p spectrum indicates that the transition state thresholds at these energies involve atomic motions that enhance the production of CO in low J_p states. The spacing between these features is comparable to the spacing between the first two pronounced steps in the PHOFEX spectra, suggesting that the states are combinations of the lowest energy hindered rotor states with an excited state of

a different vibrational mode. The excited (v = 1) C-C-O bend is a likely assignment for these thresholds because the bending motion adds or subtracts significant angular momentum from the impulsive release and broadens the CO J_p distribution. The broadening increases the yield of low J_p products and decreases the yield of J_p states near the maximum of the distribution ($J_p \approx 12$). This assignment gives a C-C-O bending energy of 250 ± 10 cm^{-1} at the transition state, which agrees very well with the *ab initio* value of 252 cm^{-1}.

The observation of steps in the rate constant supports the concept that the rate of a unimolecular reaction with a well-defined barrier (and hence transition state) is controlled by flux through quantized transition-state thresholds. The comparison of experimental and *ab initio* data given here demonstrates that many properties of the transition state are predicted by theory.

2. Transition States and Rate Constants for Unimolecular Reactions (Publication 2)

W.H. Green, Jr., C.B. Moore, and W.F. Polik

This review concentrates on the interpretation of recent experiments performed near reaction thresholds and on the potential surfaces and dynamical models necessary for their interpretation. The first section addresses reactions with barriers. First tunneling and the structure in $k(E,J)$ caused by the discrete nature of the level count $W(E,J)$ are discussed. Then the stepped structure revealed in the dissociation of ketene over a small barrier to triplet methylene and carbon monoxide is described. The quantum statistics of the dissociation rates for formaldehyde are described, along with their quantitative interpretation derived from the *ab initio* PES. The following section, on bond breaking without barriers, concentrates on the dissociation of ketene to singlet methylene and carbon monoxide and of NCNO to NC and NO. These and other data provide stringent tests for PST, variational RRKM, and other theoretical models. In the final section of this review, some limitations of the energy randomization hypothesis of statistical unimolecular reaction rate theories are discussed.

3. Work in Progress

Unimolecular reaction studies on triplet ketene are being initiated with full rotational state resolution in the initial excitation. An IR optical parametric oscillator is being set up to select a single excited rovibrational state that will then be further excited to the reaction threshold by a UV laser pulse. The carbon atom isotopic exchange reaction rate is being measured with wavenumber resolution. Sharply peaked structures in the reaction threshold region are being interpreted in terms of vibrational resonances for motion along the reaction coordinate. Quantitative theoretical analysis of these resonances with a multidimensional reaction coordinate is being carried out by William Miller's group. Ultimately these resonances will need to be studied with complete rotational resolution.

The B-state of hydrogen is being produced by tunable vacuum UV laser excitation. Experiments are being set up using a monochromator to disperse fluorescence and study collision-induced vibration-rotation energy transfers as a function of initial quantum state. Future studies are planned using a second vacuum UV laser to probe the velocity distribution of H-atom fragments from collision-induced electronic curve crossing. William Lester's group is carrying out *ab initio* theoretical work on these systems.

Energy transfer and chemical reaction rates are being studied for triplet CH_2 radicals. An infrared diode laser flash kinetic spectrometer is being used to study the reaction with O_2 in order to identify product states and intermediates. Reaction rates for radical-radical reactions are being measured. Infrared and ultraviolet spectra of intermediates in organometallic photochemistry in gas and liquid phase are being studied jointly with R.G. Bergman. Emphasis is on CH activation chemistry. Studies of CH activation systems in liquid Kr and Xe are proceeding well.

FY 1992 PUBLICATIONS AND REPORTS

Refereed Journals

1. E.R. Lovejoy, S.K. Kim, and C.B. Moore, "Observation of Transition-State Vibrational Thresholds in the Rate of Dissociation of Ketene," Science **256**, 1541 (1992); LBL-31911.
2. W.H. Green, Jr., C.B. Moore, and W.F. Polik, "Transition States and Rate Constants for Unimolecular Reactions," Ann. Rev. Phys. Chem. **43**, 591 (1992); LBL-33472.

Other Publications

3. C.B. Moore, Chair, Energy Engineering Board, Commission on Engineering and Technical Systems, National Research

Council, "Alternative Applications of Atomic Vapor Laser Isotope Separation Technology," National Academy Press, Washington, DC (1991).

LBL Reports

4. C.D. Pibel, (Ph.D. Thesis), "Reaction and Reorientation of Electronically Excited $H_2(B)$"; LBL-33473.
5. I. Garcia-Moreno, E.R. Lovejoy, C.B. Moore and G. Duxbury, "Radiative Lifetimes of $CH_2(\tilde{b}\,^1B_1)$," J. Chem. Phys. (in press); LBL-33086.
6. E.R. Lovejoy and C.B. Moore, "Structures in the Energy Dependence of the Rate Constant for Ketene Isomerization," J. Chem. Phys. (submitted); LBL-33087.

Invited Talks

7. C.B. Moore, "A Spectroscopic View of Transition States in Unimolecular Reactions," Department of Chemistry, Princeton University, November 15, 1991.
8. C.B. Moore, "Structure and Dynamics at the Transition State for Chemical Bond Breaking," IBM Almaden Research Center, San Jose, CA, March 20, 1992
9. C.B. Moore, "A Spectroscopic View of Not-So-Loose Transition States," American Chemical Society Spring Meeting, San Francisco, CA, April 7, 1992.
10. E.R. Lovejoy, "Observation of Transition State Vibrational Thresholds in the Rate of Dissociation of Ketene," XIVth International Symposium on Molecular Beams, Asilomar, CA, June 10, 1992.

Photodissociation of Free Radicals*

Daniel M. Neumark, Investigator

INTRODUCTION

While many photodissociation studies of stable molecules have been performed in recent years, it has proved difficult to extend these experiments to studies of reactive free radicals. This is largely due to the difficulty of implementing a clean, well-characterized source of free radicals. We have developed a novel approach to this problem by setting up an experiment in which free radicals are generated by photodetachment of a mass-selected anion beam, rather than the more conventional strategies in which radicals are formed by photolysis of a stable precursor or by a chemical reaction. Since nearly all radicals have a positive electron affinity, this approach should be quite general.

In the experiment, an 8-keV beam of cold mass-selected anions is photodetached with a pulser laser. The resulting neutral radicals are photodissociated with a second pulsed laser, and the photofragments are detected with high (~50%) efficiency using a microchannel plate detector that lies about 100 cm downstream from the photodissociation laser. The center of the detector is blocked so that the undissociated radicals do not impinge on it, but the photofragments move off the beam axis and strike the detector. The experiment can be operated in several modes. We can measure the total photofragment signal as a function of dissociation laser wavelength, thereby mapping out the dissociative electronic transitions of the radical. We can measure the time-of-flight distribution of the photofragments, thereby obtaining an approximated kinetic energy distribution at a fixed photodissociation wavelength. Finally, using a two-particle position and time sensing detector, we can determine detailed photofragment energy and angular distributions.

*This work was supported by the Director, Office of Energy Research, Office of Basic Energy Sciences, Chemical Sciences Division of the U.S. Department of Energy under Contract No. DE-AC03-76SF00098.

1. Adiabatic Three-Dimensional Simulations of the IHI^-, $BrHI^-$ and $BrHBr^-$ Photoelectron Spectra (Publication 3)†

R.B. Metz‡ and D.M. Neumark

In order to better characterize the transition state region for the I + HI, Br + HI, and Br + HBr reactions, the photoelectron spectra of IHI^-, IDI^-, $BrHI^-$, $BrHBr^-$, and $BrDBr^-$ have been simulated using a three-dimensional adiabatic approach. This method of simulation uses a Born-Oppenheimer separation in timescales between the fast hydrogen atom motion and the sloe halogen atom motion to greatly simplify the computational of the photoelectron spectrum. The resulting simulations are compared to the experimental photoelectron and threshold photodetachment spectra of these anions, and to "exact" simulations of the IHI^- and IDI^- spectra. The comparison with the exact simulations shows that the adiabatic method is reasonably accurate and is a considerable improvement over previous approximate simulation schemes. Potential energy surfaces for the I + HI and Br + HI reactions are evaluated based on a comparison between the simulated and experimental spectra. A three-dimensional surface for the Br + HBr reaction that reproduces the experimental photoelectron spectrum is constructed by extending a fitted collinear surface to three dimensions.

†This work is also supported in part by the Air Force Office of Scientific Research under Grant No. AFOSR-910084.

‡Department of Chemistry, University of Wisconsin, Madison, Wisconsin 53706.

2. Fast Beam Studies of NCO Free Radical Photodissociation (Publication 5)†

D.R. Cyr, R.E. Continetti,‡ R.B. Metz,§ D.L. Osborn, and D.M. Neumark

The spectroscopy and dissociation dynamics of the NCO radical have been investigated by applying fast radical beam photodissociation spectroscopy to the $B^2\Pi \leftarrow X^2\Pi$ electronic transition. Measurements of the photodissociation cross section as a function of dissociation wavelength show that even the lowest vibrational level of the $B^2\Pi$ state predissociate. Analysis of fragment kinetic energy release reveals that the spin-forbidden $N(^4S)$ + $CO(^1\Sigma^+)$ products are produced exclusively until 20.3 kcal/mol above the origin, at which point the spin-allowed $N(^2D)$ + CO product channel becomes energetically accessible. The spin-allowed channel dominates above this threshold. By determining the location of this threshold we

obtain a new $\Delta H_f°$ for NCO of 30.5 ± 1 kcal/mol, several kcal/mol lower than the previously accepted value.

†This work is also supported in part by the National Science Foundation, Grant CHE-9108145.
‡Department of Chemistry, University of California. San Diego, La Jolla, CA 92093-0314.
§Department of Chemistry, University of Wisconsin, Madison, Wisconsin 53706.

3. Photodissociation Dynamics of the N_3 Radical (Publication 8)†

R. E. Continetti,‡ D. R. Cyr, D. L. Osborn, and D. M. Neumark

The dissociation dynamics of the $B^2\Sigma_u^+$ excited state of N_3 was investigated using fast radical beam photodissociation coupled with a new coincidence wedge-and-strip-anode particle detector. With this detector, detailed photofragment kinetic energy and angular distributions can be measured as a function of excitation energy. The design of the detector is discussed, along with its calibration using predissociation of the $O_2B^3\Sigma_u^-$ state. The results for N_3 show that both spin-allowed ($N_3 \rightarrow N(^2D) + N_2(^1\Sigma_g^+)$) and spin-forbidden ($N_3 \rightarrow N(^4S) + N_2(^1\Sigma_g^+)$) dissociation processes occur from the vibrationless level of the $B^2\Sigma_u^+$ state in N_3. Bend excitation in the $B^2\Sigma_u^+$ state, however, enhances the spin-allowed dissociation process considerably. The implications of these results for the predissociation mechanism are discussed.

†This work is also supported in part by the National Science Foundation, Grant CHE9108145.
‡Department of Chemistry, University of California. San Diego, La Jolla, CA 92093-0314.

4. Work in Progress

We are now engaged in detailed investigations of photodissociation dynamics with our two-particle position and time sensing detector. We have recently examined predissociation of O_2 subsequent to excitation to the $B^3\Sigma_u^-$ state, and have found the resolution of this detector sufficient to observe individual fine structure components of the two O ^3P atoms. We are also studying the ultraviolet photodissociation dynamics of the CH_2NO_2 radical. We find that two channels occur: NO bond fission, to give CH_2NO + O, and a rearrangement/elimination channel, to give CH_2O + NO. These results are in sharp contrast to the UV photodissociation of nitromethane (CH_3NO_2), which undergoes CN bond fission to form CH_3 + NO_2. Hence, our results suggest that the dissociation dynamics of radicals may be qualitatively different from the analogous closed shell molecules.

FY 1992 PUBLICATIONS AND REPORTS

Refereed Journals

1. R.B. Metz, S.E. Bradforth, and D.M. Neumark, "Transition State Spectroscopy of Bimolecular Reactions Using Negative Ion Photodetachment," Adv. Chem. Phys. **81**,1(1992).
2. R.E. Continetti, D.R. Cyr, and D.M. Neumark, "Fast 8 kV MOSFET Switch," Rev. Sci. Instrum. **63**, 1840 (1992).
3. R.B. Metz and D.M. Neumark, "Adiabatic Three-Dimensional Simulations of the IHI^-, $BrHI^-$ and $BrHBr^-$ Photoelectron Spectra," J. Chem. Phys. **97**, 962 (1992); LBL-31880.
4. D.M. Neumark, "Transition State Spectroscopy of Bimolecular Chemical Reactions," Ann. Rev. Phys. Chem. **43**, 153 (1992).
5. D.R. Cyr, R.E. Continetti, R.B. Metz, D.L. Osborn, and D.M. Neumark, "Fast Beam Studies of NCO Free Radical Photodissociation," J. Chem. Phys. **97**, 4937 (1992); LBL-32365.
6. C.C. Arnold, Y. Zhao, and D.M. Neumark, "Study of C_6^- and C_6 with Threshold Photodetachment Spectroscopy and Autodetachment Spectroscopy," J. Chem. Phys. **97**, 6121(1992).
7. D.W. Arnold, S.E. Bradforth, E.H. Kim, and D.M. Neumark, "Anion Photoelectron Spectroscopy of Iodine-Carbon Dioxide Clusters." J. Chem. Phys. **97**, 9468 (1992).

LBL Reports

8. R.E. Continetti, D. R. Cyr, D. L. Osborn, and D. M. Neumark, "Photodissociation Dynamics of the N_3 Radical," J. Chem. Phys. (in press); LBL-33584.
9. T.N. Kitsopoulos (Ph.D. Thesis), "Threshold Photodetachment Spectroscopy of Negative Ions"; LBL-31876.
10. A. Weaver, (Ph.D. Thesis), "Spectroscopy of Transient Neutral Species via Negative Ion Photoelectron Spectroscopy"; LBL-31877.
11. R.B. Metz, (Ph.D. Thesis), "Studies of Transition States and Radicals by Negative Ion Photodetachment"; LBL-31878.

Invited Talks

12. D.M. Neumark, "Studies of Transient Species Using Negative Ion Photodetachment," University of California, Davis, October 1991.

13. D.M. Neumark, "Studies of Transient Species Using Negative Ion Photodetachment," U.S.-Japan Workshop for Young Investigators, Institute for Molecular Science, Okazaki, Japan, October 1991.
14. D.M. Neumark, "Studies of Transient Species Using Negative Ion Photodetachment," IBM Almaden, November 1991.
15. D.M. Neumark, "Studies of Transient Species Using Negative Ion Photodetachment," University of Southern California, November 1991.
16. D.M. Neumark, "Studies of Transient Species Using Negative Ion Photodetachment," University of Florida, Gainesville, December 1991.
17. D.M. Neumark, "Fast Beam Studies of Free Radical Photo Dissociation," American Chemical Society, San Francisco, CA, April 1992.
18. D.M. Neumark, "Fast Beam Studies of Free Radical Photo Dissociation," XIVth International Symposium on Molecular Beams, Pacific Grove, CA, June 1992.
19. D.M. Neumark, "Studies of Clusters with Negative Ion Photodetachment," Gordon Research Conference on Electron Spectroscopy, Wolfboro, NH, August 1992.
20. D.M. Neumark, "Photodissociation of Free Radicals," Optical Society of America Interdisciplinary Laser Science Conference, Albuquerque, NM, September 1992.

Physical Chemistry with Emphasis on Thermodynamic Properties*

Kenneth S. Pitzer, Investigator

INTRODUCTION

The purpose of this program is the discovery and development of methods of calculation of thermodynamic and related properties of important chemical systems by the use of quantum and statistical mechanics together with experimental measurements for key systems. Current emphasis is on fluid systems that include ionic or strongly dipolar components in novel ranges of conditions, including near-critical and supercritical temperatures and compositions extending from pure water or other polar solvent to pure fused salt. Reported in article 1 below is a comprehensive equation of state for the system NaCl-H_2O that is very important geologically and industrially and very complex theoretically. A recent study concerned a novel ionic system with a critical point near room temperature where it was possible to measure with high precision the near-critical properties including the critical exponent β. Earlier advances yielded improved equations for electrolyte solutions that are now being applied to a wide variety of systems of industrial or geological interest, including geothermal brines. Other recent research involved the development of a feasible method of relativistic quantum mechanical calculation for molecules containing very heavy atoms and its application to important examples. This method is now in wide use.

1. Equation-of-State Representation of Phase Equilibria and Volumetric Properties of the System NaCl-H_2O Above 573 K (Publication 10)

A. Anderko and K.S. Pitzer

A comprehensive equation of state has been developed for the system NaCl-H_2O at high temperatures and pressures. The equation consists of a reference part and a perturbation contribution. The reference part represents the properties of a mixture of hard-sphere ion pairs and dipolar solvent molecules and uses recent statistical mechanical

*This work was supported by the Director, Office of Energy Research, Office of Basic Energy Sciences, Chemical Sciences Division, of the U. S. Department of Energy under Contract No. DE-AC03-76SF00098.

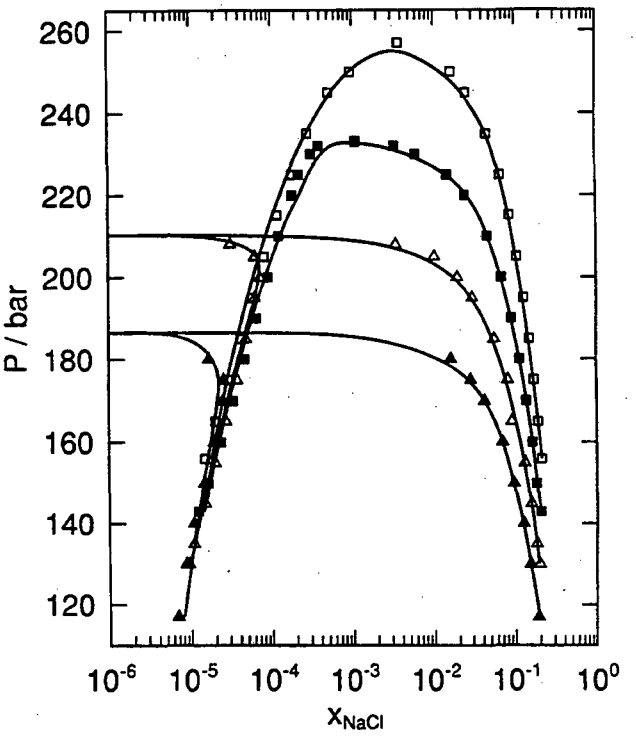

Figure 1-1. Comparison of vapor-liquid equilibria calculated from the equation of state (lines) with previously published smoothed experimental data at T = 633.15 K (▲), 643.15 K (△), 653.15 K (■), and 663.15 K (□). (XBL 937-5139)

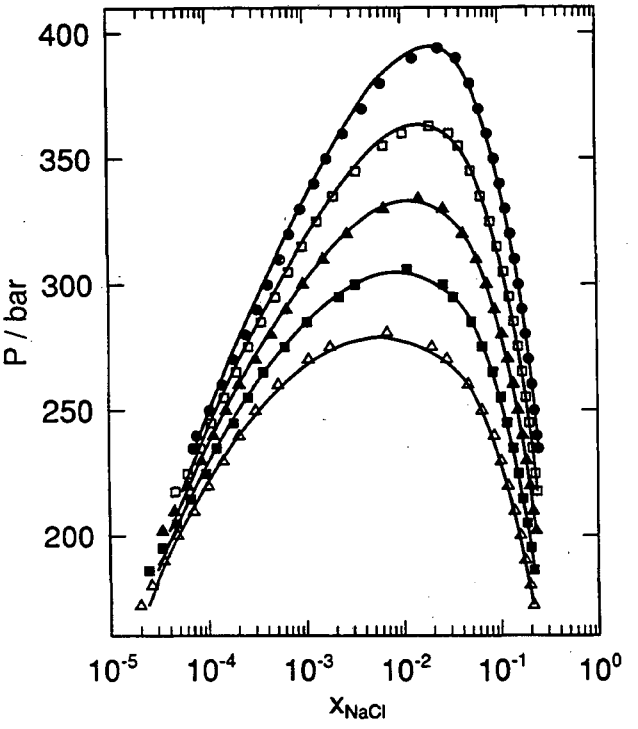

Figure 1-2. Comparison of vapor-liquid equilibria calculated from the equation of state (lines) with the smoothed experimental data at T = 673.15 K (△), 683.15 K (■), 693.15 K (▲), 703.15 K (□) and 713.15 K (●). (XBL 937-5140)

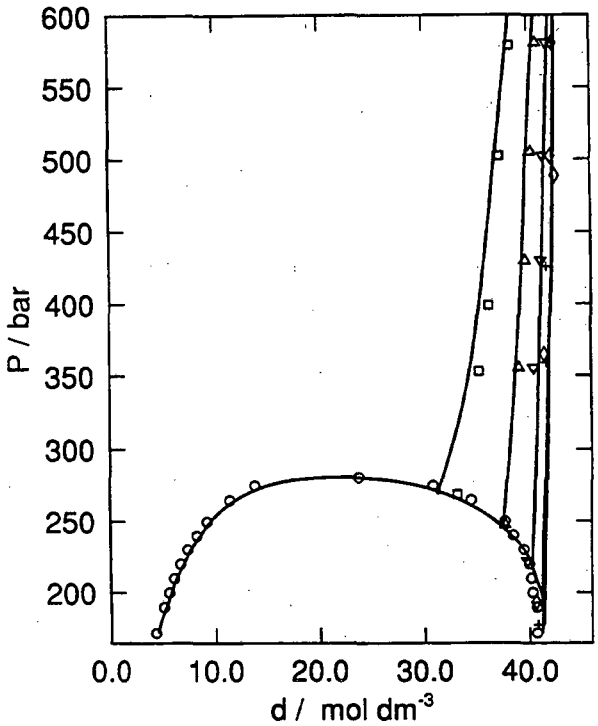

Figure 1-3. Comparison of vapor and liquid densities at T = 673.15 K calculated from the equation of state (lines) with experimental data. The circles (O) denote the saturated densities, while experimental densities in the one-phase region are shown for X_{NaCl} = 0.0331 (□), 0.0715 (△), 0.117 (▽), 0.171 (◇) and 0.201 (+). (XBL 937-5141)

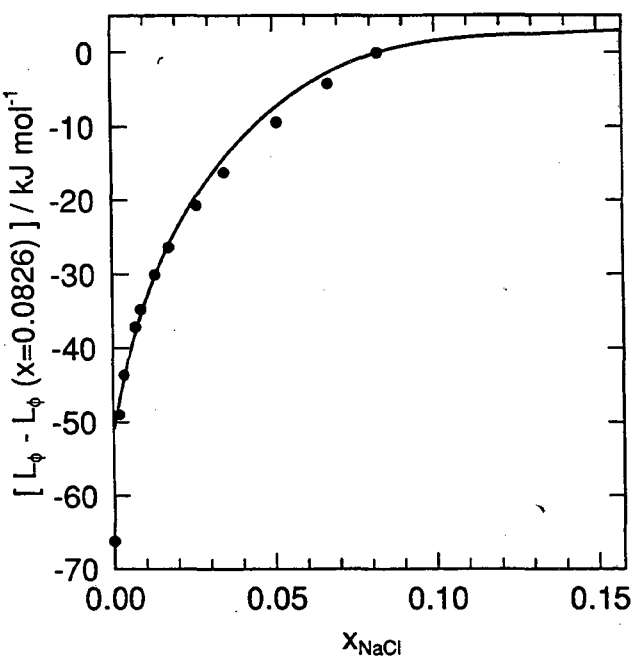

Figure 1-4. Apparent molar enthalpy of the NaCl in H_2O at 573.15 K. Shown is the value at composition X_{NaCl} relative to that with X_{NaCl} = 0.0826 with the calculated curve from the equation of state compared with circles from heat of dilution measurements. (XBL 937-5142)

theory for such systems. The perturbation part arises from all other interactions and comprises a virial-type expansion truncated after the fifth virial coefficient. Mixing rules for the perturbation part are guided by the theoretical composition dependence of virial coefficients and contain empirically determined terms for unlike-molecule interactions. The equation has been fitted to extensive experimental data in the temperature range 573–773 K and to more limited data above 773 K. In both temperature regions, the equation reproduces vapor-liquid equilibria, volumetric properties and solubilities of solid NaCl essentially within experimental uncertainty. It is valid at temperatures between 573 K and ~1200 K and pressures up to 5 kbar. Figures 1-1 to 1-4 show examples of the excellent agreement with various types of experimental data, even in the very sensitive region near the critical point.

2. Equation of State for Pure Sodium Chloride (Publication 2)

A. Anderko and K.S. Pitzer

An equation of state for pure sodium chloride has been developed on the basis of experimental data and results of Monte Carlo simulations for the restricted primitive model (RPM). The experimental database included limited vapor pressure and saturated liquid density data as well as dimerization equilibrium constants. The liquid densities have been extrapolated to the supercooled region using liquid-phase Monte Carlo data. For this purpose, the parameters of the primitive model have been calculated by assuming that sodium chloride and RPM obey the corresponding states principle over a limited range of conditions. In the near-critical region Monte Carlo data as well as results of cluster calculations have been used with parameters scaled to reproduce the critical temperature obtained by extrapolating saturation data. The RPM parameters employed in the calculations are close to those for crystalline NaCl. The experimental and scaled Monte Carlo data have been reproduced within their accuracy using a van der Waals-type equation of state with two temperature-dependent parameters a and b. The functions representing the temperature dependence of the parameters have been designed to ensure reliable extrapolation to lower and higher temperatures. Formation of Na_2Cl_2 clusters has been allowed for by using a closed-form term representing the effect of association on the compressibility factor. The performance of the equation has been additionally verified by predicting compressibility factors at low reduced temperatures outside the saturation region and comparing them with scaled Monte Carlo data.

3. Phase Equilibria in Mixtures Containing Hydrogen Fluoride and Halocarbons from an Equation of State Based on the Chemical Theory (Publication 11)

M. Lencka[†] and A. Anderko

Recently, much attention has been focused on the production of environmentally acceptable refrigerants that, in addition to desirable physico-chemical properties, do not deplete the ozone layer and do not cause the greenhouse effect. The production of such refrigerants involves the separation of multicomponent mixtures containing hydrogen fluoride, hydrogen chloride and various chlorinated and fluorinated hydrocarbons. Therefore, it is indispensable to know the phase behavior of these mixtures. While the phase behavior of refrigerant mixtures can be adequately modeled in the absence of HF using standard thermodynamic techniques, hydrogen fluoride drastically increases the complexity of the mixture because of its unusually strong association. The association of HF manifests itself in its significantly reduced gas-phase compressibility factor and the strong nonideality of mixtures containing HF and hydrocarbons or halocarbons.

This work presents an accurate yet simple association model for hydrogen fluoride and compares it with simulation data. The model is combined with a simple equation of state to yield a closed-form expression that is applicable to both pure fluids and mixtures. In addition to representing the pure-component data for HF, the theory accurately predicts phase equilibria in HF + halocarbon systems.

[†]Department of Ceramics, Rutgers University, PO Box 909, Piscataway, NJ 08855-0909.

4. Work in Progress

Extension of project 1 reported above from the binary $NaCl-H_2O$ to $KCl-H_2O$ and to the ternary system $NaCl-KCl-H_2O$ is nearly complete. The theoretically based reference function involves the collision diameters and dipole moments of each species and extends directly to three components. Additional parameters appear only for the perturbation function, and these are small and can be evaluated from the relatively limited experimental information for the ternary. This general formulation has promise for extension to other important systems for which only purely empirical treatments with no predictive power are now available.

FY 1992 PUBLICATIONS AND REPORTS

Refereed Journals

1. K.S. Pitzer and R.R. Singh, "Reply to Comment on: Rectilinear Diameters and Extended Corresponding States Theory," J. Chem. Phys. **95**, 9426 (1991); LBL-30585.
2. A. Anderko and K.S. Pitzer, "Equation of State for Pure Sodium Chloride," Fluid Phase Equilibria **79**, 103 (1992); LBL-30861.
3. K.S. Pitzer, A. Anderko, and S.M. Sterner, "Virial coefficients and Equations of State for Mixed Fluids; Application to CH_4-H_2O," Fluid Phase Equilibria **79**, 125 (1992); LBL-30899.
4. I.-M. Chou, S.M. Sterner, and K.S. Pitzer, "Phase Relations in the System $NaCl-KCl-H_2O$: IV. Differential Thermal Analysis of the Sylvite Liquidus in the $KCl-H_2O$ Binary, the Liquidus in the $NaCl-KCl-H_2O$ Ternary, and the Solidus in the NaCl-KCl Binary to 2 Kilobars Pressure, and a Summary of Experimental Data for Thermodynamic-PTX Analysis of Solid-Liquid Equilibria at Elevated P-T Conditions," Geochim. et Cosmochim. Acta **56**, 2281 (1992); LBL-31058.[†]
5. S.M. Sterner, I-M. Chou, R.T. Downs, and K.S. Pitzer, "Phase Relations in the System $NaCl-KCl-H_2O$: V. Thermodynamic-PTX Analysis of Solid-Liquid Equilibria at High Temperatures and Pressures," Geochim. et Cosmochim. Acta **56**, 2295 (1992); LBL-31059.[†]
6. S.L. Clegg and K.S. Pitzer, "Thermodynamics of Multicomponent, Miscible, Ionic Solutions: Generalized Equations for Symmetrical Electrolytes," J. Phys. Chem. **96**, 3513 (1992).
7. S.L. Clegg, K.S. Pitzer, and P. Brimblecombe, "Thermodynamics of Multicomponent, Miscible, Ionic Solutions. 2. Mixtures Including Unsymmetrical Electrolytes," J. Phys. Chem. **96**, 9470 (1992).

Other Publications

8. K.S. Pitzer, "Ion Interaction Approach: Theory and Data Correlation," Chap. 3 in Activity Coefficients in Electrolyte Solutions, 2nd Edition, K.S. Pitzer, Ed. (CRC Press, Boca Raton, Florida, 1991).
9. R.T. Pabalan and K.S. Pitzer, "Mineral Solubilities in Electrolyte Solutions," Chap. 7 in Activity Coefficients in Electrolyte Solutions, 2nd Edition, K.S. Pitzer, Ed. (CRC Press, Boca Raton, Florida, 1991).

LBL Reports

10. A. Anderko and K.S. Pitzer, "Equation-of-state Representation of Phase Equilibria and Volumetric Properties of the System $NaCl-H_2O$ above 573 K," Geochim. et Cosmochim. Acta (in press); LBL-32429.

11. M. Lencka and A. Anderko, "Phase Equilibria in Mixtures Containing Hydrogen Fluoride and Halocarbons from an Equation of State Based on the Chemical Theory," AIChE J. (in press); LBL-32434.
12. R.N. Roy, K.M. Vogel, C.E. Good, W.B. Davis, L.N. Roy, D.A. Johnson, A.R. Felmy, and K.S. Pitzer, "Activity Coefficients in Electrolyte Mixtures HCl + $ThCl_4$ + H_2O for 5° to 55°C," J. Phys. Chem. (in press); LBL-32731.†

†This work was supported by the Director, Office of Energy Research, Office of Basic Energy Sciences, Division of Engineering and Geosciences, of the U.S. Department of Energy under Contract No. DE-AC03-76SF00098.

Invited Talk

13. S.L. Clegg and K.S. Pitzer, "Multicomponent Ionic Solutions of Extended Solubility or Complete Miscibility: Equations and Applications," 12th IUPAC Conference on Chemical Thermodynamics/47th Calorimetry Conf., Snowbird, Utah, Aug. 16-21, 1992.

Chemical Physics at High Photon Energies*

David A. Shirley, Principal Investigator

INTRODUCTION

This program addresses both experimental and theoretical aspects of electron spectroscopy for the investigation of electronic structure of matter in the gaseous and condensed phases. Research is conducted using both laboratory sources at LBL and synchrotron radiation in the 5–5000 eV energy range available at SSRL and NSLS. The completion of the Advanced Light Source (ALS) and moving of the BL6-1 from SSRL to the ALS will allow us to carry out most of the experiments at LBL. A considerable effort is placed in developing the high-resolution spectroscopy in the 20–1500 eV energy range by using both modified toroidal grating monochromator (TGM) and spherical grating monochromators at SSRL. Effects are emphasized that can be refined and extended with the advent of third-generation light sources: e.g., threshold and near-edge photoexcitation phenomena, very fast processes, and processes requiring very high intensity and energy resolution. Electron correlations in atoms and molecules are studied, especially in the adiabatic (low-energy) limit, where the electronic structure of the continuum is important. Time-of-flight measurements with synchrotron radiation are used to measure angular distributions of photoelectrons and resonant photoemission phenomena in the gas phase. Of special interest are ultrahigh resolution absorption and threshold photoemission studies. Ultrahigh resolution photoelectron spectroscopy based on molecular beams is yielding new information about small molecules and about the transition from single-metal atoms to behavior characteristic of a three-dimensional solid. Employing angle-resolved, variable-energy photoemission, this program examines the electronic structure of solids. The program also studies the geometric and electronic structure of surface-adsorbate systems using photoelectron diffraction, angle-resolved photoemission extended fine structure (ARPEFS).

*This work was supported by the Director, Office of Energy Research, Office of Basic Energy Sciences, Chemical Sciences Division of the U.S. Department of Energy under Contract No. DE-AC03-76SF00098. It was performed at the National Synchrotron Light Source and Stanford Synchrotron Radiation Laboratory, which are supported by the Department of Energy's Office of Basic Energy Sciences.

1. High-Resolution K-Shell Photoabsorption in Formaldehyde (Publication 2)

G. Remmers, M. Domke, A. Puschmann, T. Mandel, C. Xue, G. Kaindl, E. Hudson, and D.A. Shirley

Inner-shell soft-x-ray absorption of formaldehyde, H_2CO, in the region of the C K and O K absorption thresholds was studied with high-energy resolution using synchrotron radiation from the SX700/II monochromator at BESSY. The absorption spectra were recorded via the total photocurrent yield. The C1s-excitation spectrum is characterized by a dominant C $1s^{-1}\,\pi^*$ resonance and weaker transitions into Rydberg states (see Figure 1-1), each exhibiting vibrational fine structure that is quantitatively analyzed in terms of the normal vibrational

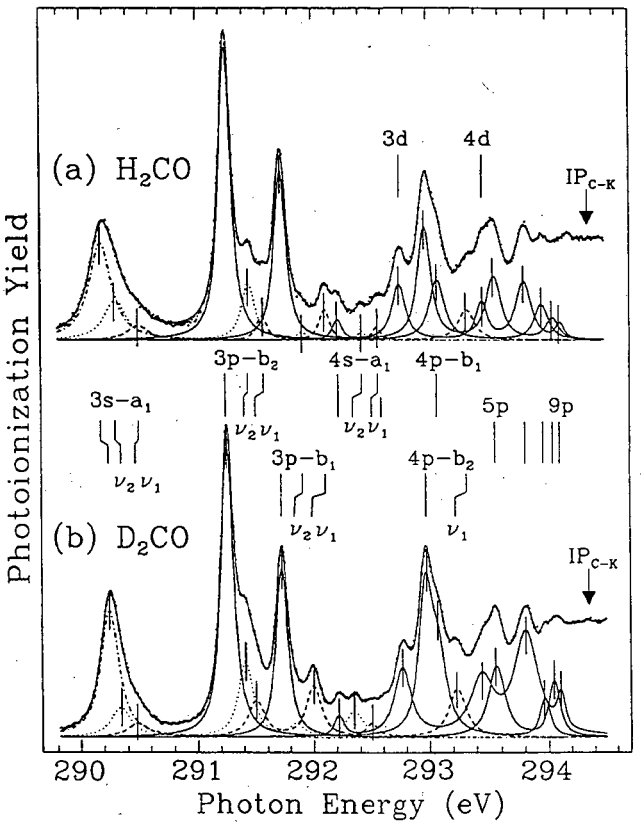

Figure 1-1. Rydberg states below the C K threshold in (a) H_2CO and (b) D_2CO. The solid lines through the data points represent the results of least-squares fits with Lorentzians convoluted by a Gaussian for instrumental resolution. The component peaks are given by solid lines if their energy positions are not changed by isotopic replacement (representing transitions to the ground vibrational level of Rydberg states). Dotted and dashed lines are used for vibrationally excited ν_2 and ν_1 modes, respectively, which exhibit decreases in vibrational energies upon replacement of H by D. The dashed-dotted component represents the ground vibrational level of the $3s–a_1$ state that exhibits a strong isotropic effect (see the text). (XBL 937-5144)

modes of H_2CO. Isotopic effects on the vibrational modes were studied by taking analogous spectra of D_2CO. A Franck-Condon analysis of the vibrationally split spectra yields equilibrium distances, molecular bond angles, and vibrational frequencies of C $1s^{-1}$-excited formaldehyde, which show strong isotopic effects. In addition, the ground vibrational level of the lowest Rydberg state (C $1s^{-1}3s$–a_1) exhibits a pronounced shift to higher excitation energies upon replacement of H by D. This shift, as well as a considerable isotope-dependent line broadening, are presumably caused by perturbations of this state by valence orbitals. Analogous isotopic effects were observed for the O $1s^{-1}3s$–a^1 Rydberg state.

2. High-Resolution He Iα Photoelectron Spectroscopy of H_2CO and D_2CO Using Supersonic Molecular Beams (Publication 4)

B. Niu, D.A. Shirley, Y. Bai, and E. Daymo

High-resolution helium Iα (584 Å) photoelectron spectra of H_2CO and D_2CO using supersonic molecular beams are reported. The excitation of the V_4 out-of-plane bending mode in the ionic ground state and the first excited state imply that formaldehyde cations in these states might have nonplanar equilibrium geometries. The different vibrational progressions observed in the first and second excited states indicate strong isotope effects on vibrational (vibronic) couplings. The AIEs and spectroscopic constants for all four ionic states are reported to a much higher accuracy than previously available.

3. High-Resolution He Iα Photoelectron Spectroscopy of H_2CCO and D_2CCO Using Supersonic Molecular Beams (Publication 5)

B. Niu, Y. Bai, and D.A. Shirley

High-resolution helium Iα (584 Å) photoelectron spectra of H_2CCO and D_2CCO using supersonic molecular beams are reported. The adiabatic ionization energies (AIEs) of the electronic first, second, and fifth excited states are determined unambiguously. The doublet-like fine structures observed in the first excited states of ketene imply the excitation of a "soft" mode that was not observed before. Strong isotope effects are observed in the vibronic (vibrational) couplings in the ground state of ketene cations. The ionic states are reported to a much higher accuracy than previously available.

4. Multiple-Scattering Enhances Depth Sensitivity of Angle-Resolved Photoemission Fine Structure (Publication 6)

Y. Zheng and D.A. Shirley

We show by analysis of experimental results that, in the structural study of adsorbed surfaces, the angle-resolved photoemission extended fine structure (ARPEFS) technique has a strong depth sensitivity that can yield unique information about adsorbate-induced substrate near-surface relaxation. Furthermore, we show by theoretical calculations that, in contrast to the generally accepted picture, the enhanced depth sensitivity of ARPEFS arises largely from multiple-scattering effects.

5. High-Resolution Measurements of Near-Edge Resonances in the Core-Level Photoionization Spectra of SF_6 (Publication 7)

E. Hudson, D.A. Shirley, M. Domke, G. Remmers, A. Puschmann, T. Mandel, C. Xue, and G. Kaindl

The X-Ray Absorption Near Edge Structure (XANES) of sulfur hexafluoride, SF_6, in the gas phase has been measured with high-energy resolution at the sulfur $L_{2,3}$ and fluorine K ionization thresholds using synchrotron radiation from the SX700/II monochromator at BESSY. Besides dominant transitions to core-excited inner-well states, several series of Rydberg states with vibrational fine structure were resolved below the sulfur $L_{2,3}$ thresholds (see Figure 5-1). Using the Rydberg formula, quantum defects of $\delta_s = 1.80$ and $\delta_d = -0.03$ were obtained for the s and d Rydberg orbitals of the central sulfur atom. A Franck-Condon analysis was used to determine the vibrational spacing and the S-F bond length of the $(S\ 2p_{3/2})^{-1}\ 4s^1$ core-excited state. The presence of vibronically-coupled transitions below the sulfur $L_{2,3}$ edges was confirmed. The derived natural linewidths of the $(S\ 2p_{1/2,3/2})^{-1}$ Rydberg states were found to be strikingly narrower than those of the $(S\ 2p_{1/2,3/2})^{-1}$ inner-well resonances. Lineshape analysis also revealed significant inhomogeneous broadening of the $(S\ 2p_{1/2,3/2})^{-1}\ a_{1g}^1$ states, which is attributed to unresolved vibrational structure. Large Lorentzian contributions to the lineshapes of the $(S\ 2p_{1/2,3/2})^{-1}\ t_{2g}^1$ resonances suggest that vibrational effects are relatively small for those states.

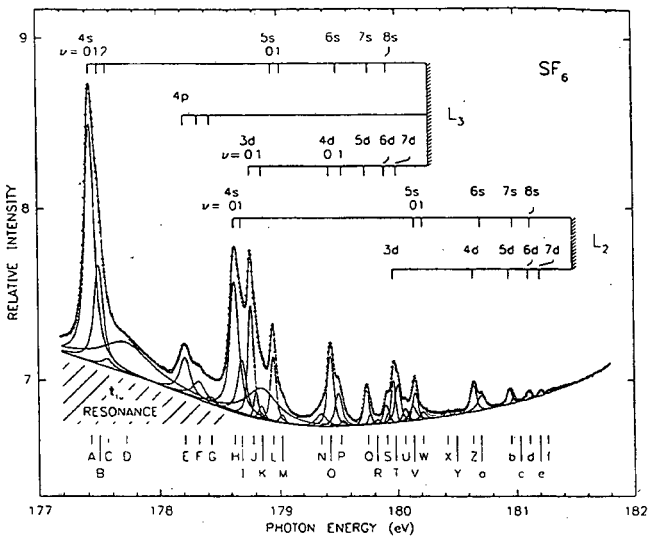

Figure 5-1. Sulfur $L_{2,3}$ pre-edge fine structure of the SF_6 photoabsorption spectrum. The shaded area indicates the contribution of the $(S\ 2p_{1/2,3/2})^{-1}t_{1u}{}^{1}$ transitions to the overall background. The line through the data points is the result of a least-squares fit. For the fit, the background was modeled by a linear contribution, the tail of a Voigt function, and several overlapping Gaussian peaks to represent the $(S\ 2p_{1/2,3/2})^{-1}t_{1u}{}^{1}$ transitions. Each of the individual component peaks is a Voigt function. The data in this figure were measured using the 2442 line/mm grating. (XBL 937-5145)

6. Structural Determination of p2mg(2×1)CO/Ni(110) Using Angle-Resolved Photoemission Extended Fine Structure (Publication 8)

Z.Q. Huang, Z. Hussain, W.T. Huff, E.J. Moler, and D.A. Shirley

The technique of angle-resolved photoemission extended fine structure has been used to study the chemisorption geometry of the dense p2mg(2×1)CO/Ni(110) overlayer at low temperatures. Photoemission intensities from the carbon 1s core level were measured in three directions as functions of photoelectron kinetic energy in the range 60–400 eV. Using multiple-scattering spherical-wave modeling, it was found that the CO molecules are adsorbed on the short-bridge sites, with adjacent CO molecules along the $[1\bar{1}0]$ direction displaced alternatively in opposite directions toward the [001] and the $[00\bar{1}]$ azimuths to form a zigzag chain geometry. The tilt angle is $16 \pm 2°$ from surface normal for the direction linking the carbon atom and the center of the nickel bridge. The carbon-nickel interatomic distance was determined to be $1.94 \pm .02$ Å. The first to second nickel layer spacing is 1.27 ± 04 Å, up from 1.10 Å for the clean Ni(110) surface, but close to the 1.25 Å Ni interlayer spacing in the bulk. Using the findings of earlier studies of this system, the C-O bond length and tilt angle were varied within small ranges (1.10–1.20 Å and 15–23°, respectively) in our MSSW simulations. At 1.16 Å and 19° the best agreement between the experimental data and the theoretical simulations was achieved. The above results yield an 0–0 distance of 2.95 Å for the two nearest CO molecules, close to twice the van der Waals radius (~1.5 Å) for oxygen.

7. High-Resolution Photoelectron Spectroscopy and Femtosecond Intramolecular Dynamics of H_2CO+ and D_2CO+ (Publication 9)

B. Niu, D.A. Shirley, and Y. Bai

High-resolution helium Iα (584 Å) photoelectron spectra of H_2CO and D_2CO are reported. The present study reveals much new vibrational structure detail in the ionic first excited state of formaldehyde. Weak excitations of the V_3 (in H_2CO) and V_1 (in D_2CO) modes along with the strong excitations of the V_2 mode in the ionic first excited states are fully resolved for the first time. The weak excitations of the V_4 out-of-plane bending mode in the ionic ground and first excited states of formaldehyde cations indicate that they may have nonplanar equilibrium geometries. Strong isotope effects on vibronic (vibrational) couplings are observed in the cation first and second excited states. Vibrational autocorrelation functions are calculated from the high-resolution photoelectron spectra. The correlation functions calculated for the first electronic excited states show rather slow decay rate on the femtosecond timescale. The ultrafast decay of the formaldehyde cations implied by the correlation functions calculated for the third electronic excited states suggest that dissociation and intramolecular dynamic processes are the main decay pathways.

8. High-Resolution Photoelectron Spectroscopy and Femtosecond Intramolecular Dynamics of H_2CCO+ and D_2CCO+ (Publication 11)

B. Niu, Y. Bai, and D.A. Shirley

High-resolution helium Iα (584 Å) photoelectron spectra of H_2CCO and D_2CCO are reported. The present spectra of the ground states of ketene cations show more vibrational fine structure than previously reported. The adiabatic ionization energies (AIEs) of the cations' first, second, and fifth excited states are determined unambiguously. The doublet-like fine structures present in the first excited states of ketene cations imply the excitation

of a "soft" mode that was not observed before. It was assigned to the V_5 mode, which is characterized by the CH_2 (CD_2) group out-of-plane wagging motion. The complexity of the photoelectron spectra obtained for the ionic first excited states is attributed to the possible dissociation and predissociation of this state. Strong isotope effects are observed in the vibronic (vibrational) couplings in most of the ionic states. Vibrational autocorrelation functions are calculated from the high-resolution photoelectron spectra for four of the six ionic states observed. The dynamics of the ground states of the cations are characterized by a wave packet oscillating with small amplitude around the minimum of the upper potential energy surfaces (PES). The decay dynamics of the ionic first and fifth excited states of ketene are characterized by ultrafast intramolecular processes such as dissociation and predissociation.

9. ARPEFS Study of the Structure of p(2×2)K/Ni(111) (Publication 12)

Z.Q. Huang, L.Q. Wang, A.E. Schach von Wittenau, Z. Hussain, and D.A. Shirley

Angle-resolved photoemission extended fine structure (ARPEFS) from the potassium 1s core level was measured for the quantitative structural determination of the p(2Y2)K/Ni(111) overlayer at 130 K. This is the first ARPEFS study of an alkali-metal adsorption system. Our analysis of the ARPEFS c(k) curves detected along [111] and [771] showed that the potassium atoms are preferentially adsorbed on the atop sites, in agreement with a previous low energy electron diffraction (LEED) study of the same system. The K-Ni bond length is 3.02 ± 0.01 Å, yielding an effective hard-sphere radius of 1.77 Å for potassium. The first- to second-layer spacing of nickel is 1.90 ± 0.04 Å, a 6.5% contraction from the bulk spacing of 2.03 Å. Furthermore, the first nickel layer shows neither lateral reconstruction (0.00 ± 0.09 Å) nor vertical corrugation (0.00 ± 0.03 Å). A comparison of the structural parameters with those determined from the LEED study is presented. The limitations of Fourier analysis for site determination and the importance of comparing ARPEFS experimental data with theoretical simulations in both k space and r space are also discussed.

10. Photoelectron Spectroscopy of Rare Gas Dimers Revisited: Vibrationally Resolved Photoelectron Spectrum of Argon Dimer (Publication 13)

T. Pradeep, B. Niu, and D.A. Shirley

Photoelectron spectra of rare gas dimers Ar_2, Kr_2, and Xe_2 have been measured using the HeI radiation at 584 Å with a resolution of 13 meV. All the six ionic states in the HeI region have been resolved for the first time, including some of the purely repulsive states. Ionization energies are presented to an accuracy ≤0.003 eV. Dissociation energies (D_0) of the ionic states are calculated using the best estimate adiabatic ionization energies. The $D^2\Sigma^+1/2g$ states of all the dimers are weakly bound, contrary to an earlier theoretical prediction. Part of the vibrational structure of two of the electronic states of Ar_2 has been resolved. For the $A^2\Sigma^+1/2u$ state as many as 14 vibrational excitations are observed. These excitations are assigned to transitions to the higher vibrational levels of v = 32–45. For the $B^2\Pi_{3/2g}$ state, three vibrational structures are resolved and are assigned to v = 2–4 of the ionic state. Accurate values of the spectroscopic constants of these are presented. The present values are compared with the values available in the literature. The D_e values for the $A^2\Sigma^+1/2u$ and the $B^2\Pi3/2g$ states are estimated to be 1.361 and 0.104 eV, respectively.

11. The Influence of Calculated Phase Shifts on the Precision and Accuracy of ARPEFS-Derived Structural Parameter (Publication 15)

Y. Zheng, Z. Hussain, and D.A. Shirley

The influence of theoretical atomic scattering phase shifts calculated by different methods in the analysis of angle-resolved photoemission extended fine structure (ARPEFS) data for structural determination of the c(2×2)S/Ni(001) surface was examined, with the goal of assessing both the precision and accuracy of derived structural parameters. It was found that the values of the S-Ni bond length obtained from the ARPEFS data analysis with different calculated atomic scattering phase shifts all fall within a total range of 0.02 Å (±0.01 Å). This result is also in excellent agreement with the currently accepted

values obtained from low energy electron diffraction (LEED) and surface extended x-ray absorption fine structure (SEXAFS), i.e., 2.19–2.20 Å. We conclude that this ARPEFS-derived structural parameter is relatively insensitive to the choice of theoretical atomic scattering phase shifts, and is both precise and accurate.

FY 1992 PUBLICATIONS AND REPORTS

Refereed Journals

1. A.E. Schach von Wittenau, Z. Hussain, L.Q. Wang, Z.Q. Huang, Z.G. Ji, and D.A. Shirley, "Reevaluation of the p(2×2)S/Cu Structure Using ARPEFS," Phys. Rev. B **45**,13614 (1992).
2. E. Hudson and D.A. Shirley, "High-Resolution K-shell Photoabsorption in Formaldehyde," Phys. Rev. A **46**, 3935 (1992).
3. Y. Zheng, Z. Hussain, and D.A. Shirley, "Amplitudes and Phase Shifts in Electron-Atom Forward Scattering: Strong Dependence on Atomic Valence Electrons," Chem. Phys. Lett. **192**, 108 (1992).
4. B. Niu, D.A. Shirley, Y. Bai, and E. Daymo, "High Resolution He Iα Photoelectron Spectroscopy of H_2CO and D_2CO Using Supersonic Molecular Beams," Chem. Phys. Lett. **201**, 212 (1992).
5. B. Niu, Y. Bai, and D.A. Shirley, "High Resolution He Iα Photoelectron Spectroscopy of H_2CCO and D_2CCO Using Supersonic Molecular Beams," Chem. Phys. Lett. **201**, 217 (1992).
6. Y. Zheng and D.A. Shirley, "Multiple-Scattering Enhances Depth Sensitivity of Angle-resolved Photoemission Fine Structure," Chem. Phys. Lett. **203**, 114 (1993).

LBL Reports

7. E. Hudson and D.A. Shirley, "High-Resolution Measurements of Near-Edge Resonances in the Core-Level Photoionization Spectra of SF_6," LBL-32054.
8. Z.Q. Huang, Z. Hussain, W.T. Huff, E.J. Moler, and D.A. Shirley, "Structural Determination of p2mg(2×1)CO/Ni(110) Using Angle-Resolved Photoemission Extended Fine Structure," LBL-32713.
9. B. Niu, D.A. Shirley, and Y. Bai, "High Resolution Photoelectron Spectroscopy and Femtosecond Intramolecular Dynamics of H_2CO+ and D_2CO+," LBL-32823.
10. B. Niu (Ph.D. Thesis), "High Resolution Photoelectron Spectroscopy and Femtosecond Intramolecular Dynamics Using Supersonic Molecular Beams," LBL-32871 .
11. B. Niu, Y. Bai, and D.A. Shirley, "High Resolution Photoelectron Spectroscopy and Femtosecond Intramolecular Dynamics of H_2CCO+ and D_2CCO+," LBL-32825.
12. Z.Q. Huang, L.Q. Wang, A.E. Schach von Wittenau, Z. Hussain, and D.A. Shirley, "ARPEFS Study of the Structure of p(2×2)K/Ni(111)," LBL-33041.
13. T. Pradeep, B. Niu, and D.A. Shirley, "Photoelectron Spectroscopy of Rare Gas Dimers Revisited: Vibrationally Resolved Photoelectron Spectrum of Argon Dimer," LBL-32925.
14. Z. Huang (Ph.D. Thesis), "Structural Studies of Molecular and Metallic Overlayers Using Angle-Resolved Photoemission Extended Fine Structure," LBL-33040.
15. Y. Zheng, Z. Hussain, and D.A. Shirley, "The Influence of Calculated Phase Shifts on the Precision and Accuracy of ARPEFS-Derived Structural Parameter," Chem. Phys. Lett. (in press); LBL-33370.

Invited Talks

16. E. Hudson, "High-Resolution Soft X-Ray Photoabsorption of SF_6 and H_2S," Department of Physics, Free University of Berlin, Germany, August 1992.
17. T. Reich, "Core Satellite Intensities in CD, C_2H_2, and C_2H_4," SSRL User's Meeting, Stanford Synchrotron Radiation Laboratory, Stanford, CA, October 22–23,1992.

Experimental Search for the Electron Electric Dipole Moment*

Eugene D. Commins, Investigator

INTRODUCTION

An atom in a nondegenerate state cannot possess a permanent electric dipole moment (EDM) unless parity (P) and time reversal invariance (T) are both violated. If an atomic EDM were to exist, it could arise from one or more of the following causes, in general: (a) intrinsic EDM of the neutron and/or proton; (b) P,T odd component of the nucleon-nucleon interaction; (c) intrinsic EDM of the electron; and (d) P,T odd component of the electron-nucleon interaction.

Experimental searches for the free neutron EDM and atomic (and molecular) EDMs are motivated by the fact that CP violation in neutral kaon decay, equivalent to T violation, still has no satisfactory explanation, in spite of almost 30 years of detailed investigation. Thus, a variety of theoretical models of CP violation have been proposed, including some that predict nucleonic and/or atomic EDMs within experimental range.[1]

One searches for an EDM by exposing a neutral system of interest to an external electric field and looking for an energy shift proportional to this field (linear Stark effect). Efforts to observe an electron EDM are aided greatly by the following: It can be shown[2] that in suitable heavy paramagnetic atoms where relativistic effects are large, the ratio R of the atomic EDM d_a to the EDM of the unpaired electron d_e is $\approx 10^2$ to 10^3 in magnitude. For example, in the ground $6^2P_{1/2}$ state of thallium (Z = 81), R = –580. Thus, in practice, one carries out an experiment to search for the atomic EDM d_a, and interprets the result in terms of d_e.

The present experiment utilizes two counter-propagating atomic beams of ^{205}Tl, laser optical pumping for state selection and analysis, two separated rf fields for magnetic resonance, and an electric field **E** in between these separated rf fields. The entire experiment is immersed in a uniform magnetic field **B**. The signal is fluorescence detected in the second optical pumping region, and the signature is an asymmetry in the fluorescent intensity proportional to **E**·**B**. The best limit on the electron EDM has been obtained in our experiment on ^{205}Tl, with the published result[3]:

$$d_e = (-2.7 \pm 8.3) \cdot 10^{-27} \text{ e cm} \quad . \qquad (1)$$

Several theoretical models of considerable current interest[1] predict that d_e should be in the range 10^{-26} e cm – 10^{-28} e cm, and thus it is very important to improve the precision of our result. Since publication in 1990, we have devoted ourselves to improving the sensitivity of the apparatus, reducing noise, and getting a firmer grip on possible sources of systematic error. During FY 1992, we also arrived at a new and powerful scheme for radical improvements in the experiment, which can be undertaken with relatively simple means, and which should eliminate a broad class of systematic errors and reduce noise. Thus, the way will be open to a very substantial improvement in precision (described briefly in Article 3).

*This work was supported by the Director, Office of Energy Research, Office of Basic Energy Sciences, Chemical Sciences Division, of the U.S. Department of Energy under Contract No. DE-AC03-76SF00098.

1. W. Bernreuther and M. Suzuki, Revs. Mod. Phys. **63**, 313 (1991).
2. P.G.H. Sandars, Phys. Lett. **14**, 194 (1965); Phys. Lett. **22**, 290 (1966).
3. K. Abdullah et al., Phys. Rev. Lett. **65**, 2347 (1990).

2. Work in Progress

We have made considerable progress in reducing overall noise (collaboration with graduate student Stephen B. Ross). The major sources of noise are: (1) fluctuations in the magnetic field, caused by (a) fluctuations in the current supplied to magnetic field coils or (b) fluctuations in the ambient field penetrating the magnetic shields; (2) 1/f noise in the atomic beams; (3) 1/f noise in laser intensity and frequency; and (4) shot noise. Of these, the dominant contribution was 1(a). During the past year, we have essentially eliminated this contribution, giving an overall reduction of noise by a factor of about 3.5. We have also reduced the fluctuations in atomic beam intensity very substantially. The total noise remaining is about three times shot noise. That in excess of shot noise is primarily in the low-frequency range, and can be eliminated by methods to be described in the following article.

The main sources of potential systematic error in the present apparatus may be classified into two categories: magnetic effects and the geometric phase effect. In the first category, all those effects are proportional to the atomic magnetic moment: the "**E x v**" effect, and possible contributions from leakage currents, charging currents, etc., which generate stray magnetic fields that change when the electric field is reversed. The geometric phase effect was discovered in the course of this experiment and has been

described in detail elsewhere.[4] It can be isolated by taking EDM asymmetry data as a function of magnetic field strength B. Whereas the true EDM effect is independent of B, the asymmetry arising from the geometric phase effect varies as B^{-2}.

We largely cancel the **Exv** effect by using two counterpropagating atomic beams with orbits defined by the same collimating slits. Small residuals remain because the beams do not have exactly the same velocity distributions, and they do not fill exactly the same regions of space, while at the same time there are unavoidable small magnetic and electric field gradients in the interaction region. These residual effects are isolated and removed by a variety of auxiliary measurements. During the past year we discovered that our program of auxiliary measurements was not entirely complete and satisfactory, but we have learned how to eliminate these residual difficulties.

The results of these various improvements in FY 1992 are as follows: We have achieved a precision of about 3×10^{-27} e cm in about 10 hours of running (a gain of approximately 12 in running time compared to our 1990 results). All the various contributions to the **Exv** effect are below the level of 1×10^{-27} e cm equivalent. Because of improvements in magnetic field stability, we can operate at sufficiently large values of B that geometric phase effects are also below the level of 1×10^{-27} e cm. We are now running the experiment and expect to complete it in its present manifestation in early spring 1993, when we expect to reach an overall precision of 2×10^{-27} e cm or better.

4. E.D. Commins, Am. J. Phys. **59**, 1077 (1991).

3. Proposal for Major Improvements

We developed a proposal for major improvements of this experiment that can be carried out with relatively simple means. The basic idea here is to employ simultaneously beams of atoms in the $6P_{1/2}$, F = 1 and $6P_{3/2}$, F = 2 states, and to switch rapidly back and forth between their fluorescent signals in the analyzer region. Only the $6P_{1/2}$ state has a large enhancement factor R, and thus a possible genuine EDM effect, whereas both $6P_{1/2}$ and $6P_{3/2}$ states exhibit identical geometric phase effects. The $6P_{3/2}$, F = 2 state is about 6 times more sensitive to magnetic systematics of all kinds as the $6P_{1/2}$, F = 1 state. Comparison of the 2 fluorescent signals by rapid switching will eliminate all low-frequency magnetic and atomic beam noise, and when used in conjunction with the up-down beam technique will cancel all magnetic systematics to very high precision. The way will thus be open to achievement of precisions better than 1×10^{-28} e cm in d_e. Further improvements can be attained by transverse laser cooling of the atomic beams.

FY 1992 PUBLICATIONS AND REPORTS

Invited Talk

1. E.D. Commins, "Atomic Parity Nonconservation and Electric Dipole Moment Experiments," Nobel Symposium #85, Saltsjobaden, Sweden, June 29–July 3, 1992.

High Energy Atomic Physics*

Harvey Gould, Investigator

INTRODUCTION

The goals of this program are to understand atomic collisions of highly relativistic heavy ions, to search for a permanent electron electric dipole moment (EDM), and to test quantum electrodynamics in a strong static Coulomb field. Recent results include the discovery at the LBL Bevalac, of a new atomic collisions process, Capture from Pair Production. In this process an electron is captured by a relativistic (bare) ion, when the electron is produced as part of an electron positron-pair by the motional Coulomb fields of the relativistic ion passing within atomic distances of a target nuclei. This process is unique because its cross sections increases with energy at relativistic energies, and because it has no electron in the initial state. It is predicted to be the dominant mechanism for beam loss for the heaviest ions at the Relativistic Heavy Ion Collider (RHIC), being built at Brookhaven National Laboratory. The measurement was made using the Advanced Positron Spectrometer (APS), a highly selective positron spectrometer that measures positron energies and angles with high acceptance and high efficiency. Present activities include (1) preparing the APS for higher energy beams at the Brookhaven Alternating Gradient Synchrotron, (2) developing a more sensitive EDM experiment using trapping and cooling of francium, (3) developing a theoretical understanding of Capture from Pair Production, and (4) continuing adherence to applicable standards for environment, health, safety, and procedure in all activities.

1. First Measurement of Capture from e^+e^- Pair Production in Relativistic Heavy Ion Collisions

A. Belkacem, H. Gould, B. Feinberg, R. Bossingham, and W. Meyerhof†

Capture from pair production is a process in which the high transient electromagnetic field from a relativistic heavy-ion atomic collision produces an electron-positron pair with the electron emerging from the collision bound to the ion. It is a recombination process with unique properties: There is no electron in the initial state, it is observed only at relativistic energies, it has a cross section that increases with increasing beam energy and is predicted to be the dominant source of beam loss at RHIC to be built at Brookhaven National Laboratory. We report, for the first time, the observation and measurement of electron capture from e^+e^- pair production. The experiment was performed at the LBL-Bevalac using 956 MeV/u uranium ions on gold, silver, and copper targets. The data from this experiment are presently being analyzed; however, preliminary results are that the cross section for capture from pair production for U92+ on a Au target is about 2 barns and free pair production (no capture of an electron) is about 3 barns.

† Stanford University, Stanford, CA 94305.

2. Work in Progress

A fully nonperturbative treatment of the time-propagation of the relativistic wavefunctions in momentum space is being applied to describe the capture from pair production process in relativistic heavy-ion collisions. Employing time reversal, this process can described by propagating the Fourier-transformed 1s-eigenfunction according to the time-dependent Dirac equation. The capture probability is obtained by projection of the final momentum distribution (obtained numerically) onto the stationary Coulomb-Dirac eigenfunctions in momentum space. Unlike coupled-channels calculations in space coordinates these calculations may be extended to very high energies (100 GeV/u).

Work has begun to develop and experiment to search for a CP-violating permanent electron electric dipole moment by the technique of laser trapping and cooling francium. Francium is highly suited to this measurement as it is an alkali with a D_2 at 718 nm and has a greater sensitivity to an electron EDM than any element yet used in an EDM experiment. ^{221}Fr is a decay product of ^{229}Th, and the feasibility of obtaining francium by evaporating it at 460°C from a ^{229}Th source has been demonstrated. An experiment with a sensitivity of 5×10^{-30} e-cm, a factor of 2000 improvement over the current limit appears feasible.

FY 1992 PUBLICATIONS AND REPORTS

LBL Reports

1. B. Feinberg, H. Gould, W.E. Meyerhof, A. Belkacem, H.-P. Hülskötter, J.R. Alonso, L. Blumenfeld, E. Dillard, N. Guardala, G.F. Krebs, M.A. McMahan, M.J. Rhoades-Brown, B.S. Rude, J. Schweppe, D.W. Spooner, K. Street,

* This work was supported by the Director, Office of Energy Research, Office of Basic Energy Sciences, Chemical Sciences Division, of the U.S. Department of Energy under Contract No. DE-AC03-76SF00098.

P. Thieberger, and H. Wegner, "Relativistic Electron Impact Ionization of Highly Stripped Heavy Ions Determined from Projectile Electron Loss in H_2 and He," Phys. Rev. A (in press); LBL-31022.

2. A. Belkacem, H. Gould, B. Feinberg, and W. Meyerhof, "An Advanced Positron Spectrometer (APS) to study Capture from Pair Production at the Bevalac" presented at the 13th DOE Atomic Physics Program Workshop, Ithaca, NY, Oct. 15–16, 1992; LBL- 31816 Abs.

Invited Talks

3. H. Gould, "Measurement of the Lamb Shift in Lithiumlike Uranium," 85th Nobel Symposium, "Heavy Ion Spectroscopy and QED Effects in Atomic Systems," Saltsjöbaden, Sweden, June 29–July 3, 1992.
4. H. Gould, "Observation and Measurement of Capture from Pair Production," presented at the 13th DOE Atomic Physics Program Workshop, Ithaca, NY, Oct. 15–16, 1992.

Atomic Physics*

Michael H. Prior, Investigator

INTRODUCTION

This program performs studies of the structure and interactions of atomic systems, to provide the most detailed description of their behavior, and to challenge and stimulate theoretical understanding of the observed phenomena. Emphasis is upon research topics that are best addressed with unique research tools and expertise available at LBL. Often topics selected have relevance to plasma behavior and diagnostics in tokamak devices or advanced laser technology. Collaborative associations with investigators from outside LBL form an essential means of bringing resources to the program, forming stimulating scientific exchange, and efficiently utilizing experimental facilities.

The research projects exploit the ability of state-of-the-art electron cyclotron resonance (ECR) ion sources at LBL to produce intense, highly charged beams for conduct of ion-atom collision and Auger spectroscopic studies. Work is carried out using the atomic physics facilities jointly established by LBL and LLNL at the LBL ion sources. These include three beamlines, several electron and optical spectrometers, a multipurpose scattering chamber with precision controlled rotating table, and data collection instrumentation. Work to date has used ion beams from the original LBL ECR source constructed in 1984 by the LBL Nuclear Science Division (NSD) to provide heavy ions for acceleration by the LBL 88-Inch Cyclotron. Two beamlines are in operation with this source; the third is attached to the recently constructed Advanced ECR source located nearby. The proximity of the two sources and facilities allows efficient use of instrumentation at either and quick switchover from one source to the other. The enhanced performance of the AECR allows mounting of experiments that require the increased intensity and/or higher charged beams available from this source.

Current emphasis is upon providing the most detailed experimental description of multiple electron capture in slow ion-atom collisions. In the past, nearly all multiple electron capture experiments have consisted of total cross-section measurements into unresolved or only partially resolved final states. Thus, whereas theorists can calculate population amplitudes into fully defined quantum states of the products, summing and averaging over much of this detail is required to obtain a total or partial cross section to compare with the much less detailed experimental data. A substantial fraction of our research conducts experiments that describe double (or more) electron transfer between uniquely characterized final states so that theoretical predictions can be tested at the finest scale possible.

The research also provides energy level structure, and decay modes of highly excited states, and insight into novel population mechanisms in ion-atom collisions, for a wide range of multiply charged ions.

*This work was supported by the Director, Office of Energy Research, Office of Basic Energy Sciences, Chemical Sciences Division of the U.S. Department of Energy under Contract No. DE-AC03-76SF00098.

1. Multiple Electron Transfer in Slow Ne^{9+}-Ne Collisions (Publication 1)

R. Herrmann,† M.H. Prior, R. Doerner,† H. Schmidt-Boecking,† C.M. Lyneis, and U. Wille‡

The combination of a multiply charged ion and a neutral atom is a highly excited system that is far from equilibrium. Their close approach, in a collision where the relative velocity is less than characteristic electron velocities, forms a transient quasi-molecule of high charge and excitation. As the collision develops, the electrons redistribute themselves among the two nuclear centers and, after separation, one has generally two ions with charges lower than that of the incident ion; these are often in excited states that decay radiatively or by the emission of Auger electrons. It is also possible, with small probability, for electrons or photons to be emitted from the quasi-molecule, that is, during the period of close approach. The study of multiple electron transfer in slow ion-atom collisions in this program is centered upon developing accurate descriptions of the final product states, from which inferences can be made about the transfer processes active during the collision.

In this work, Ne^{9+} ions at an energy of 90 keV ($v = 0.5$ au) collided with a Ne gas jet target, and the resulting product ion charges and the scattering angle of the projectile product ion were measured in coincidence. One-electron Ne^{9+} has a vacancy in the K-shell (1s), and there is a possibility that the vacancy may be transferred to the target; this would be followed by an Auger cascade that would remove several electrons from the target product ion. A vacancy in the $1s\sigma$ molecular orbital (MO), originating from the projectile K-shell, can be transferred via radial coupling to the $2p\sigma$ orbital that correlates at large separation with a K-vacancy in the target atom. The amplitude for this process peaks at an internuclear separation of about twice the atomic K-shell radius. Figure 1-1 sketches the variation with internuclear separation of the pertinent MO energy levels. During the collision the radial coupling region is passed on the incoming and outgoing parts of the trajectory. Since these two transition amplitudes cannot be distinguished experimentally by

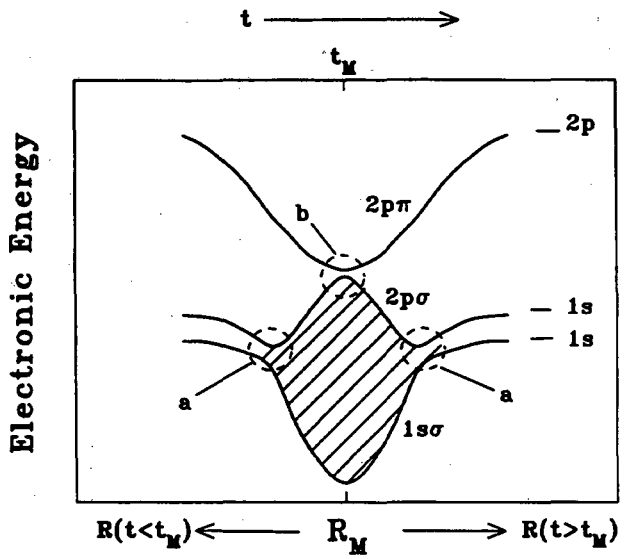

Figure 1-1. Schematic correlation diagram of the three inner-most quasimolecular orbitals. Electronic energy is plotted versus internuclear distance between projectile and target. R_M indicates the distance of closest approach. The dashed circles labeled *a* show the regions of maximum radial coupling amplitude between the 1sσ and 2pσ orbitals. The region *b* indicates the maximum of the rotational coupling between the 2pσ and 2pπ orbitals. The shaded area is proportional to the phase difference between amplitudes for K-K vacancy transfer on the incoming and outgoing parts of the trajectory. (XBL 936-943)

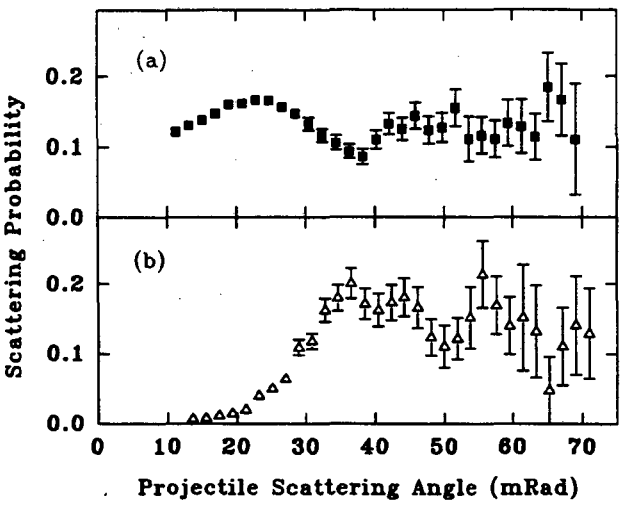

Figure 1-2. Oscillatory structure in the projectile scattering probability caused by interference in K-vacancy transfer for (a) the final charge state combinations, target q = 5+, projectile Q = 7+, and (b) the complement (7+,5+). (XBL 936-944)

measuring the total K-vacancy transfer probability, a coherent addition of the amplitudes must be made, and, depending upon the relative phase of the amplitudes, one may have constructive or destructive interference. The relative phase depends upon the minimum internuclear distance (R_M in the Fig. 1-1), that is determined by the impact parameter and the collision energy. Thus, for a fixed energy, at some impact parameters, the K-vacancy is very likely transferred, while at others the two transition amplitudes interfere destructively and there is minimal probability of transfer. At fixed collision energy, the projectile scattering angle is a function of the impact parameter; thus, the K-vacancy transfer probability should manifest itself as an oscillating structure in the projectile intensity versus scattering angle.

Figure 1-2 shows an example of this oscillatory structure observed for two sets of product ion charge states (target charge q = 5+, projectile charge Q = 7+) and the complement (q = 7+,Q = 5+). Similar oscillations were observed for other, but not all, final charge state combinations. The appearance of structure for certain final charge combinations can be explained by the KK-vacancy transfer mechanism together with the assumption that K- and L-shell charge transfer are independent processes. In this model, the appearance of interference structures occurs for those final charge state combinations that arise from intermediate states whose outer-shell populations are nearly equal, for the K-vacancy transfer channels, and are unequal for the nontransfer channels (the opposite population asymmetry produces complementary structure as shown in Fig. 1-2). Alternatively, the selective appearance of the KK-interference structure may be taken as a strong indication of independent K- and L- shell charge transfer.

The results of this study are summarized in the following points: (i) For projectile scattering angles larger than about θ = 46 mrad, a 90 keV Ne^{9+} projectile and a Ne target atom undergo a complete equilibration of their atomic shells. (ii) K- and L-shell charge transfer occur independently. (iii) The rotational coupling amplitude between the 2pσ and 2pπ quasimolecular orbitals is negligibly small. (iv) The KK-interference effect is clearly observable for certain final charge-state pairs, indicating that the different L- and outer-shell occupations on the incoming and outgoing parts of the trajectory do not influence seriously the strength of the 1sσ-2pσ radial coupling.

†Institut fur Kernphysik, U. Frankfurt, Germany.
‡Hahn-Meitner Institut, Berlin, Germany.

2. Low-Energy Electron Production in Slow Ion-Atom Collisions (Publications 2 and 6)

V.L. Plano,[†] R.R. Haar[†] and J.A. Tanis,[†] P.A. Zavodsky,[‡] L. Sarkadi,[‡] J. Palinkas,[‡] D. Schneider,[§] H. Khemliche,[||] and M.H. Prior

In earlier work[1] we showed that slow (v = 0.39 a.u.) O^{6+} collisions with. He atoms produce unbound electrons moving at near the projectile velocity and that these are almost exclusively associated with projectiles which have captured one electron. Thus the two electrons originally on the He atom are "captured" one into a projectile bound state and one into a continuum state moving with low velocity (a few eV).

To further define this process, we have recently utilized bare O^{8+} ions at v = 0.42 a.u. in collision with two-electron (He and H_2) and multi-electron (Ar) targets. In this work the electron spectrum (E < 15 eV) emitted near zero degrees (along the projectile beam) is collected in coincidence with the outgoing projectile ion charge states. For all targets, no electrons are observed coincident with outgoing O^{8+} ions, but, as with the O^{6+} study, there are a substantial number coincident with projectiles that capture one electron (i.e., with O^{7+}). Interestingly, when the target is Ar, there is nearly the same yield of electrons coincident with outgoing O^{6+} (3 active electrons, two captured, one free) as with outgoing O^{7+} (2 active electrons, one captured, one free), and there is a measurable yield of low-energy electrons coincident with outgoing O^{5+} (4 active electrons, 3 captured, one free).

A separate related experiment has measured the angular scattering of the charge analyzed O^{q+} products in coincidence with electrons emitted into all angles with energy less than about 15 eV, or with target recoil ions from He and Ar target atoms. These observations confirm the measurements made with electrons near zero degrees, and show how the projectile scattering varies with the number of active electrons. In addition to intrinsic value as diagnostics of the collisions, these measurements allow correction of the zero degree measurements for incomplete collection of the scattered projectile products.

[†]Western Michigan University.
[‡]Institute of Nuclear Research, Debrecen, Hungary.
[§]LLNL V-Division.
[||]U. Pierre et Marie Curie and LBL.
[1]J.A. Tanis et al., Phys. Rev. **A42**, 5776 (1990).

3. XUV Spectra from Highly Charged Ion-Atom Collisions (Work in Progress)

J. Crespo,[†] M.H. Prior, and D. Schneider[‡]

In collaboration with the group of E. Fill at the Max Planck Institute (MPI) for Quantum Optics, Garching, Germany, and the V-Division of LLNL, an XUV grazing incidence spectrometer has been mounted to view a gas cell located on the LBL 14-GHz Advanced ECR atomic physics beamline. The goal of studies with this instrument is determination of cross sections for the population of selected excited ion states by electron capture from atomic targets; in addition to their intrinsic interest, these are relevant to the behavior of laser-produced plasmas in contact with cold matter and related charge transfer driven, short wavelength laser designs.

[†]MPI Garching, Germany.
[‡]LLNL V-Division.

4. Amplitudes of Substates Populated in Double Electron Capture (Work in Progress)

H. Khemliche,[†] M.H. Prior, and D. Schneider[‡]

We have modified our experiment on Auger electron anisotropy following double electron capture, to measure the relative phases, magnitudes, and impact parameter dependence of the complex magnetic substate amplitudes. This requires measurement of the variation of Auger emission with respect to the scattering plane of the collision. We will do this for the same systems for which we made detailed alignment measurements, i.e., C^{5+} and B^{4+} on He. The scattering plane can be established from the beam momentum and measurement of the He^{++} recoil momentum or the complementary "recoil" of the projectile product ion. Toward realization of the former method, a prototype detector was assembled for analysis of recoil ions (both q/m and energy), and tests were conducted to determine the practicality of this approach.

In addition, the alternative method of measuring the projectile product scattering in coincidence with the Auger spectrum is being pursued. With this technique, for example, the $1s[2s2p\ ^1P]^2P$ state formed by the double capture can be described from analysis of the azimuthal (ϕ_e) dependence of the Auger electrons emitted at polar

angles (θ_e) of 45° or 135° (with respect to the beam direction) in coincidence with the scattered C^{4+} projectile products. Figure 4-1 shows how this azimuthal dependence varies with the relative phase of the amplitudes for populating the magnetic sublevels M L = 0 and ±1. Rather than rotate the electron spectrometer in angle ϕ_e, it is equivalent to hold it fixed and measure the coincident C^{4+} scattered ion position. The coordinates of each event define the collision plane for that event, and the azimuthal coordinate of the electron emission with respect to that plane will be used to construct the dependence shown in the figure. The variation of the coincident rate with the scattering angle of the projectile will give information on the impact parameter dependence of the double electron capture. (Figure 4-1 represents results averaged over all impact parameters.) To accomplish this work, a parallel plate electron spectrometer was modified to provide position sensitive detection in the exit plane. The resulting instrument provides well-resolved spectra with an efficiency gain of more than two orders of magnitude over that obtained with a similar sized instrument used with fixed slits and scanned pass energy.

†Graduate student U. Pierre et Marie Curie, Paris.
‡LLNL V-Division.

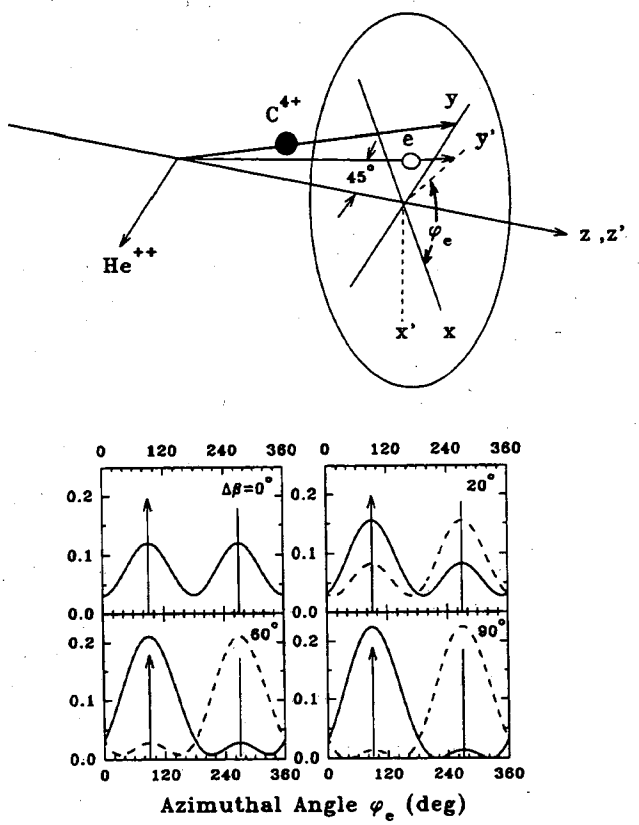

Figure 4-1. Azimuthal angular variation of Auger emission from the C^{3+} 1s[2s2p ^{1}P] ^{2}P level formed by double capture to v = 0.5 a.u. C^{5+} ions from He atoms. The upper part of the figure shows the coordinate systems relevant to the experiment and the final products of the collision. The ion-beam direction is the polar (z,z′) axis, which taken with the transverse C^{4+} momentum (greatly exaggerated here) define the scattering plane (yz). The electron spectrometer is fixed in the laboratory coordinate system (x′y′z′). The curves are for electrons emitted at polar angles of 45° (solid curves, and as shown in the upper part) or 135° (dashed curves); the vertical lines indicate location of the scattering plane. These curves are constructed from results of our alignment measurements and assumed values for the relative phase Δβ between the complex amplitudes for populating the M_L = 0 and ±1 substates. The curves represent behavior averaged over all impact parameters. (XBL 936-942)

FY 1992 PUBLICATIONS AND REPORTS

Refereed Journals

1. R. Herrmann et al., "Multiple Electron Transfer in Slow Ne^{9+}-Ne Collisions," Phys. Rev. A **46**, 5631 (1992).

Other Publications

2. R.R. Haar, J.A. Tanis, D. Schneider, M.W. Clark, M.H. Prior, K. Randall, and R.D. Dubois, "Low-Energy Continuum Electrons from O^{8+} + He Collisions," Bull Am. Phys. Soc. **37**, 1083 (1992).
3. D. Schneider, R. Bruch, T. Brage, and M.H. Prior, "Autoionization of Core-Excited Na-like $2p^5 3lnl'$ (n = 3 and 4) States in Si^{3+} Formed in 50 keV Si^{5+} + He Collisions," Abstracts of Contributed Papers of the VI International Conference on the Physics of Highly-Charged Ions, edited by P. Richard, M. Stockly, C.L. Cocke and C.D. Lin (Kansas State University), p. A9 (1992).
4. S.D. Yao, M.H. Prior and D. Schneider, "Auger Emission Following Double Electron Capture by Ne^{8+} from Helium," Abstracts of Contributed Papers of the VI International Conference on the Physics of Highly-Charged Ions, edited by P. Richard, M. Stockly, C.L. Cocke and C.D. Lin (Kansas State University), p. A10 (1992).
5. H. Khemliche, M.H. Prior, and D. Schneider, "Alignment and Orientation in Double Electron Capture Collisions," Abstracts of Contributed Papers of the VI International Conference on the Physics of Highly-Charged Ions, edited by P. Richard, M. Stockly, C.L. Cocke and C.D. Lin (Kansas State University), p. A11 (1992).
6. J.A. Tanis, R.R. Haar, D. Schneider, M.W. Clark, M.H. Prior, R.D. Dubois, and K. Randall, "Low-Energy Continuum-Electron Emission at 0° from O^{q+} + He Collisions," Abstracts of Contributed Papers of the VI International Conference on the Physics of Highly-Charged Ions, edited by P. Richard, M. Stockly, C.L. Cocke and C.D. Lin (Kansas State University), p. A44 (1992).

PROCESSES AND TECHNIQUES

CHEMICAL ENERGY

High-Energy Oxidizers and Delocalized-Electron Solids*

Neil Bartlett, Investigator

INTRODUCTION

The main aim of this program is the synthesis and characterization of new materials that may have utility in efficient storage or usage of energy. The novel materials include two-dimensional networks of high π-bonding atoms (boron, carbon and nitrogen) with structures akin to graphite. Of these the more metallic ones have possible applications as electrode materials for high-energy-density batteries and those that are semiconducting could be useful in converting light to electrical energy. Good ionic conductors are also being sought, with emphasis on lithium-ion and fluoride-ion conductors, since batteries based on lithium and fluorine would be unsurpassed in their energy density features. In addition novel oxidation-state fluorides are being synthesized and structurally characterized to provide a comprehensive basis for better theoretical models, from which an improved capability to predict physical and chemical behavior ought to be forthcoming. Previously unknown or little studied high-oxidation-state species constitute a large part of this effort. Such species are also investigated for their efficiency and specificity as chemical reagents.

1. The Remarkable Oxidizing Capabilities of Cationic Ag(III) and Ni(IV) in Anhydrous Hydrogen Fluoride Solutions (Publication 6)

G. Lucier, C. Shen, L. Chacon, W.J. Casteel Jr., and N. Bartlett

Cationic Ag(III), from AgF_3 interacting with AsF_5 in anhydrous hydrogen fluoride (AHF), oxidizes O_2 to O_2^+ AsF_6^-, RuF_6^- to RuF_6 and PtF_6^- to PtF_6, at room temperature and therefore probably surpass KrF^+ as an oxidizer. NiF_4, derived from K_2NiF_6 in AHF at –75°C acidified with BF_3, has similar oxidizing power at ~–30°C.

Silver trifluoride, prepared by displacement from a solution of $KAgF_4$ in AHF with BF_3, and washed with AHF to free it of KBF_4, may be kept indefinitely at ordinary temperatures, as a dry solid, but it does degrade to fluorine and $Ag^{2+}(AgF_4^-)_2$ in AHF in several hours. A solution of AsF_5 in AHF added to AgF_3 at room temperatures, rapidly oxidizes molecular oxygen according to the equation:

$$AgF_3 + O_2 + 3AsF_5 \rightarrow O_2^+AsF_6^- + Ag^{2+} + 2AsF_6^-.$$

The dioxygenyl salt is of slight solubility at ~–30°C and is recovered in high yield (~80% based on AgF_3) by washing (to remove Ag^{2+}) with AHF/AsF_5 at that temperature. A solution of $KPtF_6$ in AHF, acidified with AsF_5, in contact with AgF_3 liberates PtF_6 at ~20°C. The red, volatile PtF_6 separated by distillation, (along with AHF) was characterized by its quantitative interaction with O_2: $O_2 + PtF_6 \rightarrow O_2PtF_6^-$, the known salt being cubic (unit cell: $a_o = 10.032(2)$Å). A similar reaction with $KRuF_6$ generated RuF_6, again at ~20°C, the characterization of the hexafluoride again being made through the O_2^+ salt (cubic unit cell: $a_o = 10.002(4)$Å). This synthesis of RuF_6 is a particularly valuable one, since RuF_6 is thermally unstable, decomposing to liberate fluorine at ordinary temperatures. It is, therefore, difficult to obtain in even moderate yield directly from the elements. These syntheses generated each of the hexafluorides in greater than ~20% yield, based on AgF_3. A similar set of reactions in which NiF_4, produced from K_2NiF_6 with BF_3, in AHF, was brought into contact with a $KRuF_6$ or $KPtF_6$ solution at ~–30°C, produced each of the hexafluorides. These were separated by distillation, along with AHF, and mixed with oxygen to yield the $O_2^+MF_6^-$ (M = Ru or Pt) salts. Each was obtained in ~20% yield, based on NiF_4. A sample of NiF_4 in AHF, acidified with AsF_5, at –65°C, rapidly oxidized O_2 to yield the $O_2^+AsF_6^-$ salt that was characterized by its Raman spectrum with νO_2^+ at 1856 cm^{-1}.

*This work was supported by the Director, Office of Energy Research, Office of Basic Energy Sciences, Chemical Sciences Division of the U.S. Department of Energy under Contract No. DE-AC03-76SF00098.

2. Salts of Lattice Cation $(AgF_2)_3^+$, a Potent Oxidizer and Possible Metal (Publication 7)

B. Žemva, C. Shen, G. Lucier, J. Allman, and N. Bartlett

Oxidation of silver difluoride, or the salt $AgF^+BF_4^-$, by O_2^+ salts in AHF, generate strongly oxidizing salts of formulation $(AgF_2)_3^+MF_6^-$ (M = As, Sb, Au, Pt, Ru) that have perovskite-like structures and are metal-like in their magnetic behavior.

Oxidation of AgF_2 or $AgF^+BF_4^-$ by a solution of a dioxygenyl salt, $O_2^+MF_6^-$ (M = As, Sb, Au, Pt, Ru) at ~20°C, in AHF, yields a black or deeply colored salt of composition $(AgF_2)_3MF_6$: $O_2MF_6 + 3AgF_2 \rightarrow (AgF_2)_3^+MF_6^- + O_2$. These salts are isostructural and yield trifluoride-like x-ray powder diffraction patterns each of which has been indexed on the basis of a monoclinic cell containing one formula unit. For the AsF_6^- salt a = 5.6045(6), b = 5.2567(6), c = 7.8061(8)Å, ß = 96.594(9)°, V = 228.5Å^3, Z = 1, in space group P2/c. The other salts are very similar in dimensions. A single-crystal structure of the arsenic salt has been completed and shows the material to be $(AgF^+)_2AsF_6^-AgF_4^-$. Each F ligand of AsF_6^- makes a bridging contact, Ag•••F, with the six surrounding Ag species, as shown in Figure 2-1. The Ag species are of three types: one is Ag′(II) and is located in a grossly distorted octahedral environment of F ligands, with essentially linear coordination in F, each shared with a Ag″(II) atom; another {Ag(III)} is in an approximately square F ligand environment, that constitutes an anion $[AgF_4]^-$, and the third {Ag″(II)} is linearly coordinated by 2 F ligands each shared with a Ag′(II) atom. Each of the Ag(II) species is linearly coordinated by 2 F ligands and makes four long-bridge Ag•••F contacts to the four closest anions. The anions AsF_6^- and AgF_4^- are in ordered sequence along c but are not in registry with the equivalent anion arrays in neighboring cells, i.e. each anion site is 50% occupied by each anion, but the adjacent anion must always be of the other kind. Including the $[AgF_4]^-$ anion, the fluorine-bridged Ag-F (and Ag•••F) array can be viewed as a $(AgF_2)_3^+$ cage for the MF_6^- anion. This cage has sufficient oxidizing power to remove an electron from the IrF_6^- ion, which has an ionization potential of ~7 eV. Although there is a low temperature "Curie tail" in the otherwise approximately temperature-independent paramagnetism of $(AgF_2)_3^+AsF_6^-$ shown in Figure 2-2, it appears that the magnetic behavior is in accord with the Fermi-Dirac statistics appropriate for a metal. This is akin to the behavior of other $(AgF)_n^{n+}$ salts.

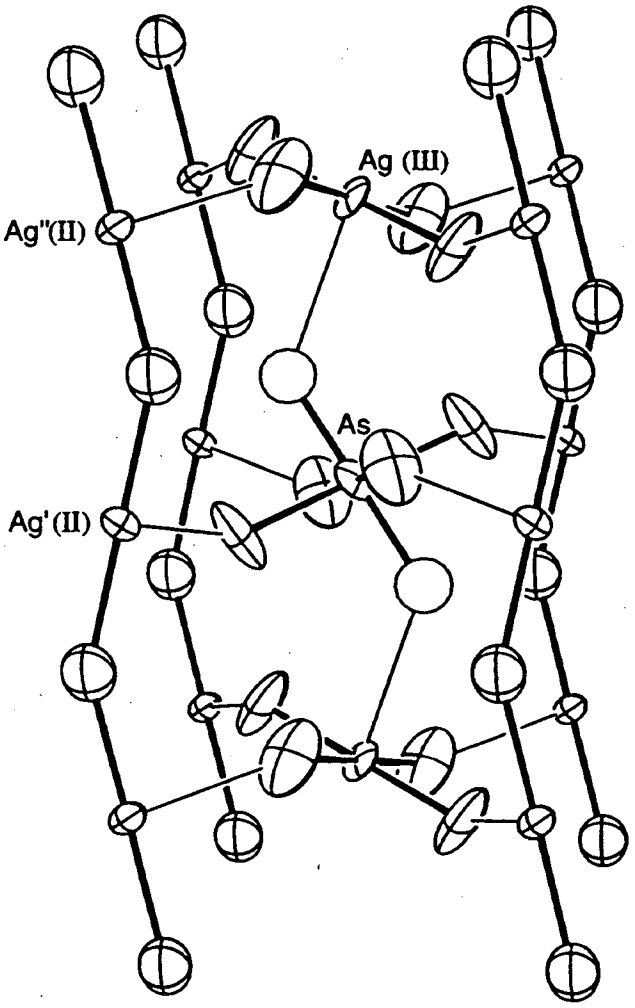

Figure 2-1. Structural arrangement in $(AgF_2)_3^+AsF_6^-$.

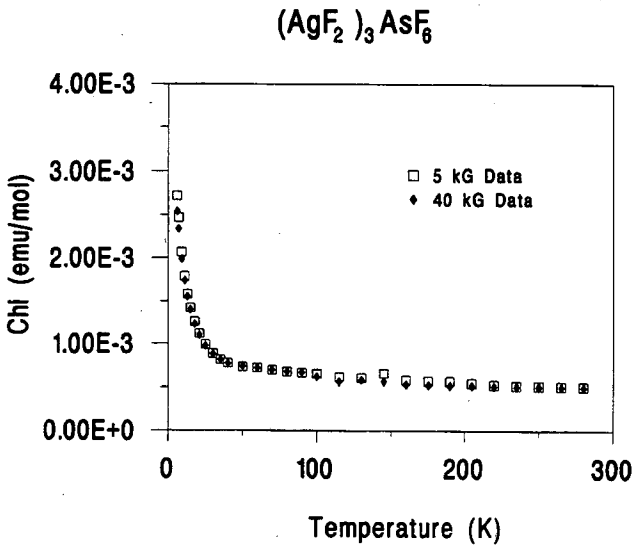

Figure 2-2. Dependence of magnetic susceptibility on temperature for $(AgF_2)_3^+AsF_6^-$.

3. The Oxidizing Properties of Cationic Ag(II) in Anhydrous Hydrogen Fluoride (Publication 8)

W.J. Casteel, Jr., G. Lucier, C. Shen, and N. Bartlett

Solvated cationic Ag(II) in anhydrous HF is a potent oxidizer and fluorinator even at dry-ice temperatures.

It is not possible to prepare the salt $AgF^+OsF_6^-$ since the chain cation $(AgF)_n^{n+}$ is able to extract the electron to liberate OsF_6. When the salt $AgF^+IrF_6^-$ is treated with AsF_5 in AHF, IrF_6 (E = 7 eV) is formed, showing that solvated Ag(II), $Ag^{2+}_{(solv)}$ in AHF is a more potent oxidizer than $(AgF)_n^{n+}$. The $Ag^{2+}_{(solv)}$ is most conveniently generated in AHF by adding two moles of AsF_5 per mole of Ag(II). Such a solution at –75°C immediately oxidizes C_6F_6 to precipitate $C_6F_6^+AsF_6^-$ (a salt previously prepared in these laboratories). Perfluoropropene is quantitatively and quickly oxidized to perfluoropropane at the same temperature: $CF_3.CF=CF_2 + 2Ag^{2+} + 2AsF_6^- \rightarrow CF_3.CF_2.CF_3 + 2AgAsF_6 + 2AsF_5$. This must occur by a sequence, of electron-oxidation followed by fluoride-ion addition, followed by a second such sequence, the lead event in each case being brought about by the very high electron affinity of the $Ag^{2+}_{(solv)}$. That this is indeed remarkably high, is shown by the fixation of O_2, as the $O_2^+AsF_6^-$ salt, at –75°C. At this temperature, the deep blue $Ag^{2+}_{(solv)}$ solution is reduced by oxygen (~2 atmospheres of gas in equilibrium with the AHF solution) to yield a colorless precipitate containing both $O_2^+AsF_6^-$ and $AgAsF_6$. On warming to –65°C, the blue color of $Ag^{2+}_{(solv)}$ is easily seen and at room temperature, the low solubility of O_2 and the large $T\Delta S$ term of the back reaction, become large enough to render the oxygen fixation negligible:

$$O_2 + Ag^{2+} + 2AsF_6^- \underset{\sim 20^\circ C}{\overset{-75^\circ C}{\rightleftharpoons}} O_2^+AsF_6^- + AgAsF_6$$

4. Some Thermodynamic Aspects of the Remarkable Oxidizing Capabilities of Fluorine/Lewis-Fluoroacid Mixtures (Publication 5)

C. Shen, R. Hagiwara, T.E. Mallouk, and N. Bartlett

Xenon and F_2 can interact to yield Xe(II) compounds without activation when fluoroacids are present to assist in the heterolytic cleavage of the F_2 and the formation of the energetically favorable $(Xe\text{-}F)^+$ bond.

Xenon and F_2, in liquid AsF_5, at –60°C interact rapidly even in the dark to yield $XeF^+AsF_6^-$. The same reaction, substituting O_2 for Xe, does not proceed to $O_2^+AsF_6^-$. This difference is attributed to the formation of a $(Xe\text{-}F)^+$ bond in a donor-acceptor concerted Xe: $\rightarrow F-F \rightarrow AsF_5$ interaction that simultaneously undoes the F-F bonding, and makes a F-As bond, in a heterolytic cleavage, there being no comparable energetic counterpart of the Xe-F bonding in the $O_2/F_2/AsF_5$ interaction. Even the modest fluoroacid, HF, brings about combination of Xe with F_2 in the dark (at 20°C) to form XeF_2. Evaluation of fluoride-ion affinities and lattice energies gives a quantitative measure of F_2-fluoroacid oxidizing effects. Enthalpy and entropy evaluations account for instability of $O_2^+BF_4^-$ and $O_2^+PF_6^-$ and the thermodynamic stability of $O_2^+AsF_6^-$ and $XeF^+AsF_6^-$ at 20°C.

5. The Preparation of KMF_6 and K_2MF_6 Second and Third Transition Series Salts from the Hexafluorides. (Publication 4)

W.J. Casteel, Jr. and T. Horowitz

High purity syntheses of KMF_6 and K_2MF_6 salts (M = Mo, Ru, Re, Os, Ir), most derived from the hexafluoride, MF_6, are described and their unit cells (and structures) defined, the rhombohedral form of $KReF_6$, isostructural with the other third transition series KMF_6 salts, having been obtained for the first time.

$KMoF_6$, $KReF_6$, $KOsF_6$, and $KIrF_6$ have been prepared in high purity by reduction of the corresponding hexafluorides with KBr in anhydrous hydrogen fluoride (AHF). Further reduction with one equivalent of KI in AHF has afforded high purity K_2MoF_6, K_2ReF_6, K_2OsF_6, and K_2IrF_6. Reduction of $KRuF_6$ with KBr has produced pure K_2RuF_6. $KReF_6$ has now been shown to crystallize in the rhombohedral $KOsF_6$ type cell, with $a_o = 5.021(3)$Å, $\alpha = 97.16(4)°$, $V = 122.7(3)$Å^3.

Table 5-1 compares the lattice parameters and unit cell volumes for the close-packed hexafluorometallate salts examined. The last row is the volume difference for the KMF_6 and K_2MF_6 pair. Because of its higher charge the MF_6^{2-} ion should be larger than the MF_6^-, hence this difference is probably slightly greater than the effective volume of K^+. The average value of 14.7Å^3 is only slightly greater than the sphere volume given by the Pauling radius, which is 13.3Å^3.

Table 5-1. A Comparison of Lattice Parameters and Unit Cell Volumes for Some Close-packed Hexafluorometallate Salts

	Re	Os	Ir	Pt[10],[11]	Ru
KMF_6 a_o(Å)	5.012(4)	4.987(1)	4.9744(7)	4.96	4.968(1)
KMF_6 α(°)	97.15(4)	97.18(1)	97.399(9)	97.4	97.40(1)
KMF_6 V(Å^3)	122.7(3)	120.8(1)	119.72(5)	118.7	119.3(1)
K_2MF_6 a_o(Å)	5.852(2)	5.824(2)	5.798(2)	5.76	5.755(2)
K_2MF_6 c_o(Å)	4.594(3)	4.617(2)	4.617(2)	4.64	4.657(4)
K_2MF_6 V(Å^3)	137.4(2)	135.6(2)	134.4(2)	133.3	133.6(2)
ΔV (Å^3)	14.7	14.8	14.7	14.7	14.3

FY 1992 PUBLICATIONS AND REPORTS

Refereed Journals

1. W.J. Casteel, Jr., A.P. Wilkinson, H. Borrmann, R.E. Serfass, and N. Bartlett, "The Preparation and Structure of Ruthenium Tetrafluoride and a Structural Comparison with Ruthenium Trifluoride and Ruthenium Pentafluoride," Inorg. Chem. **31**, 3124 (1992).
2. W.J. Casteel, Jr., G. Lucier, R. Hagiwara, H. Borrmann, and N. Bartlett, "Structural and Magnetic Properties of Some AgF^+ Salts," J. Solid State Chem. **96**, 84 (1992).
3. M. Lerner, R. Hagiwara, and N. Bartlett, "Synthesis of Main-Group Graphite Fluoroanion Salts with Chlorine-Assisted Oxidation by Lewis-Acid Fluorides," J. Fluorine Chem. **57**, 1 (1992).
4. W. Casteel, Jr. and T. Horowitz, "The Preparation of KMF_6 and K_2MF_6 Second and Third Transition Series Salts from the Hexafluorides," European J. of Solid State and Inorg. Chem. **29**, 649 (1992).

LBL Reports

5. C. Shen, R. Hagiwara, T.E. Mallouk, and N. Bartlett, "Some Thermodynamic Aspects of the Remarkable Oxidizing Capabilities of Fluorine/Lewis-Fluoroacid Mixtures," to be published in Advances in Chemistry Series, Fluorine and Fluorine-Containing Substituent Groups; LBL-31263.
6. G. Lucier, C. Shen, L. Chacon, W.J. Casteel Jr., and N. Bartlett, "The Remarkable Oxidizing Capabilities of Cationic Ag(III) and Ni(IV) in Anhydrous Hydrogen Fluoride Solutions"; LBL-33690.
7. B. Žemva, C. Shen, G. Lucier, J. Allman, and N. Bartlett, "Salts of the Lattice Cation $(AgF_2)_3^+$, a Potent Oxidizer and Possible Metal"; LBL-33691.
8. W.J. Casteel, Jr., C. Shen, G. Lucier, and N. Bartlett, "The Oxidizing Properties of Cationic Ag(II) in Anhydrous Hydrogen Fluoride"; LBL-33692.
9. N. Bartlett, Bonner Chemiepreis Lecture, "Some Advances in High Oxidation-State Fluorine Chemistry of the Past Forty Years," October 19, 1992, Bonn, Germany, LBL-33612.

Invited Talks

10. N. Bartlett, "High Oxidation-State Silver Fluoride Chemistry," Simon Fraser University, Burnaby, British Columbia, Canada, January 15, 1992.
11. N. Bartlett, "Remarkable Oxidizing Capabilities of Fluorine/Lewis-Fluoroacid Mixtures," Fluorine Symposium at the Spring American Chemical Society National Meeting, San Francisco, CA, April 6, 1992.
12. N. Bartlett, "The Fluorides of Silver," at the Gordon Conference on Solid-State Chemistry, Plymouth, NH, July 31, 1992.

Catalytic Hydrogenation of CO*

Alex T. Bell, Investigator

INTRODUCTION

The purpose of this program is to develop an understanding of the fundamental processes involved in the catalytic conversion of carbon monoxide and hydrogen to gaseous and liquid fuels. Attention is focused on defining the factors that limit catalyst activity, selectivity, and resistance to poisoning, and the relationship between catalyst composition/structure and performance. To meet these objectives, a variety of surface diagnostic techniques are used to characterize supported and unsupported catalysts before, during, and after reaction. The information thus obtained is combined with detailed studies of reaction kinetics to elucidate reaction mechanisms and the influence of modifications in catalyst composition and/or structure on the elementary reactions involved in carbon monoxide hydrogenation.

1. An Infrared Study of the Interactions of CO and CO_2 with Cu/SiO_2 (Publication 6)

D.B. Clarke, I Suzuki, and A.T. Bell

The adsorption of CO and CO_2 on Cu/SiO_2 have been investigated by means of infrared spectroscopy. CO adsorbs on Cu with a heat of adsorption of 8.4 kcal/mol, whereas CO_2 weakly adsorbs on both Cu and SiO_2 with a heat adsorption of 6.9 kcal/mol. As much as 24% of the adsorbed CO_2 is associated with Cu and the rest, with the silica support. On freshly reduced Cu/SiO_2, adsorbed CO exhibits an infrared band 2103 cm^{-1}, whereas CO_2 exhibits a band at 2340 cm^{-1} when adsorbed on both SiO_2 and Cu surfaces. A band at 2118 cm^{-1} is also observed during CO_2 exposure. This feature is attributable CO associated with Cu^+ formed via the dissociation of CO_2 into CO_s and O_s. The extent of CO_2 dissociation on Cu is measured to be about 20%. During CO_2 exposure the coverage of adsorbed CO increases rapidly, goes through a maximum, and then decays. This transient is attributable to the competition of CO and CO_2 for Cu sites. The effects on the CO_2 dissociation transient of temperature, pressure, space velocity, catalyst preoxidation, and H_2 addition can be explained with the proposed mechanism.

*This work was supported by the Director, Office of energy Research, Office of Basic Energy, Chemical Sciences Division, of the U.S. Department of Energy under Contract No. DE-AC03-76SF00098.

2. Temperature-Programmed Desorption Studies of the Interaction of H_2, CO, and CO_2 with Cu/SiO_2 (Publication 7)

M.J. Sandoval and A.T. Bell

The interactions of H_2, CO, and CO_2 with a Cu/SiO_2 catalyst have been investigated using temperature-programmed desorption spectroscopy. The heat of adsorption of H_2 and CO were obtained from an analysis of the experimentally observed spectra. The activation energy for H_2 adsorption was obtained from isothermal measurements of the adsorption rate. The heat of adsorption of H_2 is found to increase from 10.1 to 13.8 kcal/mol from $0.007 \leq \theta_H \leq 0.26$. The activation energy for H_2 adsorption is found to be 10.5 kcal/mol and the activation energy for the desorption of H_2 is found to increase from 20.6 to 24.3 kcal/mol for $0.07 \leq \theta_H \leq 0.26$. The heat adsorption of CO decreases from 16.4 to 12.5 kcal/mol for $0.01 \leq \theta_{CO} \leq 0.18$. The coverage by molecularly adsorbed CO_2 was below the detectable limits for adsorption temperatures above 250 K. Evidence was found, however, for a small amount of dissociatively adsorbed CO_2. The present findings are in very good agreement with recent studies on Cu single crystal surfaces, and in particular for Cu(110) and Cu(311) surfaces.

3. Mechanistic and Dynamic Studies of Methanol Decomposition on Cu/SiO_2 (Work in Progress)

D.B. Clarke, I. Suzuki, D.-K. Lee, M. Sandoval, and A.T. Bell

The mechanism and dynamics of methanol decomposition over a Cu/SiO_2 catalyst are being investigated by combined temperature-programmed infrared spectroscopy and temperature-programmed desorption spectroscopy. This approach makes possible the simultaneous observation of species on the surface and in the gas phase and thereby provides a level of mechanistic detail not previously possible. At room temperature, methanol is found to adsorb molecularly on Cu. As the temperature is elevated, infrared bands appear that are attributable to methoxide groups, CH_3O. The dissociative adsorption of methanol is accompanied by the desorption of methanol. At somewhat higher temperatures, formaldehyde appears in the gas phase. The infrared spectra taken at this stage reveal the presence of first of bis-methyleneoxy groups, $(CH_2)OO$, followed by adsorbed formaldehyde. The decomposition of methanol is accompanied by the appearance of bidentate formate groups, HCOO. Finally, above 450 K, CO_2, and H_2 are released into the gas phase in 1:1 proportions, as the formate groups undergo

decomposition. Work currently in progress focuses on the effects of Cu preoxidation and the influence of H_2O adsorption on the pathway of methanol decomposition.

4. Effects of Olefin Reabsorption on the Dynamics of Chain Propagation and Termination during Fischer-Tropsch Synthesis over Ru/TiO_2 (Work in Progress)

T. Komaya and A.T. Bell

The dynamics of chain growth and termination during Fischer-Tropsch synthesis over Ru were investigated using transient-response isotopic-tracer techniques. Of particular significance was to establish whether the rate coefficients determined from such experiments are independent of carbon number. During the course of these experiments it was observed that both the steady-state product distribution and the time constants of the transient response associated with each product is a function of the residence time of the reactants over the catalyst. Analysis reveals that these effects are attributable to the physisorption of olefins on the support and their subsequent surface diffusion to the particles of dispersed Ru. Simulation of the experimentally observed transients using a model that incorporates the effects of physisorbed olefins on the initiation of chain growth results in the determination of rate coefficients for chain propagation and termination, a result not achievable using previously published models of the Fischer-Tropsch process. Work is currently in progress to determine the effects of Ru particle size on the intrinsic rate coefficients for chain initiation, propagation, and termination.

5. Raman Studies of the Structure of Niobia Dispersed on Titania (Work in Progress)

R. Pittman and A.T. Bell

The structure of niobia dispersed on the anatase phase of titania is being investigated by means of Raman spectroscopy. In contrast to earlier work with vanadia, niobia is found to agglomerate more readily even at relatively low loadings. Raman spectroscopy reveals that only for loadings of 1% Nb, or less, is evidence found for isolated niobyl species, or oligomers of such species. At higher loadings, amorphous niobia is formed. Calcination of the dispersed niobia shows that the amorphous niobia is stable to 773 K, but above this temperature is gradually transformed in to the TT, T, and finally H phases of crystalline Nb_2O_5. Calcination at temperatures between 973 K and 1073 K results in the formation of only a small amount of rutile, in contrast to what is observed if pure anatase is calcined. The structural stabilization of the support is attributed to the formation of an Nb-O-Ti phase, observable by XRD. The interactions of dispersed niobia with H_2, H_2O, and NH_3 at elevated temperatures is currently under investigation.

FY 1992 PUBLICATIONS AND REPORTS

Refereed Journals

1. G.T. Went, L.-J. Leu, and A.T. Bell, "Quantitative Structural Analysis of Dispersed Vanadia Species in TiO_2(Anatase)-Supported V_2O_5," J. Catal. **134**, 479 (1992); LBL-30656.
2. G.T. Went, L.-J. Leu, S.J. Lombardo, and A.T. Bell, "Raman Spectroscopy and Thermal Desorption of NH_3 Adsorbed on TiO_2(Anatase)-Supported V_2O_5," J. Phys. Chem. **96**, 2335 (1992); LBL-30568.
3. G.T. Went, L.-J. Leu, R. Rosin, and A.T. Bell, "The Effects of Structure on the Catalytic Activity and Selectivity of V_2O_5/TiO_2 for the Reduction of NO by NH_3," J. Catal. **134**, 492 (1992); LBL-30569.
4. K.R. Krishna and A.T. Bell, "The Role of C_2 Intermediates in Fischer-Tropsch Synthesis over Ruthenium," Catal. Lett. **14**, 305 (1992); LBL-32007.

LBL Reports

5. K.R. Krishna and A.T. Bell, "Estimates of the Rate Coefficients for Chain Initiation, Propagation, and Termination during Fischer-Tropsch Synthesis over Ru/TiO_2," J. Catal. (in press); LBL-31801.
6. D.B. Clarke, I. Suzuki, and A.T. Bell, "An Infrared Study of the Interactions of CO and CO_2 with Cu/SiO_2," J. Catal. (in press); LBL-33129.
7. M.J. Sandoval and A.T. Bell, "Temperature-Programmed Desorption Studies of the Interactions of H_2, CO, and CO_2 with Cu/SiO_2," J. Catal. (submitted); LBL-33564.
8. A.T. Bell, L.E. Manzer, N.Y. Chen, V.W. Weekman, L.L. Hegedus, and C.J. Pereira, "Applications of Catalysis for the Protection of the Environment," Science (submitted); LBL-33460.

Invited Talks

9. A.T. Bell, "Effects of Catalyst Structure on the Performance of V_2O_5/TiO_2 Catalysts for NO Reduction by NH_3," Gas Research Institute Inorganic Chemistry Review, Chicago, IL, October 9, 1991.
10. A.T. Bell, "Applications of the Bond-Order-Conservation-Morse-Potential Approach in the Field of Catalysis," BIOSYM Technologies, Inc., La Jolla, CA, October 24, 1991.

11. A.T. Bell, "Effects of Catalyst Structure on the Performance of V_2O_5/TiO_2 Catalysts for NO Reduction by NH_3," Ethyl Corp., Baton Rouge, LA, November 26, 1991.
12. A.T. Bell, "Design of Fischer-Tropsch Catalysts," ACS Meeting, San Francisco, CA, April 5–10, 1992.
13. A.T. Bell, "Mechanism of Hydrocarbon and Alcohol Synthesis from CO and CO_2," National Taiwan University, Taipei, Taiwan, April 13, 1992.
14. A.T. Bell, "Application of NMR Spectroscopy in Catalysis," National Tsing-hua University, Tsinchu, Taiwan, April 14, 1992.
15. A.T. Bell, "The Effect of Catalyst Structure on the Performance of Titania-Supported Catalysts for SCR of NO," Chinese Petroleum Corp., Chia-Yi, Taiwan, April 16, 1992.
16. A.T. Bell, "The Effects of Catalyst Structure on the Performance of V_2O_5/TiO_2 Catalysts for the Selective Catalytic Reduction of NO_x," Laboratoire de Catalyse Hétérogène et Homogène, Université des Science et Technique de Lile 1, Villeneuve d'Ascq, France, May 20, 1992.
17. A.T. Bell, "The Effects of Catalyst Structure on the Performance of V_2O_5/TiO_2 Catalysts for the Selective Catalytic Reduction of NO_x," Laboratoire de Chimie Organique Appliquée, Ecole Europeéne des Hautes Etudes des Industries Chimiques de Strasbourg, Strasbourg, France, May 17, 1992.
18. A.T. Bell, "Mechanistic Studies of Hydrocarbon and Alcohol Synthesis from CO and CO_2," Laboratoire de Réactivité de Surface et Structure, Université Pierre et Marie Curie, Paris, France, June 2, 1992.
19. A.T. Bell, "The Effects of Catalyst Structure on the Performance of V_2O_5/TiO_2 Catalysts for the Selective Catalytic Reduction of NO_x," Institut de Petrol Francais, Rueil-Malmaison, France, June 3, 1992.
20. A.T. Bell, "The Effects of Catalyst Structure on the Performance of V_2O_5/TiO_2 Catalysts for the Selective Catalytic Reduction of NO_x," Laboratoire de Catalyse et Spectrochimie, Université de Caen, Caen, France, June 5, 1992.
21. A.T. Bell, "The Effects of Catalyst Structure on the Performance of V_2O_5/TiO_2 Catalysts for the Selective Catalytic Reduction of NO_x," Institut de Recherches sur La Catalyse, Villeurbanne, France, June 12, 1992.
22. A.T. Bell, "The Effects of Catalyst Structure on the Performance of V_2O_5/TiO_2 Catalysts for the Selective Catalytic Reduction of NO_x," Laboratoire des Matériaux Minéraux, Ecole Nationale Supérieure de Chimie, Mulhouse, France, June 18, 1992.
23. A.T. Bell, "The Effects of Catalyst Structure on the Performance of V_2O_5/TiO_2 Catalysts for the Selective Catalytic Reduction of NO_x," Laboratoire de Catalyse en Chimie Organique, Université de Poitiers, France, June 23, 1992.
24. A.T. Bell, "Mechanistic Studies of Hydrocarbon and Alcohol Synthesis from CO and CO_2," Laboratoire de Chimie Organique Appliquée, Ecole Europeéne des Hautes Etudes des Industries Chimiques de Strasbourg, Strasbourg, France, June 26, 1992.
25. A.T. Bell, Langmuir Lecture: "Relationships between the Structure and Performance of Heterogeneous Catalysts," ACS Meeting, Washington, DC, August 23–28, 1992.
26. A.T. Bell, "Isotropic Tracer Studies of Oxygen Exchange on Silica-Supported Cu," AIChE Annual Meeting, Los Angeles, CA, November 21, 1991.
27. A.T. Bell, "The Influence of Vanadia Structure on the Activity and Selectivity of V_2O_5/TiO_2 Catalysts for NO Reduction by NH_3, AIChE Annual Meeting, Los Angeles, CA, November 21, 1991.
28. A.T. Bell, "Infrared Study of CO_2 Adsorption and Dissociation on Cu/SiO_2," The California Catalysis Society Meeting, Menlo Park, CA, April 2–3, 1992.
29. A.T. Bell, "Isotopic Tracer Studies of Chain Propagation and Termination during Fischer-Tropsch Synthesis over Ru/TiO_2," 10th International Congress on Catalysis, Budapest, Hungary, July 19–24, 1992.
30. A.T. Bell, "Isotopic Tracer Studies of the Kinetics of CO and CO_2 Hydrogenation," Mitsubishi Kasei, Yokohama, Japan, September 21, 1992.

Transition Metal Catalyzed Conversion of CO, NO, H_2 and Organic Molecules to Fuels and Petrochemicals*

Robert G. Bergman, Principal Investigator

INTRODUCTION

The goals of this program are the development of new chemical reactions in which transition metals interact with organic materials and the understanding of how these reactions work. A recent discovery on this project was the finding that certain cyclopentadienyliridium and -rhodium complexes undergo oxidative addition into the carbon-hydrogen bonds of completely saturated hydrocarbons (M + R–H → R–M–H). This finding was the first example of a long-sought "alkane C–H activation" reaction; research is now being directed at examining the scope, selectivity, and mechanism of the process, extending it to other systems, and developing ways to convert the activated metal complexes X–M–H into functionalized organic molecules. During the current year, progress was made in two areas. In the first, the highly reactive, unsolvated C-H activating intermediate $(\eta^5\text{-}C_5H_5)Rh(CO)_2$ was detected spectroscopically in the gas phase, and the rate of its reaction with alkanes and other molecules was directly determined. In the second project, progress was made on the synthesis of C-H activating iridium complexes containing an indenyl rather than a cyclopentadienyl ligand, as an approach to the development of methods for converting alkanes into functionalized organic molecules.

1. Gas-Phase Rates of Alkane C-H Oxidative Addition to a Transient CpML Complex (Publication 1)

E.P. Wasserman, C.B. Moore, and R.G. Bergman

Because alkanes and alkyl chains make up a large percentage of natural materials, there is an incentive to develop methods for converting these unactivated C-H bonds into more reactive, and therefore useful, organic functional groups. Several years ago it was discovered in this laboratory that irradiation of complexes having the general formula $Cp(L)MH_2$ (where Cp is an abbreviation for the five-membered ring π-bound ligand $\eta^5\text{-}C_5H_5$ or $\eta^5\text{-}C_5(CH_3)_5$, L represents a trialkylphosphine ligand, and the metal M is iridium) leads to the generation of a reactive intermediate, presumed to have the formula CpML. This species is capable of undergoing oxidative addition into the carbon-hydrogen bonds of simple alkanes (Eq. (1)).

$$CpML + R\text{-}H \rightarrow Cp(L)M(R)(H) \qquad (1)$$

More recently it was shown that the complexes of general structure $CpRhL_2$ also undergo this reaction via the intermediates CpRhL. In the present study the gas-phase irradiation of $CpRh(CO)_2$ was examined using a time-resolved infrared laser system capable of detecting the infrared (IR) spectra of transient species and measuring their rapid rates of decay. "Naked" (unsolvated) CpRh(CO), having a carbonyl stretching absorption band at 1985 cm^{-1}, was detected, and direct measurements of the rates of reaction of this very short-lived complex with alkane carbon-hydrogen bonds were made. Figure 1-1 illustrates typical transient digitizer traces for the decay of CpRh(CO) (compound **2** in Figure 1-2) in the gas phase containing argon and the hydrocarbon neopentane and the concomitant rise of absorption at 2037 cm^{-1} due to the formation of the C-H activation product Cp(CO)Rh(neopentyl)(H) (4, R = $CH_2C(CH_3)_3$). The data in Table 1-1 summarize the rate constants measured for reaction of CpRh(CO) with CO, H_2, alkanes, and isotopically substituted molecules D_2 and CD_4. Also tabulated are the efficiencies of these reactions (i.e., the fraction of collisions that result in conversion to product). The most dramatic aspect of these data is that all of the rates are within an order of magnitude of the calculated gas-kinetic values. Therefore, reactions are occurring (even in the case of H-H and C-H oxidative addition) on nearly

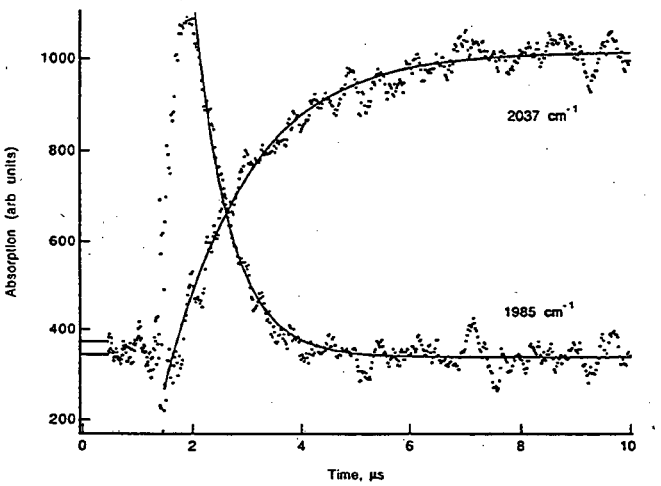

Figure 1-1. Transient absorption traces taken at 1985 and 2037 cm^{-1} that follow the decay of CpRh(CO) and the formation of $Cp(CO)Rh[CH_2C(CH_3)_3](H)$, respectively, from the reaction of CpRh(CO) with neopentane. Pressure of gases: 12.6 torr Ar and ~0.08 torr neopentane. The shock wave transients were removed from these traces. (XBL 939-4563)

*This work was supported by the Director, Office of Energy Research, Office of Basic Energy Sciences, Chemical Sciences Division of the U.S. Department of Energy under Contract No. DE-AC03-76SF00098.

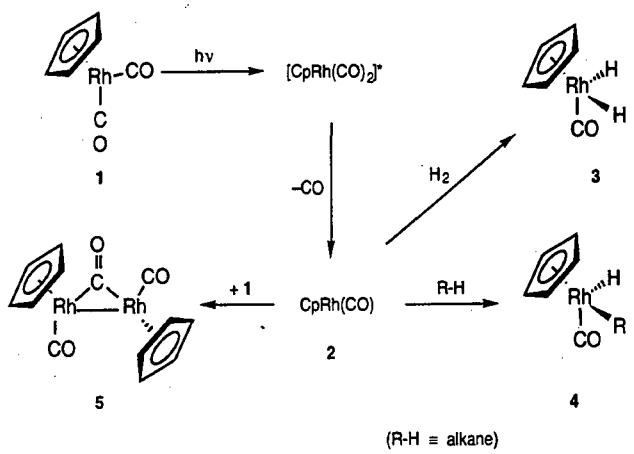

Figure 1-2. Proposed reactions occurring during the gas-phase photolysis of $Cp^*Rh(CO)_2$. (XBL 939-4564)

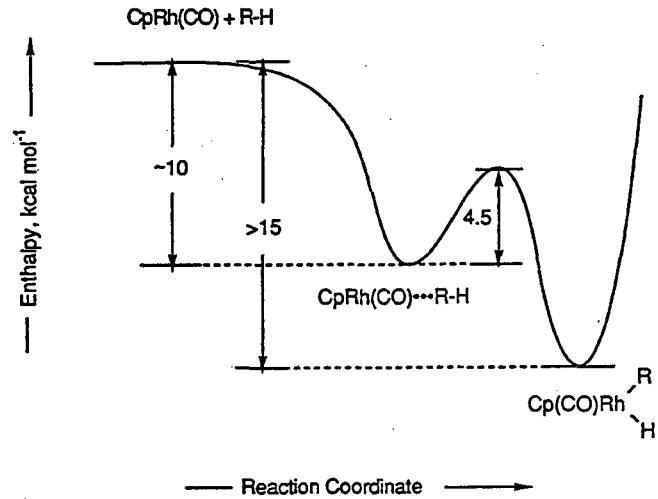

Figure 1-3. Proposed reaction coordinate diagram for the gas-phase reaction of CpRh(CO) with alkane R-H to give oxidative addition product Cp(CO)Rh(R)(H). Estimated energy differences are based on both solution and gas-phase determinations. (XBL 939-4565)

every collision. Also notable is the fact that the rate of reaction with alkanes increases with increasing size of the hydrocarbon.

The reaction coordinate diagram illustrated in Fig. 1-3 is proposed to account for both the rapid rates of reaction measured here and the ~4.5 kcal/mole barrier measured earlier for the cyclohexane and neopentane complex-to-alkyl hydride reactions measured in liquid krypton solvent. As one follows the reaction path from left to right, the system passes from the separated reactants to a pair of potential wells. The first well represents the energy of the σ-type alkane complex postulated earlier, and the second is the alkyl hydride Rh(III) C-H oxidative addition product. The first stage of the reaction is the formation of a collision complex between CpRhCO and the alkane. In the experimentally demonstrated high-pressure limit, this complex undergoes vibrational deactivation at approximately the gas-kinetic collision rate (about $9 \times 10^7 s^{-1}$ at 10 torr Ar) and little redissociation of the initially formed, vibrationally excited alkane complex to CpRhCO and free alkane occurs. At pressures sufficient to cause vibrational deactivation of the initial rhodium-alkane complex, formation of the complex is the rate-determining step of the reaction. If there is little or no barrier to this initial reaction step (which seems reasonable), the overall process may occur at or near the gas-kinetic rate, as is observed.

Table 1-1. Rate constants for reactions of CpRh(CO)

Reactant	k_{obsd} (10^{10} $cm^3molec^{-1}s^{-1}$)[a]	Efficiency[b]
CO	1.5 ± 0.3	0.43
H_2	1.6 ± 0.3	0.17
D_2	1.6 ± 0.7	0.22
CH_4	0.58 ± 0.26	0.14
CD_4	0.47 ± 0.10	0.11
C_2H_6	1.8 ± 0.5	0.49
$C(CH_3)_4$	2.1 ± 0.6	0.60
c-C_6H_{12}	2.8 ± 0.9	0.82

[a]All rate constants were calculated by averaging at least 20 runs; errors are quoted as the standard deviation of these independent measurements.
[b]Fraction of gas-kinetic value.

2. Synthesis and C-H Activation Reactions of η^5-Indenyl(trimethylphosphine)iridium Alkyl and Hydride Complexes (Publication 2)

T. Foo and R.G. Bergman

A primary goal of research on alkane carbon-hydrogen bond activation is the development of methods for the conversion of the alkyl(hydrido)metal complexes formed on C-H oxidative addition into functionalized organic compounds. To obtain C-H oxidative addition products susceptible to further chemical transformation, the synthesis of a series of indenyliridium complexes that parallel the pentamethylcyclopentadienyl systems shown earlier to successfully activate alkane carbon-hydrogen bonds have been developed. Efficient routes to several members of the series (η^5-C_9H_7)Ir(PMe_3)(X)(Y), where X and Y are alkyl, aryl, and hydride ligands, are described. The structure of the (methyl)(phenyl)iridium complex (η^5-C_9H_7)Ir(PMe_3)(CH_3)(Ph) (**4b**, Figure 2-1) has been determined by x-ray diffraction. In spite of the increased

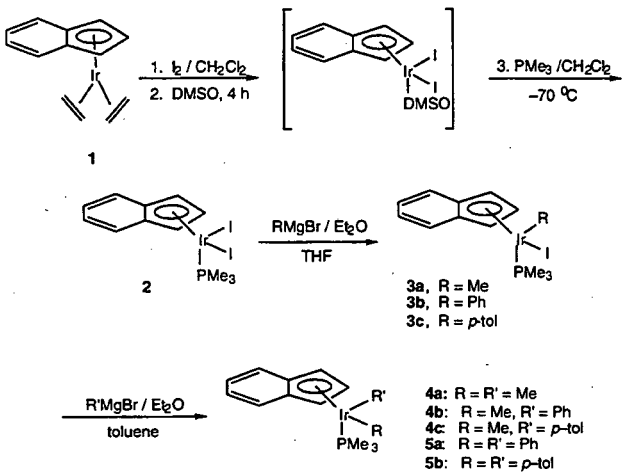

Figure 2-1. Synthesis of indenyliridium complexes. (XBL 939-4566)

liability of these complexes caused by the presence of the indenyl ligand, they retain both the thermal and photochemical C-H activating properties associated with the corresponding pentamethylcyclopentadienyl complexes. Thus as shown in Figure 2-2, $(\eta^5\text{-}C_9H_7)Ir(PMe_3)H_2$ (**7**)

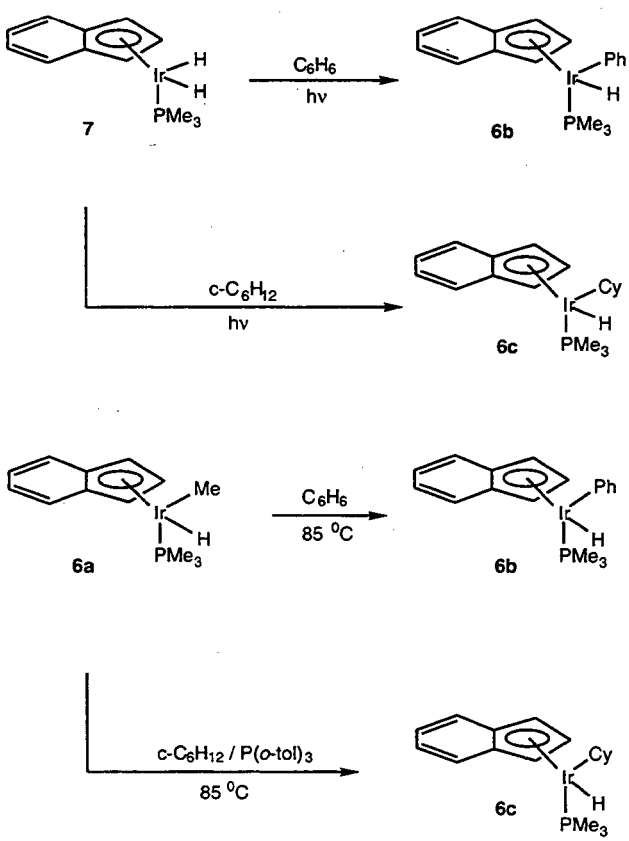

Figure 2-2. C-H activating reactions of indenyliridium complexes. (XBL 939-4567)

undergoes loss of H_2 on irradiation, and in benzene and cyclohexane solvent leads to $(\eta^5\text{-}C_9H_7)Ir(PMe_3)(C_6H_5)(H)$ (**6b**) and $(\eta^5\text{-}C_9H_7)Ir(PMe_3)(C_6H_{11})(H)$ (**6c**), respectively. Thermolysis of $(\eta^5\text{-}C_9H_7)Ir(PMe_3)(CH_3)(H)$ (**6a**) occurs to eliminate methane at lower temperature than its $\eta^5\text{-}C_5(CH_3)_5$ analogue, and in benzene and cyclohexane once again leads successfully to the phenyl and cyclohexyl hydrides **6b** and **6d**.

3. Migratory Insertion Reactions of Indenyliridium Dialkyls and Alkyl and Aryl Hydrides (Publication 3)

T. Foo and R.G. Bergman

Complexes of general formula $(\eta^5\text{-Ind})(PMe_3)Ir(R)(R')$ (R = alkyl or aryl and R' = alkyl, aryl or hydride; compounds **4**, **5**, **6** illustrated in Figure 3-1), whose syntheses are described in the previous section, react with dative ligands L such as t-butylisonitrile and CO. These transformations lead to η^5 to η^1 isomerization of the

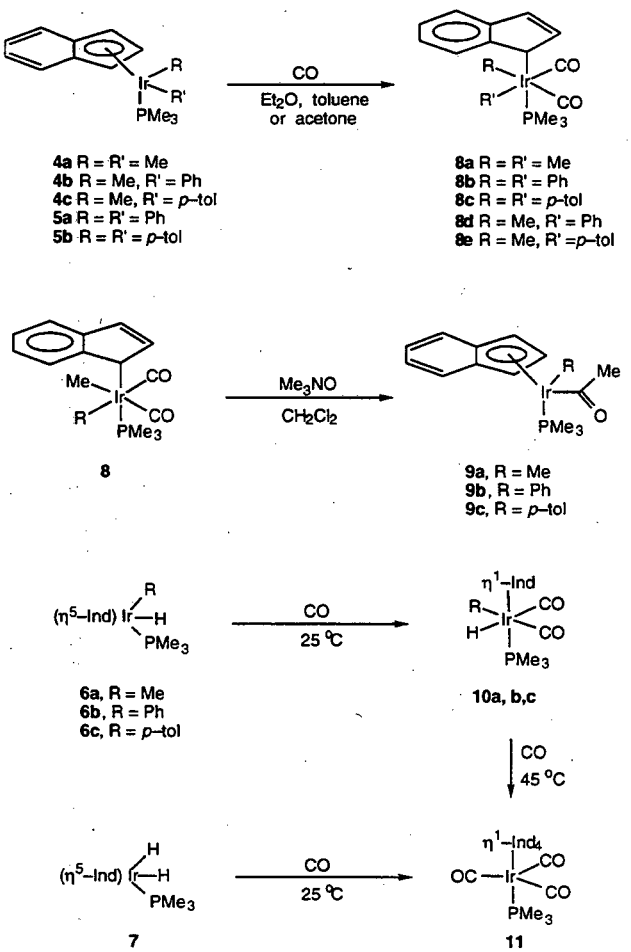

Figure 3-1. CO migratory insertion and alkane reductive elimination reactions of indenyliridium complexes. (XBL 939-4568)

indenyl ligand, giving octahedral iridium complexes of general formula (η^1-Ind)(PMe_3)$(L)_2$Ir(R)(R') (**8, 9, 10**). Treatment of the methyl aryl and dimethyl η^1-indenyl complexes **8a, 8d**, and **8e** with trimethylamine oxide removes CO, allowing the indenyl ligand to re-establish η^5-coordination by inducing CO migratory insertion to give acyl complexes **9**. Reaction of η^1-indenyl, aryl, and methyl hydrides **6** (as well as the dihydride (η^5-Ind)(PMe_3)IrH_2 (**7**)) with CO leads to reductive elimination of arene or H_2 rather than migratory insertion, forming (η^1-Ind)$(CO)_3$(PMe_3)Ir (**11**) as the organometallic product. In contrast, as shown in Figure 3-2 treatment of methyl hydride **6a** with alkynes leads to the methyl vinyl complexes (η^5-Ind)(PMe_3)Ir(Me)(CR=C(R')(H)) (**12**) and reaction of **6a** with ethylene gives the methyl ethyl complex (η^5-Ind)(PMe_3)Ir(Me)(Et) (**13**). Isotope labeling, stereochemistry and kinetic studies have been carried out on the insertion reaction of **6a** with 3,3-dimethyl-1-butyne. The results of these experiments are most consistent with the mechanism of the reaction of **6a** with t-butylacetylene to give **12b** illustrated in Figure 3-3. This involves initial reversible coordination of alkyne to the metal center (probably with concurrent η^5-η^3 isomerization of the indenyl ligand, giving **14**) followed by irreversible migration of the metal-bound hydrogen to the t-butyl substituted carbon of the alkyne and then rapid re-coordination of the indenyl group.

4. Work in Progress

Research is in progress in the following areas: (1) expansion of time-resolved infrared studies of the fast reactions of several C-H activating intermediates in liquid xenon and liquid krypton solutions, using a new spectrometer equipped with a diode probe laser; (2) attempts to utilize complexes known to undergo C-H activation of alkanes to carry out C-F activation of

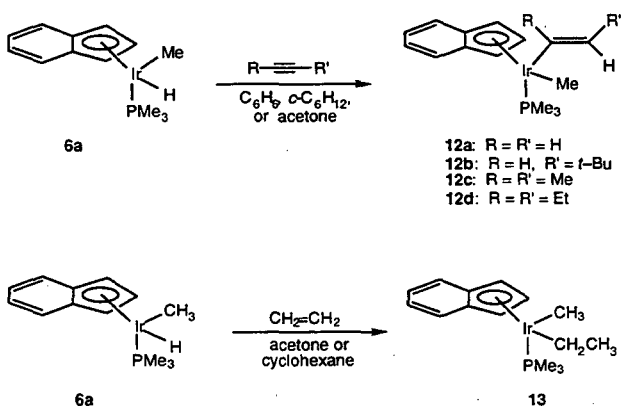

Figure 3-2. Alkyne and ethylene migratory insertion reactions. (XBL 939-4569)

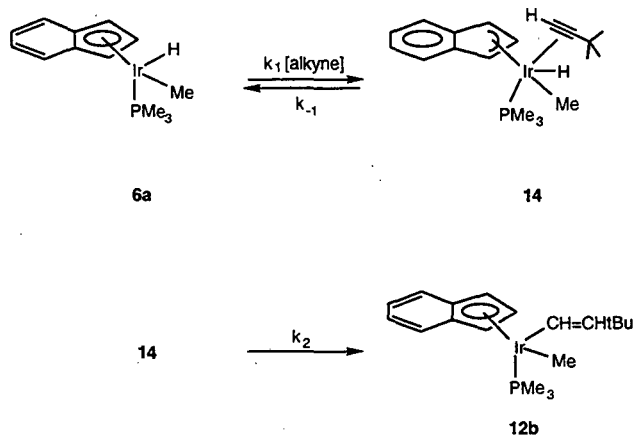

Figure 3-3. Proposed mechanism of t-butylacetylene migratory insertion reaction. (XBL 9311-4584)

fluorocarbons; (3) studies of new iridium-based C-H activation systems involving the conversion of Ir(III) to Ir(V) rather than Ir(I) to Ir(III); (4) synthesis of C-H activation precursors that are stereospecifically labeled with deuterium to investigate the role played by alkane complexes in solution C-H activation reactions.

FY 1992 PUBLICATIONS AND REPORTS

Refereed Journals

1. E.P. Wasserman, C.B. Moore, R.G. Bergman, "Gas-Phase Rates of Alkane C-H Oxidative Addition to a Transient CpRh(CO) Complex," Science **255**, 315 (1992); LBL-31099.
2. T. Foo and R.G. Bergman, "Synthesis and C-H Activation Reactions of η^5-Indenyl(tri-methylphosphine)iridium Alkyl and Hydride Complexes," Organometallics **11**, 1801 (1992); LBL-31249.
3. T. Foo and R.G. Bergman, "Migratory Insertion Reactions of Indenyliridium Dialkyls and Alkyl and Aryl Hydrides," Organometallics **11**, 1811 (1992); LBL-31250.

Other Publications

4. R.G. Bergman, "Activation of Carbon-Hydrogen Bonds in Alkanes and Other Organic Molecules Using Organotransition Metal Complexes" *Homogeneous Transition Metal Catalyzed Reactions*; W.R. Moser, D.W. Slocum, Eds., Am. Chem. Soc., Washington, D.C. (1992), p. 211.

Invited Talks

5. R.G. Bergman, "Stoichiometric and Catalytic Carbon-Nitrogen Bond Forming Reactions Mediated by

Organotransition Metal Imido Complexes," University of Iowa, Iowa City, October 25, 1991.

6. R.G. Bergman, "Stoichiometric and Catalytic Carbon-Nitrogen Bond Forming Reactions Mediated by Organotransition Metal Imido Complexes," Princeton University, Princeton, NJ, November 6, 1991.
7. R.G. Bergman, "Using Kryptochemistry to Deal with Xenophobia: Alkane C-H Activation in Liquefied Noble Gas Solvents," Frontiers in Chemical Research Lecture Series, Texas A&M University, College Station, TX, November 11, 1991.
8. R.G. Bergman, "Stoichiometric and Catalytic Reactions of Early-Late Heterobinuclear Transition Metal Complexes," Frontiers in Chemical Research Lecture Series, Texas A&M University, College Station, TX, November 12, 1991.
9. R.G. Bergman, "Synthesis, Chemistry, and Hydrogen Bonding Properties of Complexes with Transition Metal-Heteroatom Bonds," Frontiers in Chemical Research Lecture Series, Texas A&M University, College Station, TX, November 13, 1991.
10. R.G. Bergman, "Stoichiometric and Catalytic Carbon-Nitrogen Bond Forming Reactions Mediated by Organotransition Metal Imido Complexes," Frontiers in Chemical Research Lecture Series, Texas A&M University, November 14, 1991.
11. R.G. Bergman, "Stoichiometric and Catalytic Carbon-Nitrogen Bond Forming Reactions Mediated by Organotransition Metal Nitrene Complexes," Ralph Hirschmann Lecture Series, University of Wisconsin, Madison, February 17, 1992.
12. R.G. Bergman, "Stoichiometric and Catalytic Reactions of Early-Late Heterobinuclear Transition Metal Complexes," Ralph Hirschmann Lecture Series, University of Wisconsin, Madison, February 18, 1992.
13. R.G. Bergman, "Synthesis, Chemistry, and Hydrogen Bonding Properties of Complexes with Transition Metal-Heteroatom Bonds," Ralph Hirschmann Lecture Series, University of Wisconsin, Madison, February 20, 1992.
14. R.G. Bergman, "Stoichiometric and Catalytic Carbon-Nitrogen Bond Forming Reactions Mediated by Organotransition Metal Nitrene Complexes," Colorado State University, Fort Collins, February 24, 1992.
15. R.G. Bergman, "Stoichiometric and Catalytic Carbon-Nitrogen Bond Forming Reactions Mediated by Organotransition Metal Imido Complexes," Frontiers in Chemistry Lecture Series, Scripps Research Institute, La Jolla, CA, March 5, 1992.
16. R.G. Bergman, "Stoichiometric and Catalytic Carbon-Nitrogen Bond Forming Reactions Mediated by Organotransition Metal Nitrene Complexes," Shell Development Company, Houston, TX, March 23, 1992.
17. R.G. Bergman, "Selective Transformations of Organic Compounds Mediated by Transition Metal Complexes," ACS Meeting, San Francisco, CA, April 7, 1992.
18. R.G. Bergman, "Activation of Carbon-Hydrogen Bonds in Alkanes and Other Organic Molecules Using Organotransition Metal Complexes," ACS Meeting, San Francisco, CA, April 9, 1992.
19. R.G. Bergman, "Stoichiometric and Catalytic Reactions of Transition Metal Nitrene Complexes with Organic Compounds," University of Chicago, Chicago, IL, April 24, 1992.
20. R.G. Bergman, "Stoichiometric and Catalytic Carbon-Nitrogen Bond Forming Reactions Mediated by Organotransition Metal Imido Complexes," Cornell University, Ithaca, NY, April 27, 1992.
21. R.G. Bergman, "Stoichiometric and Catalytic Carbon-Nitrogen Bond Forming Reactions Mediated by Organotransition Metal Nitrene Complexes," Karl Pfister Lecture, Massachusetts Institute of Technology, Cambridge, MA, April 28, 1992.
22. R.G. Bergman, "Transition Metal Catalyzed Conversion of CO, NO, H*2 and Organic Molecules to Fuels and Petrochemicals," Department of Energy Peer Review, Washington, D.C., May 13, 1992.
23. R.G. Bergman, "Selective Transformations of Organic Compounds Mediated by Transition Metal Complexes," Eastman Kodak, Rochester, NY, June 11, 1992.
24. R.G. Bergman, "Stoichiometric and Catalytic Reactions of Organotransition Metal Nitrene Complexes," Union Carbide, South Charleston, WV, June 15, 1992.
25. R.G. Bergman, "The Use of Organotransition Metal Complexes in the Formation and Cleavage of Carbon-Carbon, Carbon-Hydrogen, and Carbon-Heteroatom Bonds," Gordon Conference on Organometallic Chemistry, Newport, RI, July 27, 1992.
26. R.G. Bergman, "Activation of C-H and Other Bonds in Organic Molecules Using Soluble Transition Metal Complexes," Amoco Oil Company, Naperville, IL, August 20, 1992.

Formation of Oxyacids of Sulfur from SO_2*

Robert E. Connick, Investigator

INTRODUCTION

The research is concerned with the basic chemistry of inorganic sulfur species in aqueous solution. Sulfur dioxide produced in coal-burning power plants is the major source of acid rain. Currently the primary method of removing it from flue gas is by absorption into aqueous scrubber solutions as bisulfite ion, which can undergo oxidation by oxygen in the water. The present research is focused on understanding the kinetics and mechanism of oxidation of bisulfite ion by oxygen—a reaction of importance not only in flue gas desulfurization but also in the formation of sulfuric acid from sulfur dioxide in atmospheric water droplets.

1. Work in Progress

In the study of the chain reaction of oxygen with bisulfite ion convincing evidence was found for the species peroxymonosulfate ion as an intermediate in the reaction. Its fate is to react with bisulfite ion to give ultimately two sulfate ions and two hydrogen ions. The study of this latter reaction in the pH region 3.75 to 7.9 has now been completed. From the results it is possible to calculate the steady state concentration of HSO_5^- in the O_2-HSO_3^- reaction. For example, with oxygen present and at 25°C, 0.008 M HSO_3^-, and pH 4.50 the concentration of HSO_5^- is calculated to be 1.3×10^{-7} M. This concentration is much too small to be detected directly, yet all of the atoms of the O_2 pass through this species, and it plays a key role in the initiation reaction of the chain and in the formation of a second intermediate, $S_2O_7^{2-}$.

A study of the effect of inhibitors on the reaction previously led to important insights regarding the mechanism of the O_2-HSO_3^- reaction. A remarkably abrupt decrease in rate with increasing concentration of inhibitor was observed for methanol, ethanol, and 2-propanol, but not for tertiary butyl alcohol. The same effect is found with arsenious acid. In the case of both 2-propanol and arsenious acid, the rate of reaction becomes dependent on the oxygen concentration with the most unusual result that the rate decreases as the oxygen concentration increases, even though the overall reaction consumes oxygen. In an experiment where the rate had been decreased about 30 fold by the addition of arsenious acid, permitting the oxygen concentration to drop four fold brought the rate back nearly to its original value. The rate without any arsenious acid present does not depend on the oxygen concentration.

Thiosulfate ion also inhibits the O_2-HSO_3^- reaction; the rate is cut in half by the addition of 5×10^{-8} M $S_2O_3^{2-}$ under the following conditions: 0.010 M HSO_3^-, 1.6×10^{-4} M O_2, pH 4.50, and 25°C. The rate of reaction does not appear to depend on the oxygen concentration and the sharp fall-off with increasing inhibitor concentration is not observed. As the reaction proceeds the rate gradually increases back to the value with no thiosulfate present, showing that the inhibitor is being destroyed. This opens the possibility of measuring a lower limit for the chain length of the reaction.

FY 1992 PUBLICATIONS AND REPORTS

LBL Reports

1. E. Connick, S. Lee, and R. Adamic, "Kinetics and Mechanisms of the Oxidation of HSO_3^- by HSO_5^-," LBL-32424.

*This work was supported by the Director, Office of Energy Research, Office of Basic Energy Sciences, Chemical Sciences Division, of the U.S. Department of Energy under Contract No. DE-AC03-76SF00098.

Potentially Catalytic and Conducting Polyorganometallics*

K. Peter C. Vollhardt, Investigator

INTRODUCTION

Soluble organotransition metal clusters have great potential as catalysts for known and new organic transformations, and as building blocks for novel electronic materials. While much is known about how such clusters are assembled and disassembled, their chemistry is largely unpredictable and/or uncontrollable. This project constitutes an interdisciplinary approach to the designed construction of polymetallic arrays, anchored rigidly on novel π-ligands that enforce hitherto unprecedented metallic topologies. For this purpose, new synthetic organic methodology has been developed that allows the stepwise chemo-, regio-, and loco- (i.e., identity of the metal sequence in heterometallic systems) specific building-up of cluster-chains. Many of their physical and chemical properties are unparalleled and include: extreme ligand deformations, highly strained metal-metal bonds, intramolecular organic fragment migrations, intrachain electron transfers, and thermally reversible photochemical storage processes.

1. Hexabutadiynylbenzene: A Remarkable Potential π-Ligand (Publication 5)

R. Boese,† J.R. Green, J. Mittendorf, D.L. Mohler, and K.P.C. Vollhardt

Hexaalkynylbenzenes are of interest as novel discotic liquid crystals and precursors to new organic solids with unusual properties (hardness, thermal and electric conductivity, lubrication). They are new, very electron-rich, reactive hydrocarbons with high C/H ratios. In synthesis they are precursors to allotropes of carbon, such as C_{60}, substrates in CpCo-catalyzed cocyclizations with monoalkynes on route to multiphenylenes, and potential multidentate ligands to transition-metal clusters. Along these lines, hexabutadiynylbenzene **1d** was deemed a particularly attractive target, because it is the first $C_{30}H_6$ hydrocarbon and it contains 54(!) conjugated π-electrons, which might give rise to unusual spectral properties

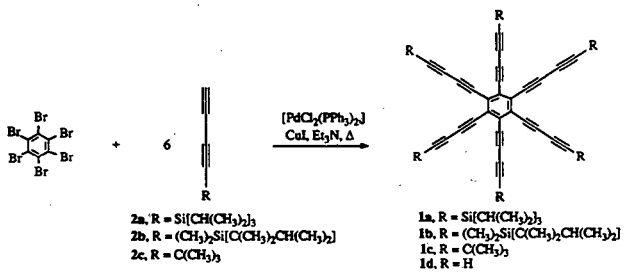

Figure 1-1. Pd-catalyzed coupling of hexabromobenzene with butadiynes to give **1**. (XBL 932-214)

indicative of σ-delocalization. A successful approach to **1** is shown in Figure 1-1.

The substituted butadiynes **2** required for the Pd-catalyzed coupling with hexabromobenzene were made by published (**2a,c**) or adapted (**3b**) literature procedures. The coupling step (with toluene: **1a**, 18%; **1b**, 11%; without toluene: **1c**, 36%) proceeded with a facility and efficiency that is remarkable in light of the reactivity of the species involved. The compounds were obtained as yellow crystals, stable to air, but losing x-ray diffraction capability in the absence of the solvent of crystallization. Their NMR and IR absorptions are found at the expected positions and compare well to those of hexaethynylbenzene **3** and related models. The clearest manifestation of the change in electronic structure on going from **3** to **1** is provided by UV measurements (see Figure 1-2); a pronounced shift of all the spectral bands to higher wavelengths ($\Delta\lambda_{max} \approx 50$ nm), a generally dramatic increase of the associated molar absorptivities, and the detection of a new set of higher energy transitions is observed. The quite striking hexagonal symmetry of **1** was confirmed by an x-ray structural determination of **1c** (see Figure 1-3). The compound crystallized from THF with two solvent

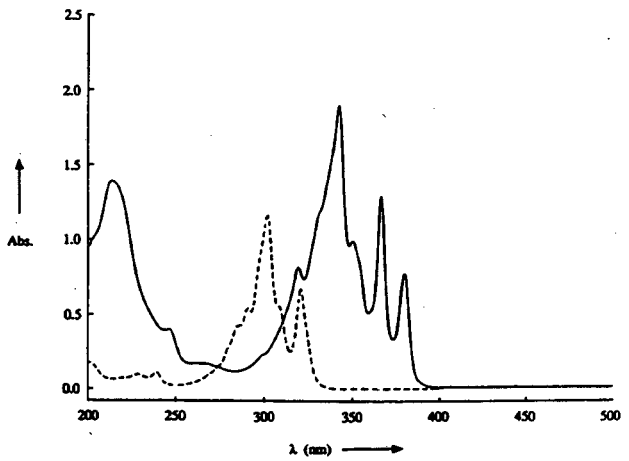

Figure 1-2. Electronic spectra of **3** (---) and **1a** (—) in hexane (7.64×10^{-6} M). A = absorption. (XBL 932-215)

*This work was supported by the Director, Office of Energy Research, Office of Basic Energy Sciences, Chemical Sciences Division of the U.S. Department of Energy under Contract No. DE-AC03-76SF00098.

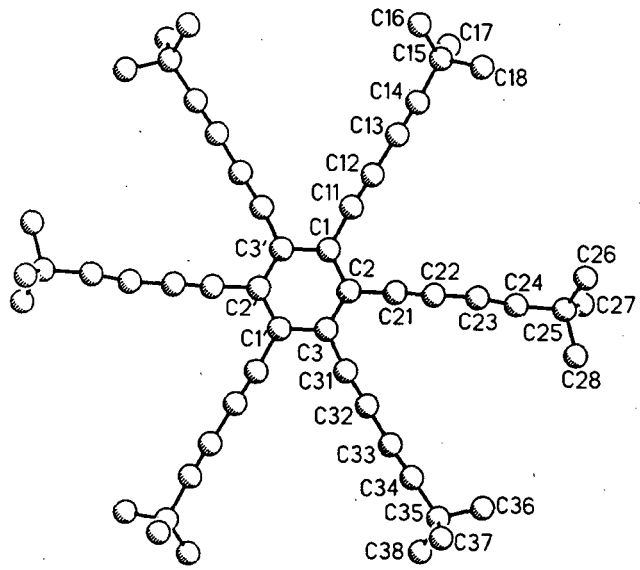

Figure 1-3. Molecular structure of **1c**. Mean distances [Å]: C_{arom}-C_{arom} 1.39(2), C_{arom}-C ≡ 1.42(2), C ≡ 1.19(1), ≡C-C≡1.38(2), sC-C(CH_3)$_3$ 1.48(2). (XBL 932-216)

molecules in intermolecular spaces (see Figure 1-4) and had to be kept in the mother liquor to enable acceptable diffraction measurements. An additional complication is presented by the mobility of the diyne substituents, evidenced by the increase in the value of the atomic displacement parameters with increasing distance from the ring. As a consequence, the degree of accuracy of the structural details is diminished.

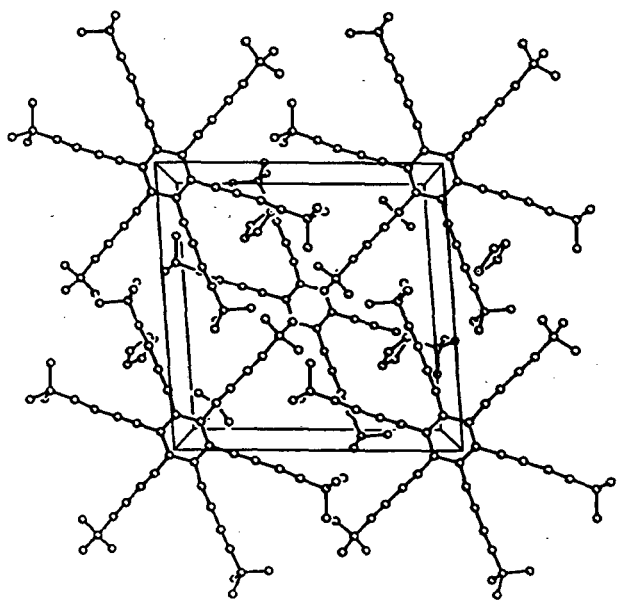

Figure 1-4. The unit cell of the crystal structure of **1c**. (XBL 932-217)

A few qualitative experiments probing the reactivity of **1** have been moderately encouraging. Surprisingly, **1a-c** show remarkable resilience to irradiation (at 254, 300, 350 nm) in solution and as solids. However, **1a** and **1c** react in the presence of [$CpCo(CO)_2$] and [$L_3Cr(CO)_3$](L = CH_3CN) to form new complexes, they appear to undergo charge-transfer complexation, and they reveal promising electrochemistry.

†Permanent address: Institute of Inorganic Chemistry, University-GH Essen, D-4300 Essen 1, Germany.

2. Total Synthesis of Angular [4]Phenylene and [5]Phenylene (Publication 4)

R.H. Schmidt-Radde and K.P.C. Vollhardt

Biphenylene or [2]phenylene, **1**, is a key polycyclic hydrocarbon with which to probe the effect of fusing a classical antiaromatic frame of benzene. Activated molecules of this nature are important fundamentally, because their study sheds light on the limits of chemical bonding to carbon, and, in a more practical vein, because they are protagonists in current efforts directed toward the elucidation of the mechanism(s) of carcinogenesis by polycyclic benzenoid hydrocarbons; the activation of benzene and related petroleum and coal-derived compounds as a source of industrial raw materials; the development of organic electroactive materials, such as potential conductors, ferromagnets, memory storage devices; and the organometallic chemistry of the strained and electronically reactive π-framework. The discovery that "CpCo" facilitates the cocyclization of *o*-diethynylarenes with alkynes to generate this otherwise difficult to assemble structural moiety has led previously to the construction of a number of biphenylenes, as well as several benzocyclobutadienologs, i.e., the linear [3]-, [4]-, and [5]- and the angular [3]phenylenes, **2-5** (see Figure 2-1).

In a nutshell, the trends in the physical properties exhibited along the linear series **1-4** appear to strongly indicate complete nonadherence to the Hückel [4*n* + 2] rule, the electronic spectra reflecting a rapidly diminishing HOMO-LUMO gap, and the ^{1}H NMR data indicating an increasing degree of paratropism of the internal "benzene" rings. An important question that has awaited an experimental answer is the behavior of the corresponding angular isomers **5-7** of **2-4**. Recent theoretical work has suggested that, while the linear phenylenes should be more aromatic (on thermodynamic grounds), they might also be more reactive, as indicated by their HOMO-LUMO separation, than the angular systems. The first experimental verification of some of these notions has now

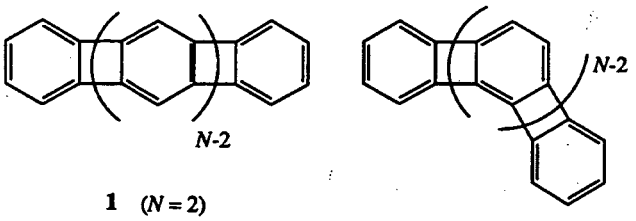

1 (*N* = 2)
2 (*N* = 3)
3 (*N* = 4)
4 (*N* = 5)

5 (*N* = 3)
6 (*N* = 4)
7 (*N* = 5)

Figure 2-1. The linear and angular phenylenes. (XBL 932-218)

been obtained by the syntheses of the novel angular phenylenes **6** and **7**.

The synthetic approach relies on "CpCo" to assemble the aromatic cycles by [2 + 2 + 2] cycloaddition of

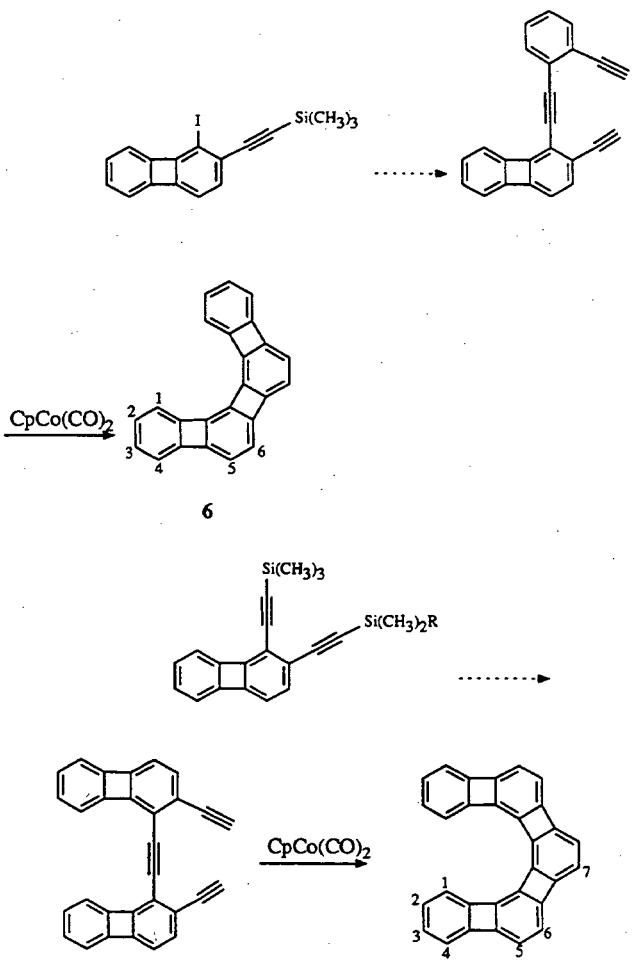

6

Figure 2-2. Synthesis of **6** and **7**. (XBL 932-219)

appropriate alkynes, on Pd to ensure the construction of the required alkynylarene precursors, and on silicon to provide functional group protection and regiocontrol to ultimately furnish the desired targets, intensely yellow **6** and yellow-orange **7** (see Figure 2-2).

As predicted by theory, the HOMO-LUMO gap decreases much less along the angular series compared to its linear counterpart. Most strikingly, the ^{1}H NMR chemical shifts of the "internal" benzene hydrogens (H5,6,7) reveal incremental *deshielding*, in stark contrast to the linear analogs [cf. (C_6D_6) 2,3-bis(trimethylsilyl)biphenylene, δ_{H5} = 6.64 ppm; 2,3,7,8-tetrakis(trimethylsilyl)[3]phenylene, δ_{H5} = 6.23 ppm; 2,3,8,9-tetrakis(trimethylsilyl)[4]phenylene, δ_{H5} = 5.89 ppm; and 2,3,9,10-tetrakis(trimethylsilyl)[5]phenylene, δ_{H6} = 5.56 ppm). It is difficult to provide a rationale for this unusual behavior, a task that constitutes an obvious challenge to theoretical chemists. We propose that the physical properties of the linear phenylenes are governed by the antiaromaticity (hence paratropism) associated with the overriding presence of cyclobutadienoid circuits. On the other hand, the angular systems are best described by invoking varying (and diminishing) degrees of bond alternation. Thus, **5** contains an internal "cyclohexatriene," maximizing the "aromaticity" of the flanking two benzene rings. Bond localization is increasingly attenuated along the series **5**, **6**, **7**, as more and more ($4n$ + 2) circuits contribute to the π-structure.

3. Synthesis and Fluxional Behavior of [Bis(trialkylphosphine)nickelio]anthracene (Alkyl = Et, Bu) (Publication 1)

A. Stanger[†] *and K.P.C. Vollhardt*

The title compounds were prepared from the respective $(R_3P_2)NiCl_2$ complexes and magnesium-anthracene-$(THF)_3$ (or anthracene in the presence of Mg or C_8K). The assignment of the anthracene proton NMR signals was made by NOE in conjunction with magnetization-transfer techniques. The complexes undergo haptotropic rearrangements in which the $(R_3P)_2Ni$ moiety migrates between the two terminal rings of the coordinated anthracene. The rates of these processes are concentration independent and unaffected by the presence of free anthracene and tris(trialkylphospine)nickel. Kinetic studies in the temperature range –60 to +70°C using lineshape analysis and spin saturation transfer techniques gave $\Delta H^{\neq}$ = 13.6 kcal mol^{-1} and $\Delta S^{\neq}$ = –4.3 eu for the haptotropic rearrangement in the butyl system, and similar values were found for the ethyl derivative. According to ^{1}H, ^{13}C, and ^{31}P NMR data, the coordination number between the

anthracene and the $(R_3P)_2Ni$ moiety is 4. However, an equilibrium between two η^2 structures with $\Delta G^{\neq} \leq 4$ kcal mol^{-1} cannot be ruled out.

†Permanent address: Technion-Israel Institute of Technology, Haifa 32000, Israel.

4. Ab Initio Study of σ- and π-Effects in Benzenes Fused to Four-Membered Rings: Rehybridization, Delocalization, and Antiaromaticity (Publication 3)

R. Faust, E.D. Glendenning, A. Streitwieser, and K.P.C. Vollhardt

The geometries of benzene incrementally fused to cyclobutenes, 3,4-dimethylenecyclobutenes, and cyclobutadienes (see Figure 4-1) were investigated with *ab initio* SCF-MO methods and by natural bond orbital (NBO)/natural resonance theory (NRT) analysis. These systems show various degrees of bond alternation in the six-membered ring with fused bonds elongated and bonds adjacent to the site of annelation contracted compared to those of benzene. NBO analysis reveals significant strain in the σ-frame as evidenced by strong rehybridization at the annelated carbon centers. This effect accounts, in part, for the bond alternation in the cyclobutadieno-fused benzenes, but has negligible influence on that of the cyclobuteno- and 3,4-dimethylenecyclobuteno-fused analogs. The relative contributions of the two Kekulé resonance forms are assessed by NRT analysis and are found to be in accord with the postulate originally presented by Mills and Nixon. The results suggest that the principal source of bond alternation is either hyperconjugation (in cyclobuteno-fused benzenes) or conjugation (in benzenes annelated to 3,4-dimethylenecyclobutene or cyclobutadiene). In all cases, deletion of these delocalizing interactions from the wavefunction leads to a more symmetrical benzene geometry.

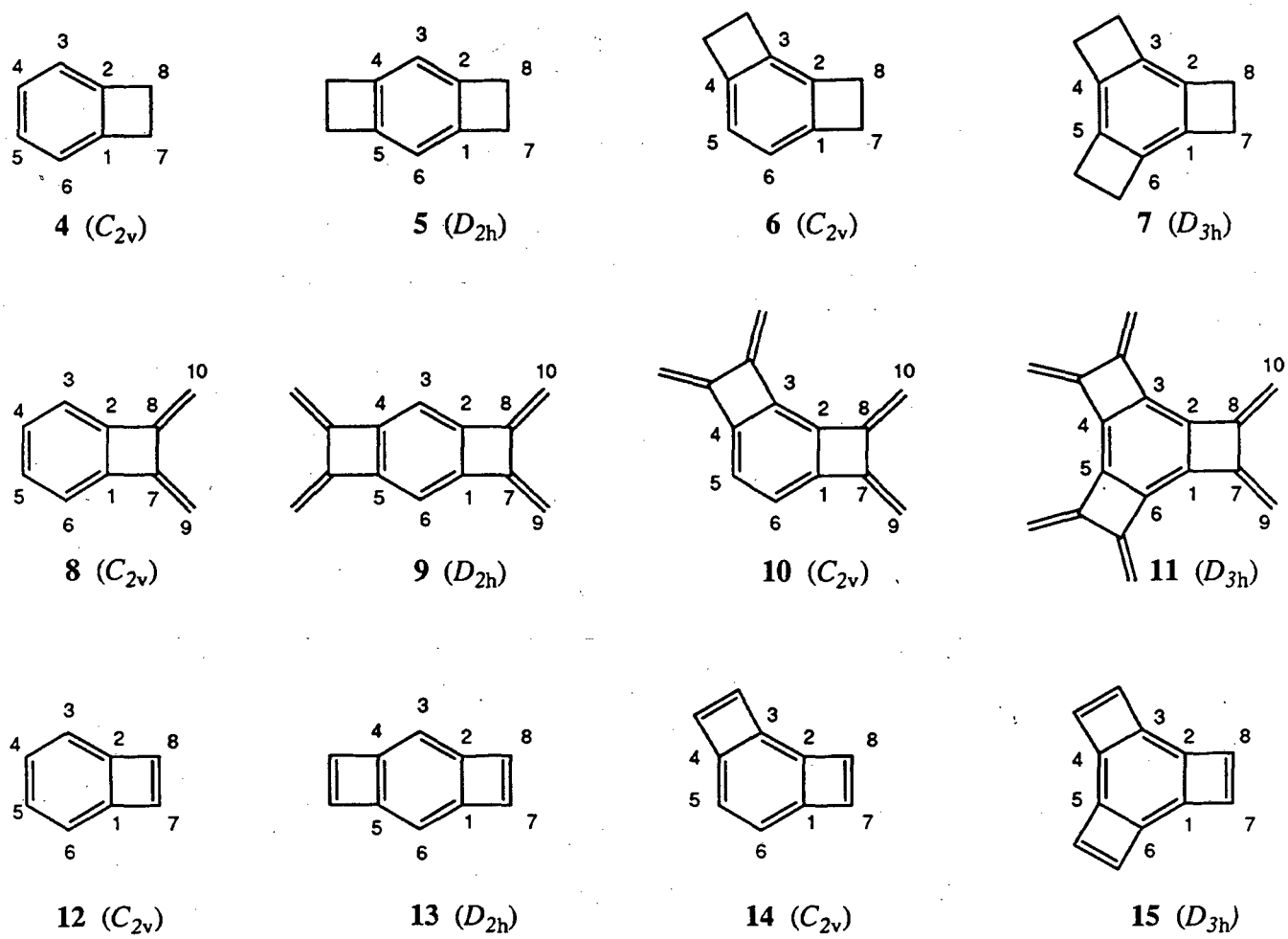

Figure 4-1. Structures of the hydrocarbons investigated. (XBL 932-220)

FY 1992 PUBLICATIONS AND REPORTS

Refereed Journals

1. A. Stanger and K.P.C. Vollhardt, "Synthesis and Fluxional Behavior of [Bis(trialkylphosphine)nickelio]anthracene (Alkyl = Et, Bu)," Organometallics **11**, 317 (1992); LBL-31990.
2. D. Brown, M.-H. Delville-Desbois, K.P.C. Vollhardt, and D. Astruc, "Specific Metal Recognition in the Redox Chemistry of the Heterobinuclear Fulvalene Complexes [WM(fulvalene)$(CO)_5$], M=Fe or Ru and Access to Tetranuclear Difulvalene Complexes," New J. Chem. **16**, 899 (1992); LBL-33619.
3. R. Faust, E.D. Glendenning, A. Streitwieser, and K.P.C. Vollhardt, "Ab Initio Study of σ- and π-Effects in Benzenes Fused to Four-Membered Rings: Rehybridization, Delocalization, and Antiaromaticity," J. Am. Chem. Soc. **114**, 8263 (1992); LBL-33620.
4. R.H. Schmidt-Radde, and K.P.C. Vollhardt, "Total Synthesis of Angular [4]Phenylene and [5]Phenylene," J. Am. Chem. Soc. **114**, 9713 (1992); LBL-33621.
5. R. Boese, J. Green, J. Mittendorf, D.L. Mohler, and K.P.C. Vollhardt, "The First Hexabutadiynylbenzenes: Synthesis and Structures," Angew. Chem. **104**, 1643 (1992); Angew. Chem., Int. Ed. Engl. **31**, 1643 (1992); LBL-33622.
6. U. Bunz, K.P.C. Vollhardt, and J.S. Ho, "Tetraalkynylmethanes: Synthesis of Diethynyldipropargyl- and Tetrapropargylmethane," Angew. Chem. **104**, 1645 (1992); Angew. Chem., Int. Ed. Engl. **31**, 1648 (1992); LBL-33623.
7. K.P.C. Vollhardt, "The Phenylenes," Pure and Appl. Chem. **65**, 151 (1993); LBL-33624.

LBL Reports

8. D.L. Mohler (Ph.D. Thesis), "The Synthesis, Properties, and Reactivity of Angular, Bent, and Triangular Phenylenes," LBL-33618.

Invited Talks

9. K.P.C. Vollhardt, "Cobalt-Mediated Total Synthesis of Natural and Unnatural Products," 5th Symposium on Natural Products Chemistry, Karachi, Pakistan, January 5-9, 1992; University of Reno, Nevada, February 27, 1992; SUNY Stony Brook, NY, March 27, 1992; European Stereochemistry Conference, Bürgenstock, Switzerland, April 26–May 2, 1992; Université Pierre et Marie Curie, Paris, France, June 9, 1992; Pierre Fabre Company, Toulouse, France, June 10, 1992; Rhone Poulenc Company, Lyon, France, June 11, 1992; Ecole Normale Superieure, Paris, France, June 16, 1992; Bristol Myers Company, Aulnais Sur Bois, France, June 18, 1992; Roussel-Uclaf Company, Romainville-Paris, France, June 22, 1992; CNRS Thiais, France, June 23, 1992; Abbott Laboratories, Chicago, Illinois, July 28, 1992; 2nd International Symposium on Transition Metals in Organic Synthesis, Bristol, England, September 22–24, 1992.
10. K.P.C. Vollhardt, "The Phenylenes," 7th International Symposium on Novel Aromatic Compounds, Victoria, Canada, July 19–24, 1992.
11. K.P.C. Vollhardt, "Oligocyclopentadienylmetals: Remarkable Organometallic Materials," University of Essen, Germany, September 11, 1992.

HEAVY-ELEMENT CHEMISTRY

Actinide Chemistry*

Norman M. Edelstein, Richard A. Andersen, and Kenneth N. Raymond, Investigators

GENERAL INTRODUCTION

Development of new technological processes for the use, safe handling, storage, and disposal of actinide materials relies on the further understanding of basic actinide chemistry and the availability of a cadre of trained personnel. This research program is a comprehensive, multifaceted approach to the exploration of actinide chemistry and to the training of students. Research efforts include synthetic organic and inorganic chemistry for the development of new chemical agents and materials, the chemical and physical elucidation through various characterization techniques, and thermodynamic and kinetic studies for the evaluation of complex formation.

The development and understanding of complexing agents that specifically and effectively sequester actinide ions is one program aspect. Such agents are intended for the decorporation of actinides in humans, in the environment, and in systems related to the nuclear fuel cycle. Extensive studies are under way to prepare organometallic and coordination compounds of the f-block elements that show the differences and similarities among the f-elements, and between the f- and d-transition series elements. Optical and magnetic studies on actinides as isolated ions in ionic solids, and in molecules, provide information about electronic properties as a function of atomic number.

SPECIFIC SEQUESTERING AGENTS FOR THE ACTINIDES

INTRODUCTION

The coordination chemistry of the actinides and lanthanides is being studied in order to create agents that selectively and strongly bind f transition elements in their +4 and +3 oxidation states. Characterization of these compounds includes the use of NMR spectroscopy, x-ray crystallography, potentiometric and spectrophotometric titrations, and electrochemistry. Possible applications for these ligands include magnetic resonance imaging (MRI), plutonium decorporation, uranium extraction from sea water and waste actinide extraction, and long-term storage.

1. Stereognostic Coordination Chemistry: The Design and Synthesis of Chelators for the Uranyl Ion (Publication 1)

T.S. Franczyk, K.R. Czerwinski, P.H. Walton, and K.N. Raymond

Following the first paper in this series,[1] which described a new approach to the ligand design for the sequestration of metal-oxo cations, we report herein a new generation of ligands in this class to chelate uranyl. The new approach to ligand design, called stereognostic coordination chemistry, incorporates a traditional Lewis base coordination to the metal center and a hydrogen-bond donor to interact with the oxo atom. Two new tripod ligands tris-N,N′,N″-[2-(2-carboxy-phenoxy)ethyl]-1,4,7-triazacyclononane bis-hydrochloride (ETAC.2HCl) and tris-N,N′,N″-[2-(2-carboxy-4-decyl-phenoxy)ethyl]-1,4,7-triazacyclononane tris-hydrochloride (DETAC.3HCl) have been prepared. They chelate uranyl with a tris-carboxylate coordination sphere and provide a hydrogen bond donor through a protonated amine on the triazacyclononane macrocycle to interact with an oxo atom. The ligand design is new insofar as CPK models predict that upon uranyl binding the hydrogen bond donor must point directly toward the oxo atom, enforcing a stereognostic interaction. Both ligands chelate the uranyl ion, the latter one is a powerful extractant and will quantitatively extract uranyl into an organic phase at pH 2.5 and above. The predicted extraction coefficient is estimated to be approx. 10^{14} in neutral aqueous conditions. The O^{18} labeling of uranyl in conjunction with an infrared spectrum study of the labeled uranyl-ligand complex confirmed, for the first time, a stereognostic type coordination to uranyl.

*This work was supported by the Director, Office of Energy Research, Office of Basic Energy Sciences, Chemical Sciences Division, of the U.S. Department of Energy under Contract No. DE-AC03-76SF00098.

[1] T.S. Franczyk, K.R. Czerwinski, K.R. Raymond, J. Am. Chem. Soc. **114**, 8138 (1992).

2. Pu(IV) Coordination (Publication 2)

J. Xu, D.W. Whisenhunt Jr., and K.N. Raymond

New types of octadentate terephthalamide ligands have been synthesized including the first tetraterephthalamide macrocyclic cage (BHCAM) and its noncyclic analogs.[2] Although the cage macrocycle can remove only 56% of the Pu(IV) from contaminated mice, its non-cyclic analog (MeTAM) can remove 77% of the Pu(IV) from contaminated mice.

A series of new polydentate 3-hydroxy-2-pyridones have been synthesized. The hexadentate Tren-3,2-HOPO is one the most promising ones in terms of Pu(IV) removal from mice. This ligand is able to remove up to 82% of the Pu(IV) and up to 89% of the Am(III) from contaminated mice. The ligand is also orally active and can remove 76% of the Pu(IV) and 87% of the Am(III) when delivered orally. Even large doses of the ligand (500 mmol/kg twice a day) proved to be non-toxic to mice.

Stability constants of Desferrioxamine B (DFO) and DFO analogs (hydroxamate based ligands) with actinide (IV) ions have been determined using competition spectrophotometric titrations. The ligands show much promise as specific sequestering agents for actinide(IV) ions. These ligands high thermodynamic stability (log K ≈ 26–42) and ease of functionalization make them likely candidates as liquid/liquid or solid/liquid extractants.

3. Work in Progress

$[Gd(DTPA)(H_2O)]^{2-}$ is one of only two lanthanide containing MRI agents currently approved by the FDA. Neutral derivatives of this complex are of interest as they are non-ionic, which reduces toxicity, and have been shown to be relatively more stable than $[Gd(DTPA)(H_2O)]^{2-}$ in the presence of physiological concentrations of Ca^{2+}, Cu^{2+}, Zn^{2+} and H+.[3] The x-ray crystal structure of [Gd(DTPA-bisethylamide)(H_2O)], studied in collaboration with a research group at Salutar, Inc.[4] has revealed that both amide oxygens are bound to the metal in the solid state. Analogous bis-amide macrocyclic chelators are being synthesized in order to fully encapsulate the metal and to explore solution state coordination geometry and isomerization processes in these macrocyclic systems.

NMR spectroscopy of the lanthanide complexes is being employed to study the dynamics of complex isomerization and their solution state structures. Two-dimensional correlation spectra are being used for peak assignments, to which calculated chemical shifts based on an initial assumed complex geometry are iteratively fit.

In addition, stability constant measurements of these macrocycles and analogs that lack amide or carboxylate ligating groups are in progress to deconvolute factors influencing complex stability and mechanism of ligand exchange.

SYNTHETIC STUDIES

4. New Synthetic Routes to Cyclopentadienyl-uranium(IV) Fluorides; Redox and Atom-Abstraction Reactions (Publication 13)

M. Weydert and R.A. Andersen

New synthetic routes for the synthesis of $(RC_5H_4)_3UF$ compounds have been developed that fall into two general classes, (a) redox reactions and (b) atom-abstraction reactions. The redox reactions involve oxidation of trivalent uranium metallocenes by a fluoride-ligand transfer reductant such as AgF, COF_2, or tritylfluoride. The other synthetic route, viz. atom-abstraction is the more interesting since it involves intermolecular C-F activation processes. Thus $(MeC_5H_4)_3U\text{-}CMe_3$ reacts with aromatic or aliphatic fluorocarbons to give $(MeC_5H_4)_3UF$ and various organic products depending on the identity of the solvent and temperature. In toluene, for example, the relative amounts of the organic products at 25°C are $Me_3CC_6F_5$:HC_6F_5:isobutane:isobutene in ratio 1:2:2:1. As the temperature is raised, the amount of $Me_3CC_6F_5$ decreases and the relative ratio of isobutane to isobutene approaches 1:1. Since the rate of the reaction depends upon the concentration of C_6F_6, a bimolecular reaction mechanism is suggested. This implies that in the transition state, the fluorocarbon is coordinated to the uranium center before uranium-carbon bond homolysis occurs. The driving force for the exothermic reaction is that the strong C-F and U-F bonds largely cancel so that the weak U-C bond is more than compensated by the formation of the C-C bond.

The temperature dependence of the ^1H NMR spectral resonances for $(MeC_5H_4)_3UF$ follow Curie Law behavior from –90°C to +90°C in toluene-d_8 or tetrahydrofuran-d_8. This behavior is normal for compounds of the type Cp_3UX and corrects some misleading information in the literature.

[2] J. Xu, T.D.P. Stack, K.N. Raymond, Inorg. Chem. **31**, 4903 (1992).
[3] W.P. Cacheris, S.C. Quay, and S.M. Rocklage, Mag. Reson. Imag. **8**, 467 (1990).
[4] M.S. Konings, W.C. Dow, D.B. Love, et al., Inorg. Chem. **29**, 1488 (1990).

5. Spectroscopic Studies and Crystal Field Analyses of Am $^{3+}$and Eu^{3+} in the Cubic Symmetry Site of ThO_2 (Publication 20)

S. Hubert, P. Thouvenot, and N. Edelstein

Fluorescence and excitation spectra of Am^{3+} diluted in ThO_2 are reported at room and liquid helium temperatures along with fluorescence data for Eu^{3+} diluted in ThO_2. The Eu^{3+} data can be assigned primarily to magnetic dipole transitions, but the Am^{3+} data appear to be primarily phonon-assisted electric-dipole transitions. Figure 5-1 shows the $^5D_1' \rightarrow {}^7F_2'$ magnetic dipole-allowed transition plus some forced-electric dipole transitions for Am^{3+}/ThO_2. Earlier electron paramagnetic resonance (EPR) data on Pu^{3+} diluted in ThO_2 have set limits on the possible ratios of the crystal field parameters B_0^4/B_0^6 for this system. Assuming the same ratio should hold for Am^{3+}/ThO_2, the observed transitions were assigned and the values for the crystal field parameters $B_0^4 = -6731\ cm^{-1}$, $B_0^6 = 714\ cm^{-1}$ were obtained. Figure 5-2 shows the agreement between the experimental energies and those calculated from the best-fit parameters of the empirical Hamiltonian. The B_0^4 value is the same order of magnitude as found earlier in inelastic neutron scattering experiments for UO_2 and NpO_2, but B_0^6 for Am^{3+}/ThO_2 is much smaller than determined in the neutron experiments.

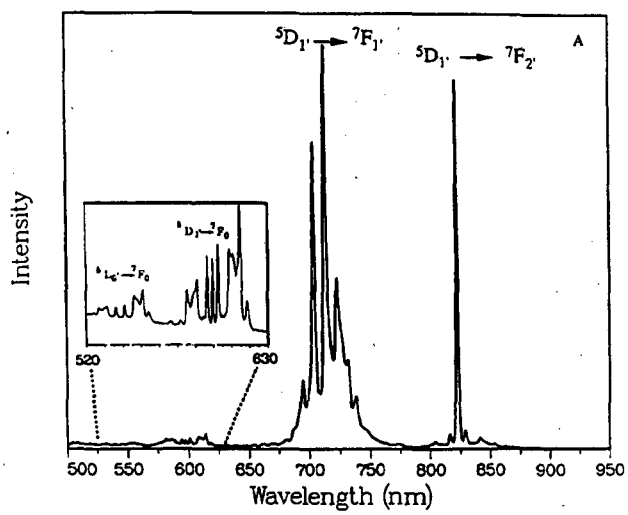

Figure 5-1. Some fluorescence data for Am^{3+}/ThO_2 at room temperature. (XBL 931-171)

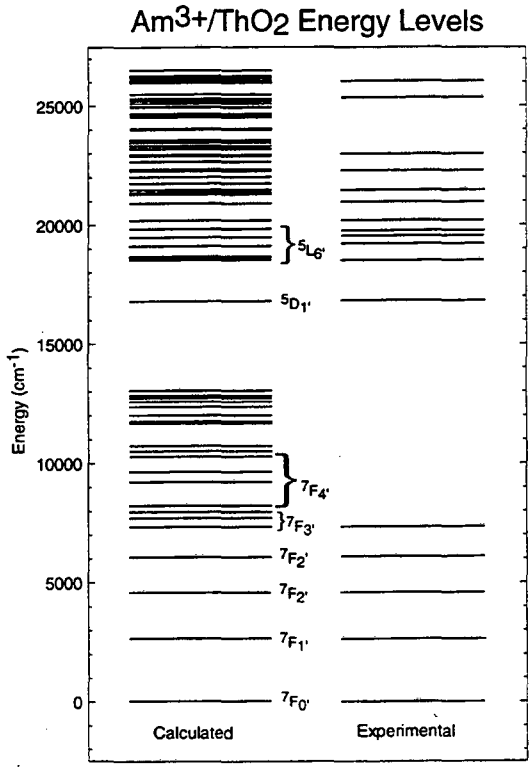

Figure 5-2. Experimental and calculated energy levels for Am^{3+}/ThO_2. (XBL 931-170)

6. Two-Photon Excitation of the $4f^1 \rightarrow 5d^1$ Transitions of Ce^{3+} in $LuPO_4$ and YPO_4 (Publication 21)

J. Sytsma, D. Piehler, N.M. Edelstein, L.A. Boatner, and M.M. Abraham

Two-photon excitation (TPE) spectra of the $4f^1 \rightarrow 5d^1$ transitions of Ce^{3+} in $LuPO_4$ and YPO_4 have been investigated. For Ce^{3+} in $LuPO_4$, transitions to four out of the five $5d^1$ levels are observed as zero-phonon lines. Figure 6-1 shows the TPE spectrum for the second and third $5d^1$ components. Figure 6-2 shows the TPE spectrum for the fourth $5d^1$ component. The symmetry properties of the levels were obtained from the polarization dependence of the TPE signals. Measurements on Ce^{3+} in YPO_4 support the given assignments. Although a crystal-field fit yields a satisfactory RMS energy deviation, an unrealistic value of the spin-orbit coupling parameter, ζ_{5d1}, is obtained. The vibronic coupling appears to be smaller than for the single-photon absorption spectra, and the vibronic bands show a rich structure. There are striking differences between the energies and the relative intensities of the vibronic lines and the associated zero-phonon lines. The vibronic coupling is also found to be strongly dependent on the Ce^{3+} concentration.

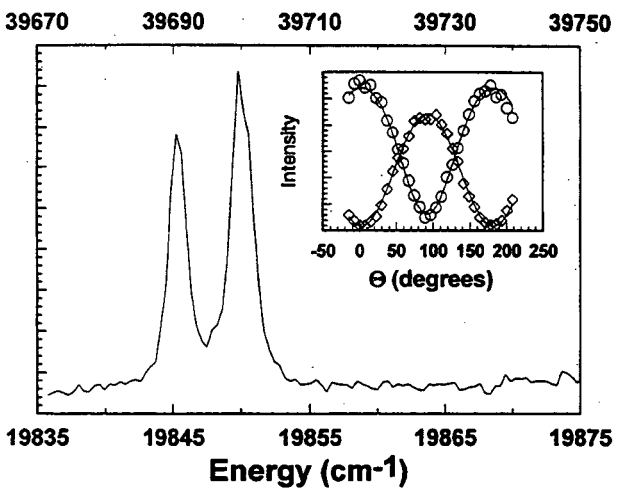

Figure 6-1. Two-photon excitation spectrum of Ce^{3+} in $LuPO_4$ to the second and third $5d^1$ component for different polarizations of the excitation light. The insert shows the TPE signal as a function of the polar angle θ of the polarization vector $\hat{\varepsilon}$. Excitation is at 19,845.3 cm^{-1} (O) and at 19,849.8 cm^{-1} (◊). (XBL 931-167)

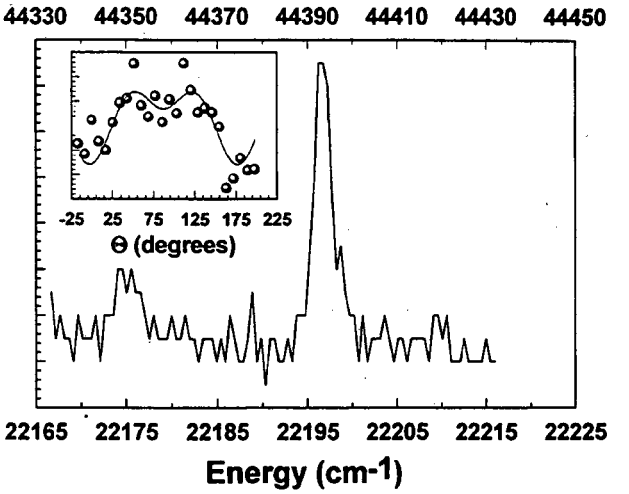

Figure 6-2. Two-photon excitation spectrum of Ce^{3+} in $LuPO_4$ to the fourth of the $5d^1$ components. The polarization of the excitation light was parallel to the $\hat{z}$ axis. The insert shows the TPE signal as a function of the polar angle θ of the polarization vector $\hat{\varepsilon}$. Excitation is at 22,196.5 cm^{-1}. (XBL 931-166)

7. Electron Paramagnetic Resonance (EPR) of Pu^{3+} and Cf^{3+} in Single Crystals of $LuPO_4$ (Publication 19)

W.K. Kot, N.M. Edelstein, M.M. Abraham, and L.A. Boatner

Electron paramagnetic resonance (EPR) spectroscopy has been used to investigate the ground-state properties of the actinide ions Pu^{3+} ($5f^5$) and Cf^{3+} ($5f^9$) incorporated as dilute impurities in single crystals of the tetragonal-symmetry host $LuPO_4$. The g-values of the electronic ground states were determined experimentally at a sample temperature of 4 K (see Figure 7-1). These values are compared to those calculated using the free-ion parameters available from previous crystal-field analyses of Pu^{3+} and Cf^{3+} ions diluted in $LaCl_3$ host single crystals and a set of "crystal-field" parameters reported earlier for Cm^{3+} ($5f^7$) ions in $LuPO_4$. These crystal-field parameters were obtained from spin-Hamiltonian parameters using operator-equivalent factors and the assumption that the zero-field splitting of the ground state of the $5f^7$ ion is due primarily to intermediate-coupling effects. The relatively poor agreement between the experimental and calculated g-values indicates that the crystal-field parameters obtained for Cm^{3+} in $LuPO_4$ cannot be used to predict the correct electronic ground-state properties of the other actinide ions Pu^{3+} and Cf^{3+} in the identical host single crystal $LuPO_4$. Accordingly, in the case of actinide impurity ions in single crystals, there is no simple correspondence between the spin-Hamiltonian parameters and the crystal-field parameters.

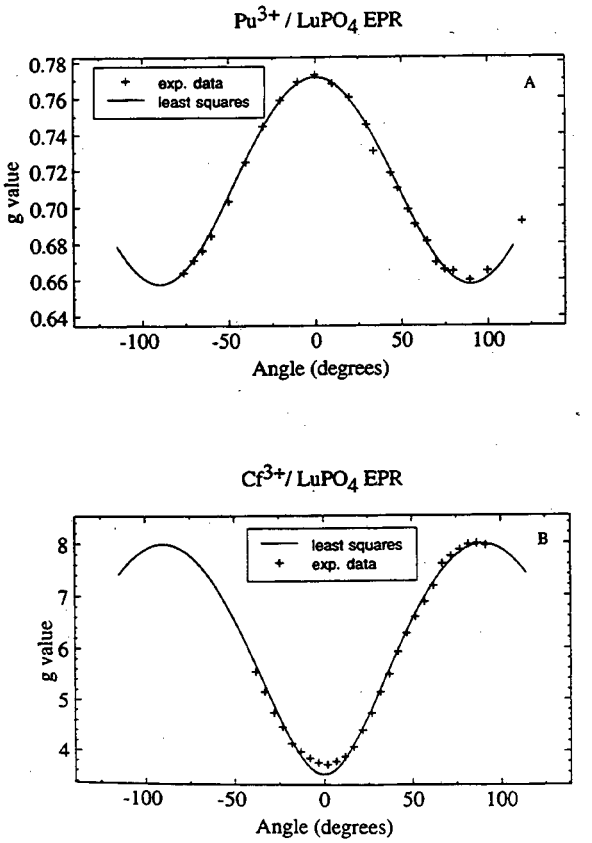

Figure 7-1. Experimental EPR measurements as a function of the angle between the crystallographic c axis and the magnetic field. The solid curves represent a least-squares fit of the data to the expression $g^2 = g_{\parallel}^2 \cos^2\theta + g_{\perp}^2 \sin^2\theta$. (A) $Pu^{3+}/LuPO_4$, microwave frequency = 9.223 GHz, $g_{\parallel} = 0.772(2)$, and $g_{\perp} = 0.658(2)$. (B) $Cf^3/LuPO_4$, microwave frequency = 9.217 GHz, $g_{\parallel} = 3.56(2)$ and $g_{\perp} = 7.79(3)$. (XBL 931-168)

8. K_2UBr_5 —Nuclear and Magnetic Structure (Publication 17)

K. Krämer, L. Keller, P. Fischer, B. Jung, N.M. Edelstein, H.-U. Güdel, and G. Meyer

Magnetic susceptibility measurements show an antiferromagnetic ordering phenomenon for K_2UBr_5. There is a broad maximum in the χ versus T curve at about 10 K (see Figure 8-1). In order to determine the magnetic structure of K_2UBr_5, powder neutron diffraction investigations were performed. The nuclear structure of K_2UBr_5 (K_2PrCl_5 type of structure) was refined at 15 K in the paramagnetic state. According to the temperature dependence of the intensity of the 010 and 111 magnetic peaks the Néel temperature is 2.8(3) K. Presumably, there is a short-range magnetic ordering along the $[UBr_3Br_{4/2}]^{2-}$ chains giving rise to the maximum of χ at T = 10 K, followed by long-range (three-dimensional) ordering at 2.8 K. The magnetic structure, which was determined from a measurement at 1.5 K in the magnetically ordered state, belongs to the Shubnikov space group Pn'm'a' with k = 0. In the uranium chains along [010] there is an antiferromagnetic ordering of the magnetic moments with components in the (010) plane only. The magnetic moments of neighboring chains are perpendicular to each other within the error limit. Each U^{3+} has an ordered magnetic moment of 2.31(4) μ_B.

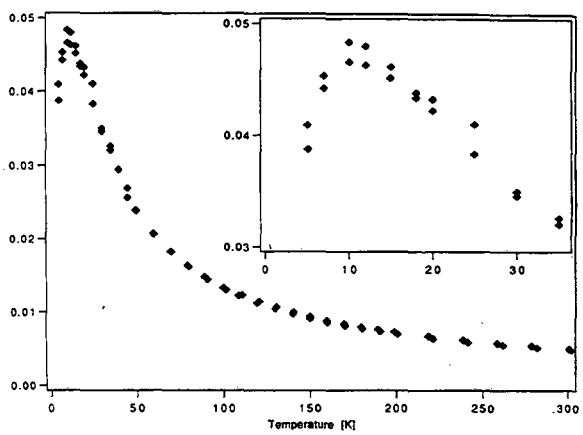

Figure 8-1. The magnetic susceptibility of K_2UBr_5. The inset shows a magnification of the magnetic susceptibility data at the highest transition temperature. (XBL 931-165)

9. Spectroscopic and Magnetic Studies of Tetravalent Pa and Trivalent Th Compounds (Publication 18)

N.M. Edelstein and W.K. Kot

Before 1940, the elements Th, Pa, and U (atomic numbers 90–92) were placed below their 5d counterparts Hf, Ta, and W (atomic numbers 72–74) in the Periodic Table because of the similarity of their chemical properties to those 5d elements. However, it had long been predicted theoretically that a new transition series should begin somewhere around uranium in the Periodic Table, and many early studies suggested this shell should consist of 5f electrons. Today it is known experimentally that the first appearance of 5f electrons in the free gaseous atoms of the present-day actinide series occurs at element 91, Pa, whose ground configuration is $5f^26d7s^2$ outside the closed radon shell. For all the early actinide gaseous atoms and ions, there are a number of low-lying electron configurations. Placing these ions in compounds or crystals can cause perturbations to the relative energies of these configurations due to the effects of the crystal field. The most notable example is for the one structurally characterized compound of trivalent Th, $Cp_3''Th$ ($Cp'' = \eta^5\text{-}C_5H_3\text{-}(SiMe_3)_2$). In the free trivalent Th ion, the lowest configuration is $5f^1$ with the $6d^1$ configuration starting at 9192.84 cm^{-1}. In $Cp_3''Th$, the ground configuration is $6d^1$ with the $5f^1$ configuration beginning at 15,350 cm^{-1}. Thus placing the Th^{3+} ion into this compound results in a stabilization of the lowest 6d energy level by greater than 24,000 cm^{-1}. Similar, though less dramatic, effects occur in Pa compounds. Recent electronic and magnetic studies on Pa^{4+} and Th^{3+} compounds are reviewed in this paper.

10. Crystal-field Excitations and Magnetic Properties of $TmPO_4$ (Publication 15)

C.-K. Loong, L. Soderholm, M.M. Abraham, L.A. Boatner, and N.M. Edelstein

The magnetic-excitation spectrum of $TmPO_4$ has been studied using inelastic neutron scattering techniques. Sharp crystal-field transitions were observed in spectra obtained at 15 and 100 K, yielding new information regarding the energy-level structure of the Tm^{3+} ground multiplet splitting. Figure 10-1 shows the energy level diagram and

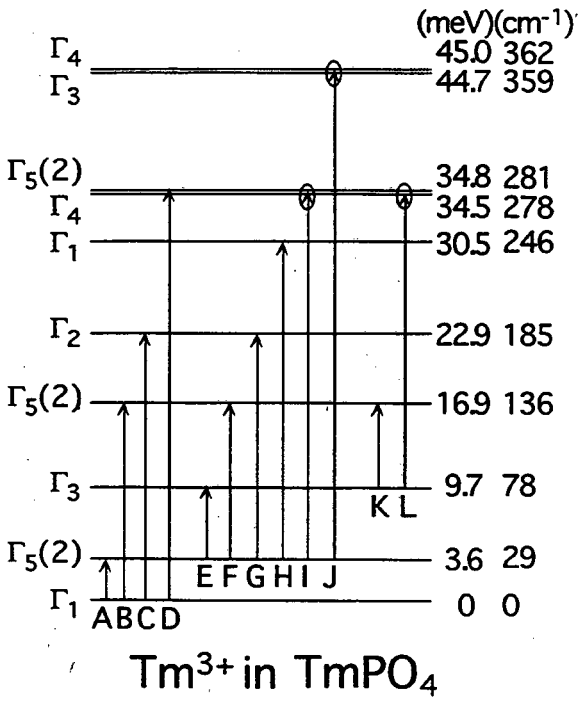

Figure 10-1. A schematic diagram of the splitting of the Tm^{3+} $^3H_6$ ground multiplet by crystal field into 7 singlets, $2\Gamma_1 + \Gamma_2 + 2\Gamma_3 + 2\Gamma_4$, and 3 doublets, $3\Gamma_5$ (D_{2d} symmetry). The transitions labels refer to the experimentally observed transitions in the inelastic neutron scattering spectra. (XBL 931-169)

observed transitions for $TmPO_4$. The data were analyzed using a Hamiltonian that included the atomic free-ion and crystal-field interactions for an f^{12} configuration. Using the Tm free-ion parameters derived from optical spectroscopy of Tm^{3+} diluted in a $LuPO_4$ host, a set of crystal-field parameters were obtained for Tm^{3+} in pure $TmPO_4$. The calculated magnetic spectra of $TmPO_4$ agree very well with the results of neutron and Raman measurements. The calculated bulk magnetic susceptibility of $TmPO_4$ exhibits a large anisotropy at low temperature and is in good agreement with the experimental data. A significant contribution to the specific heat from the Tm^{3+} crystal field states was found at temperatures below 100 K.

11. Rare-Earth Energy Levels and Magnetic Properties of $HoPO_4$ and $ErPO_4$ (Publications 14 and 16)

C.-K. Loong, L. Soderholm, J.P. Hammonds, M.M. Abraham, L.A. Boatner, and N.M. Edelstein

The static and dynamic magnetic response of $HoPO_4$ and $ErPO_4$ has been studied by means of neutron spectroscopy and magnetic susceptibility measurements. The inelastic neutron-scattering spectra exhibit well-defined transitions characteristic of crystal-field excitations of the rare-earth ions. The data were analyzed using a Hamiltonian that included atomic free-ion and crystal-field interactions for an f^N configuration (N = 10 and 11 for Ho^{3+} and Er^{3+}, respectively). Using the free-ion parameters derived from optical spectroscopy of the corresponding rare-earth ions diluted in a YPO_4 host, crystal-field parameters for both $HoPO_4$ and $ErPO_4$ were obtained. Figures 11-1 and 11-2 show the energy level diagrams and observed transitions for $HoPO_4$ and $ErPO_4$, respectively. A comparison of the neutron data with optical absorption and both nonresonance and resonance Raman scattering measurements has been made. The derived crystal-field-level structure provides a basis for explaining the low-temperature magnetic properties of both compounds. The calculated and measured paramagnetic susceptibilities agree well for $HoPO_4$ and $ErPO_4$ in the temperature range of 5–300 K. The highly anisotropic, saturated magnetization of the ground doublet in $HoPO_4$ may act as a "bootstrap" for a long-range magnetic ordering of the moments parallel to the c-axis at low temperatures. The nearly spherically symmetric moments of the low-lying Kramers doublets of $ErPO_4$, however, tend to couple less effectively via exchange interactions. The effective

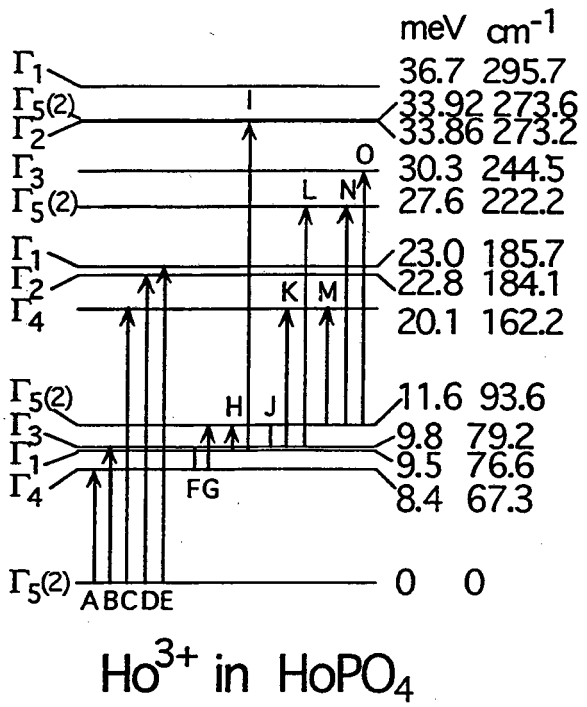

Figure 11-1. A schematic diagram of the splitting of the Ho^{3+} $^5I_8$ ground multiplet by the crystal field into 9 singlets, $3\Gamma_1 + 2\Gamma_2 + 2\Gamma_3 + 2\Gamma_4$, and 4 doublets, $4\Gamma_5$ (D_{2d} symmetry). The transitions labels refer to the experimentally observed transitions in the inelastic neutron scattering spectra. (XBL 931-173)

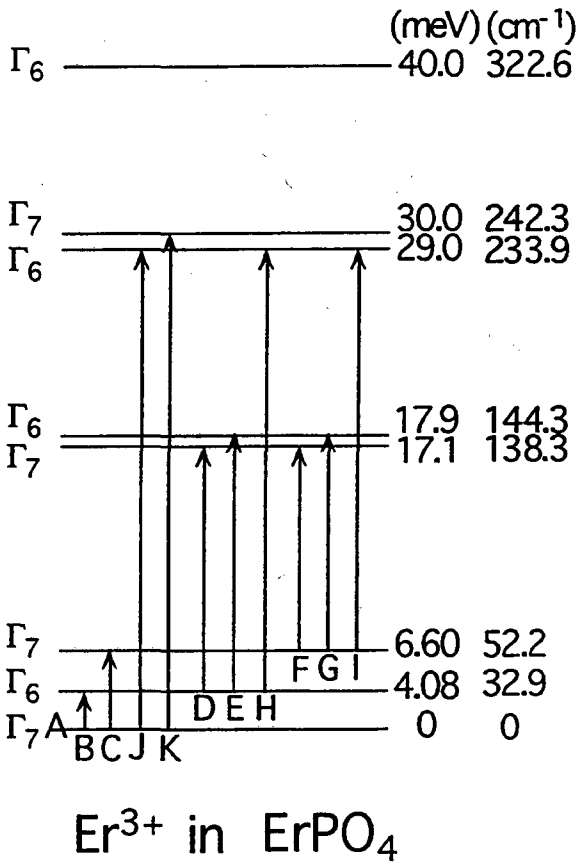

Figure 11-2. A schematic diagram of the splitting of the Er^{3+} $^4I_{15/2}$ ground multiplet by the crystal field into 4 Γ_6 and 4 Γ_7 Kramers doublets (D_{2d} symmetry). The transitions labels refer to the experimentally observed transitions in the inelastic neutron scattering spectra. (XBL 931-172)

exchange field in antiferromagnetic $HoPO_4$, as estimated based on the crystal-field-level scheme and a molecular-field approximation, is found to be in good agreement with that reported from a specific-heat analysis. The paramagnetic specific heat, spectroscopic splitting g-factors of the low-lying doublet states, and the saturated moments for $HoPO_4$ and $ErPO_4$ obtained from the present study are applicable to interpreting specific-heat, hyperfine interaction, EPR, and neutron diffraction measurements.

ACTINIDE SYNCHROTRON RADIATION PROGRAM

INTRODUCTION

An actinide beamline at the Advanced Light Source (ALS) has been proposed and is based upon a branchline of an insertion device beamline that covers the photon energy range of ~20–300 eV. A workshop entitled "Synchrotron Radiation in Transactinium Research" was held at LBL on October 1–2, 1992 that explored the wide range of the scientific opportunities that would be made available by an actinide beamline facility at the ALS. The speakers, as well as the attendees, clearly demonstrated and strongly supported the construction of a beamline dedicated to actinide-related science, both basic and applied in nature. Furthermore, all of the workshop participants clearly expressed great interest in becoming actively involved with the development of the proposed beamline and endstations. Perhaps of primary importance, the safety concerns regarding the proposed actinide beamline facility were openly and critically discussed. The conclusions were that, properly designed and operated, an actinide beamline facility would exceed safety requirements ensuring no risk to the ALS.

The preliminary designs of the actinide beamline, safety enclosure system, and all safety systems have been completed. In addition, the requirements for the actinide beamline solid state endstation capabilities have been delineated and conceptually designed. An interim solid state synchrotron endstation, without a safety enclosure, is currently being fabricated for use at ALS to investigate the surface chemistry of uranium-based materials.

Synchrotron radiation (SR) investigations of actinide materials with x-ray (2.5–25 keV) rather than vacuum ultraviolet (VUV) radiation is an additional regime that presents extremely attractive opportunities with which to investigate actinide science. The prime advantage of x-ray SR techniques is that the x-ray beamlines employed do not share vacuum with the storage ring nor do they require elaborate endstations. Use of radioactive materials is

simplified by doubly encasing them in simple protective claddings and the access-limited, radiation shielded experimental hutches are ideal. These SR x-ray techniques provide a method for investigating actinide materials in solution, which are of the utmost concern for waste remediation and long-term storage projects. These techniques can also be extended to surface studies of active materials with the incorporation of UHV capabilities.

12. X-Ray Absorption Spectroscopy of the Rare Earth Orthophosphates (Work in Progress)†

D.K. Shuh, L.J. Terminello, L.A. Boatner, and M.M. Abraham

There is a rich history of rare earth (RE) 3d x-ray absorption measurements that has been augmented recently by improvements in both experimental and theoretical techniques. X-ray Absorption Spectroscopy (XAS) of the RE $M_{4,5}$ edges (3d levels) yields sharp peaks near the edges as a result of strong quasi-atomic $3d^{10}4f^n \rightarrow 3d^94f^{n+1}$ transitions that exhibit a wealth of spectroscopic features. Although the purpose of XAS experiments is to obtain information on the RE ground state, the technique images the excited electronic final states. The total $3d^94f^{n+1}$ multiplets for the REs are quite complex, and even with dipole selection rules limiting the allowed transitions from the ground state, give rise to a large number of possible final states. The technique of total electron yield (TY) x-ray absorption spectroscopy has been shown to be a useful technique for investigation of 4f occupancy, 4f hybridization, and valence issues in RE containing materials since the TY measurements are known to be proportional to the x-ray absorption coefficient.

The electronic structures of the RE ions in the orthophosphates (La, Ce, Nd,...)PO_4 are of particular interest since the valence state is clearly defined as tripositive and are analogs of the corresponding actinide orthophosphates, which have been considered as materials for primary nuclear waste containment and disposal. Preliminary x-ray absorption measurements of the single crystal rare earth orthophosphates (RE = La, Ce, Pr, Nd, Sm, Eu, Tb, Er) at the $M_{4,5}$ edges were performed on the LLNL/UC PRT Beamline 8–2 SGM. The spectra were measured with the monochromatic x-ray beam (700–1300 eV) incident at ~45° to the surface normal, monitoring the photon flux with an Au grid and by recording the total electron yield from a Channeltron. Figure 12-1 shows the XAS spectra of the Ce 3d ($M_{IV,V}$) edges in $CePO_4$ and is

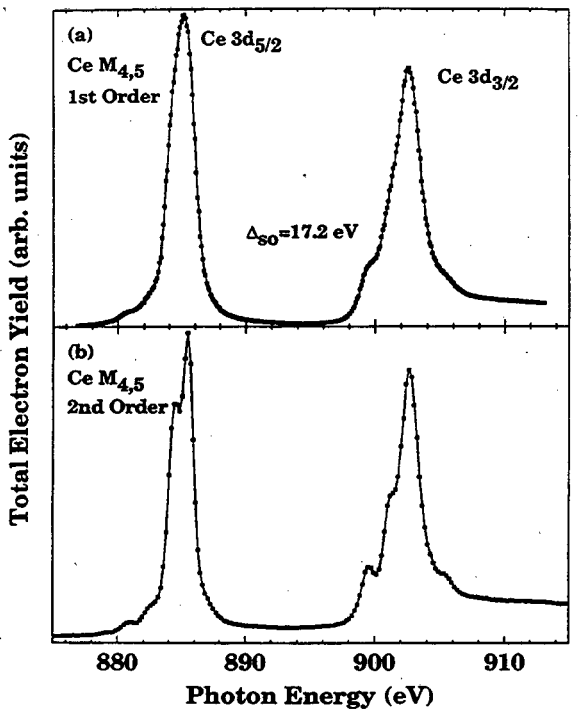

Figure 12-1. Representative XAS spectra of the Ce 3d edge ($M_{IV,V}$) from single crystal $CePO_4$. Spectrum (a) was collected with the monochromator diffraction grating satisfying the n = 1 condition, whereas (b) was recorded utilizing second order light (n = 2) to improve spectral resolution. (XBL 932-223)

representative of the total RE-PO_4 electron yield spectra. The spin-orbit split Ce $3d_{5/2}$ and $3d_{3/2}$ peaks are the predominant features of the spectrum, whereas the exchange interaction provides the observed fine structure. The RE-PO_4 edges actually appear a few eV prior to the true RE edges, as a result of the strong core-hole/4f Coulomb interaction that lowers the energy of the final state. The intensity distribution between the spin-orbit pairs in the second order spectra are very slightly skewed, since the photon flux monitor primarily accounts for the distribution of first order light.

The XAS spectra of the RE ions in the orthophosphate matrix generally resemble that of the corresponding RE metal. This is not unexpected and emphasizes the major contribution of the trivalent state to the electronic transitions at the RE 3d edges. These spectra unequivocally identify the transitions originating from well-characterized RE cores and correlate well with previous theoretical investigations. New features are observed in several of the RE-PO_4 materials as a result of the high resolution measurements. The results of these measurements show that XAS of actinide and other active elements, safely contained in similar glass matrices, is feasible and will yield valuable electronic information.

† This work was done at SSRL, which is operated by the Department of Energy, Division of Chemical Sciences.

13. Determination of the Oxidation States of Uranium and Thorium Compounds by NEXAFS (Work in Progress)‡

D.K. Shuh, J.J. Bucher, N.M. Edelstein, B. Jung, W. Lukens, H. Nitsche, P. Torretto, and M.F. Lappert

In recent years, a number of new organometallic compounds of Th have been synthesized. One of these compounds has been shown to be Th in the tripositive oxidation state, a most unusual valence state for a molecular Th compound. Further synthetic efforts have resulted in the isolation of a compound that may have the Th ion in the dipositive state. A number of thorium and uranium organometallic compounds were synthesized and dissolved in THF (tetrahydrofuran) or hexane. In addition, solid thorium and uranium compounds were prepared along with aqueous solutions of UO_2Cl_2.

Near Edge X-ray Absorption Fine Structure (NEXAFS) data were collected from these samples on beamline 4-1 at SSRL for the purpose of charge state determination. Preliminary examination of the data for the thorium compounds, such as ThI_2, ThI_3, Th metal, and Th(IV) organometallic compounds showed no significant, systematic charge state energy shifts that can be attributed to different oxidation states. However, it should be noted that in general the metal ion concentrations of the Th samples were not ideal.

The uranium data show significant shifts between the U(VI) compounds and U(III) compounds employed as standards. This enables the oxidation state of unknown uranium compounds to be obtained and will be exploited in future work.

FY 1992 PUBLICATIONS AND REPORTS

Refereed Journals

1. T.S. Franczyk, K.R. Czerwinski, and K.N. Raymond, "Stereognostic Coordination Chemistry I: The Design and Synthesis of Chelators for the Uranyl Ion," J. Am. Chem. Soc. **114**, 8138 (1992); LBL-32465.
2. J. Xu, T.D.P. Stack, and K.N. Raymond, "An Eight-Coordinate Cage: Synthesis and Structure of the First Macrotricyclic Tetraterephthalamide Ligand," Inorg. Chem. **31**, 4903 (1992); LBL-33014.
3. G.N. Stradling, S.A. Gray, M. Ellender, J.C. Moody, A. Hodgson, M. Pearce, I. Wilson, R. Burgada, T. Bailly, Y.G.P. Leroux, D. El Manouni, K.N. Raymond, and P.W. Durbin, "The Efficacies of 3,4,3-LIHOPO and DTPA for Enhancing the Excretion of Plutonium and Americium from the Rat: Comparison with other Siderophore Analogues," Int. J. Rad. Biol. **62**, 487 (1992); LBL-31871.
4. Y. Hinatsu, T. Fujino, and N. Edelstein, "Magnetic Susceptibility of $LiUO_3$," J. Solid State Chem. **99**, 182 (1992); LBL-32779.
5. H.-D. Amberger, C. Hagen, G. Shalimoff, and N. Edelstein, "The Electronic Structure of Highly Symmetric Compounds of F-Elements-XXIII. How Large are the Crystal Field Splitting Effects in Tris(bis(trimethylsilyl)amido) Complexes of the Lanthanoids?" Spectrochimica Acta **48A**, 1107 (1992); LBL-32980.
6. Y. Hinatsu, T. Fujino, and N. Edelstein, "Studies on Magnetic Susceptibility, Electron Paramagnetic Resonance, and Absorption Spectrum of Li_3UO_4, an Octahedral U^{5+} Compound with a Small Tetragonal Distortion," J. Solid State Chem. **99**, 95 (1992); LBL-32778.
7. N. Edelstein, W.K. Kot, and J.-C. Krupa, "The 5f → 6d Absorption Spectrum of Pa^{4+}/Cs_2ZrCl_6," J. Chem. Phys. **96**, 1 (1992); LBL-31108.
8. P.C. Becker, G.M. Williams, N.M. Edelstein, J.A. Koningstein, L.A. Boatner, and M.M. Abraham, "Observation of Strong Electron-Phonon Coupling Effects in $YbPO_4$," Phys. Rev. B **45**, 5027 (1992); LBL-32117.
9. H. Reddmann, H. Schultze, H.-D. Amberger, G.V. Shalimoff, and N.M. Edelstein, "The Electronic Structure of Organometallic Complexes of the f Elements XXVIII. Interpretation of the Optical and Magnetochemical Data of a Cyclohexylisocyanide Adduct Derived from Tris(η^5-Cyclopentadienyl)-Samarium(III)," J. Alloys and Compounds **180**, 337 (1992); LBL-30570.

LBL Reports

10. K.N. Raymond and P.W. Durbin, "The Design, Synthesis and Evaluation of Sequestering Agents Specific for Plutonium(IV)," presented at The First Hanford Separation Science Workshop, July 23–25, 1992; LBL-31872.
11. L.C. Uhlir, P.W. Durbin, N. Jeung, and K.N. Raymond, "Specific Sequestering Agents for the Actinides. 21. Synthesis and Initial Biological Testing of Octadentate Mixed Catechoylate Hydroxypyridinonate Ligands," submitted to J. Med. Chem.; LBL-32464.
12. V. Volf, R. Burgada, K.N. Raymond, and P.W. Durbin, "Chelation Therapy of Incorporated Pu-238 and Am-241: Comparison of LILHOPO, DFO-HOPO, DTPA-DX, DTPA and DFOA in Rats," submitted to Int. J. Rad. Biol.; LBL-33616.
13. M. Weydert and R.A. Andersen, "New Synthetic Routes to Cyclopentadienyluranium(IV) Fluorides; Redox and Atom-Abstraction Reactions," ACS Symposium, San Francisco, CA; LBL-33299.
14. C.-K. Loong, L. Soderholm, J.P. Hammonds, M.M. Abraham, L.A. Boatner, and N.M. Edelstein, "Neutron Study of Crystal-field Transitions in $ErPO_4$," J. Appl. Phys. (in press); LBL-33491.
15. C.-K. Loong, L. Soderholm, M.M. Abraham, L.A. Boatner, and N.M. Edelstein, "Crystal-Field Excitations and Magnetic Properties of $TmPO_4$," J. Chem. Phys. (in press); LBL-33198.

‡ This work was done at SSRL, which is operated by the Department of Energy, Division of Chemical Sciences.

16. C.-K. Loong, L. Soderholm, J.P. Hammonds, M.M. Abraham, L.A. Boatner, and N.M. Edelstein, "Rare-Earth Energy Levels and Magnetic Properties of $HoPO_4$ and $ErPO_4$," submitted to J. Phys. Condens. Matter; LBL-33490.
17. K. Krämer, L. Keller, P. Fischer, B. Jung, N. Edelstein, H.-U. Güdel, and G. Meyer, "Magnetic and Crystal Structure Determination of K_2UBr_5," submitted to J. Solid State Chem.; LBL-32909.
18. N.M. Edelstein and W.K. Kot, "Spectroscopic and Magnetic Studies of Tetravalent Pa and Trivalent Th Compounds," in Proceedings of Rare Earths '92 in Kyoto, Japan, June 1–5, 1992, J. Alloys and Compounds (in press); LBL-32473.
19. W.K. Kot, N.M. Edelstein, M.M. Abraham, and L.A. Boatner, "Electron Paramagnetic Resonance of Pu^{3+} and Cf^{3+} in Single Crystals of $LuPO_4$," Phys. Rev. B (in press); LBL-32511.
20. S. Hubert, P. Thouvenot, and N. Edelstein, "Spectroscopic Studies and Crystal Field Analyses of Am^{3+} and Eu^{3+} in the Cubic Symmetry Site of ThO_2," submitted to Phys. Rev. B; LBL-33524.
21. J. Sytsma, D. Piehler, N.M. Edelstein, L.A. Boatner, and M.M. Abraham, "Two-Photon Excitation of the $4f^1 \rightarrow 5d^1$ Transitions of Ce^{3+} in $LuPO_4$ and YPO_4," submitted to Phys. Rev. B; LBL-33593.
22. N.M. Edelstein, "Magnetic and Optical Properties of Np and Pu Ions and Compounds," in Transuranium Elements: A Half Century, Proceedings of the Symposium on "50th Anniversary of the Discovery of Transuranium Elements," Washington, D.C. (American Chemical Society, 1992), p. 145; LBL-29305.

Invited Talks

23. K.N. Raymond, "Metal-Ion Specific and Sterognostic Coordination Chemistry," University of New Mexico, Albuquerque, NM, Feb.7, 1992; University of British Columbia, Vancouver, March 23–24, 1992.
24. K.N. Raymond, "Siderophore Mediated Iron Transport: Microbial Geritol," Xerox Lectures in Industrial or Applied Chemistry, University of British Columbia, Vancouver, March 23–24, 1992.
25. K.N. Raymond, "New Macrocyclic Actinide Sequestering Agents," Symposium on Complexing Agents for Ions and Molecules Applied to Environmental Separations, ACS Meeting, San Francisco, CA, April 8, 1992.
26. K.N. Raymond, "Plutonium Sequestering Agents: Their Chemistry and Biological Evaluation," Symposium on Metal Ions in Medical Biotechnology, ACS Meeting, San Francisco, CA, April 8, 1992.
27. K.N. Raymond, "Metal-Ion Specific Sequestering Agents: Stereognostic Coordination Chemistry," 1992 Monie A. Ferst Symposium Honoring Dr. Fred Basolo, Georgia Tech, May 14–15, 1992.
28. K.N. Raymond, "Siderophore-based and Macrocyclic Iron(III) Sequestering Agents," 3rd NIH-Sponsored Symposium on the Development of Iron Chelators for Clinical Use, Gainesville, FL, May 20–22, 1992.
29. K.N. Raymond, "Metal Ion Specific and Stereognostic Coordination Chemistry," The University of Michigan, Ann Arbor, MI, Oct. 5, 1992.
30. R.A. Andersen, "Organometallic Chemistry of the f-Block Elements," University of Seville, Spain, June 17, 1992; Athens Polytechnique, Greece, June 24, 1992; University of South Dakota, April 15, 1992; Los Alamos National Laboratory, August 5, 1992; University of Konstanz, Germany, August 21, 1992; Technical University, Berlin (Germany), August 28, 1992.
31. N.M. Edelstein, "Spectroscopic and Magnetic Studies of Actinide Compounds," Rare Earths '92 Conference, Kyoto, Japan, June 1–5, 1992.
32. N.M. Edelstein, "Optical and Magnetic Properties of $5f^1$ Ions," University of Hong Kong, May 20, 1992; City Polytechnic of Hong Kong, May 21, 1992.

CHEMICAL ENGINEERING SCIENCES

Molecular Thermodynamics for Phase Equilibria in Mixtures*

John M. Prausnitz, Investigator

INTRODUCTION

Phase equilibria are required for design of efficient separation processes and for design of new products in the chemical and related industries. In this context, "efficient" refers to optimum use of raw materials and to conservation of energy.

Since the variety of technologically important fluid mixtures is extremely large, it is not possible to obtain all equilibria from experiment. Therefore, the objective of this research is development of molecular thermodynamics for interpretation and correlation of reliable experimental data toward confident prediction of phase equilibria for engineering. The correlations are expressed through semi-theoretical, physicochemical models in a form suitable for computer-aided design. Particular attention is given to those materials that may be useful for innovative low-energy-consuming separation processes such as polymers and gels, and polyelectrolyte systems with possible applications in biotechnology. However, attention is also devoted to conventional materials for applications in fuel technology and for recovery of solutes from wastewater.

Development of molecular thermodynamics calls for a combination of theoretical, computational, and experimental work. Further, it requires simultaneous awareness of progress in molecular science and of realistic requirements for engineering design.

1. Thermodynamic Properties of Aqueous α-Chymotrypsin Solutions from Membrane Osmometry Measurements (Publication 1)

C.A. Haynes, K. Tamura, H.R. Körfer, H.W. Blanch, and J.M. Prausnitz

Osmotic pressure data at 25°C are reported for ternary aqueous solutions containing α-chymotrypsin and potassium sulfate or sodium phosphate buffer. Protein number-average molecular weights and apparent osmotic second virial coefficients are reported over a range of solution pH and ionic strength. The data show that significant aggregation of α-chymotrypsin occurs at pH 8.3. Protein osmotic second virial coefficients depend strongly on pH and ionic strength. The molecular theory of fluids is used to develop a potential-of-mean-force expression useful for correlating osmotic pressures of dilute to concentrated aqueous α-chymotrypsin solutions.

2. Swelling Equilibria for Acrylamide-Based Polyampholyte Hydrogels (Publication 2)

J.P. Baker, D.R. Stephens, H.W. Blanch, and J.M. Prausnitz

Polyampholyte hydrogels were synthesized by copolymerizing acrylamide with the cationic monomer methacrylamidopropyl trimethylammonium chloride and the anionic monomer sodium styrene sulfonate. The total nominal charge density of the hydrogels was held constant at 4.7 ± 0.1 mol %(dry basis), while the molar ratio of anionic to cationic moieties within the hydrogels was varied. Swelling equilibria were measured in water and in aqueous sodium chloride solutions ranging in ionic strength from 10^{-5} to 1.0 M. the hydrogels showed increasing insensitivity to ionic strength as the molar ratio of anionic to cationic moieties in the hydrogel approached unity. Donnan membrane equilibria qualitatively explain the experimental results.

3. Liquid-Liquid Equilibria for Aqueous Systems Containing N,N-Diethylmethylamine and Sodium Chloride or Sodium Sulfate (Publication 3)

A.M. Ting, S. Lynn, and J.M. Prausnitz

Liquid-liquid equilibria were measured to study the feasibility of using N,N-diethylmethylamine (DEMA) for extractive crystallization of sodium chloride or sodium sulfate. The experimental results show that DEMA selectively extracts water from saturated sodium chloride solution at low temperatures (5–10°C), causing sodium chloride crystals to precipitate. DEMA also selectively extracts water from saturated sodium sulfate solution at moderate temperatures (21–25°C), precipitating sodium sulfate decahydrate.

*This work was supported by the Director, Office of Energy Research, Office of Basic Energy Sciences, Chemical Sciences Division of the U.S. Department of Energy under Contract No. DE-AC03-76F00098.

4. Vapor-Liquid Equilibria for Polyatomic Fluids from Site-Site Computer Simulations: Pure Hydrocarbons and Binary Mixtures Containing Methane (Publication 4)

J.J. de Pablo, M. Bonnin, and J.M. Prausnitz

Densities and enthalpies of vaporization for several alkanes have been calculated by dividing the molecules into sites (or groups) and then using Monte Carlo simulation with site-site Lennard–Jones potential energy functions. The properties of uniphase systems have been determined from simulations in the isobaric-isothermal ensemble. The properties of saturated (two-phase) systems have been computed by simulations in the Gibbs ensemble. The intermolecular potential energy functions used in these simulations are similar to those presented by Jorgensen, Madura and Swenson.[1] However, to cover an appreciable range of external conditions, the characteristic energy ε used here is a linear function of site density. Site-site potential functions provide the microscopic analog of group contribution methods for estimation of thermodynamic properties. Good agreement with experiment is achieved for several pure hydrocarbons and for a few binary mixtures containing methane.

1. Jorgensen et al., J. Am. Chem. **106**, 6638 (1984).

5. Extractive Bioconversions in Aqueous Two-Phase Systems: Enzymatic Hydrolysis of Casein Proteins (Publication 5)

S. Mukataka, C.A. Haynes, H.W. Blanch, and J.M. Prausnitz

Partition coefficients in poly(ethylene glycol)/dextran aqueous two-phase systems are reported for mixed-casein and its components, α, β, and κ-casein. Rates of casein proteolysis by α-chymotrypsin and by trypsin are reported in single-phase and aqueous two-phase reactor systems. The advantages resulting from selective partitioning of substrates, enzymes, and products are examined in terms of relative volumetric reaction rates.

6. Buffer Effects on Aqueous Swelling Kinetics of Polyelectrolyte Gels (Publication 6)

L. Chou, H.W. Blanch, R.A. Siegel, and J.M. Prausnitz

Electrolytes are often added to a gel-swelling medium under the assumption that the important conditions that characterize swelling rates are the solution's pH and ionic strength, with little emphasis on the nature of the electrolyte. Previous research by Siegel et al. has indicated that the presence of the un-ionized acidic form of an electrolyte buffer is a primary rate determinant for swelling of a polybase gel. A systematic swelling study on two separate gels, 2-hydroxyethylmethacrylate co-polymerized with methacrylic acid (HEMA/MAA) and N,Ndimethylaminoethyl methacrylate (HEMA/DMA), has been performed to investigate the influence of the concentration of the unionized buffer by three principal factors: (1) total buffer concentration, (2) solution pH, and (3) buffer pK_a. Swelling and deswelling kinetics were obtained. In the presence of an electrolyte buffer, a dramatic swelling rate increase is observed for the HEMA gels, with substantial gains in rate obtained as total buffer concentration rises. Results also emphasize that to enhance swelling kinetics, the pH must be such that the buffer is essentially unionized.

7. High Pressure Phase Equilibria With Three-Phase Flash for Multicomponent Systems of Hydrogen, Water, and Hydrocarbons (Publication 7)

A.P. Bunz, R. Dohrn, and J.M. Prausnitz

A three-phase flash algorithm has been used in combination with a modified Redlich-Kwong equation of state for calculating high-pressure phase equilibria. To start the flash calculations, experimental data or rough estimates for the phase compositions can be used as initial values. The applicability of the flash algorithm is demonstrated for ternary and quaternary systems containing hydrogen, water and hydrocarbons at elevated pressures and temperatures. Upon application of mean interaction parameters, it is possible to predict the occurrence of two- and three-phase regions at temperatures and pressures where no experimental data are available.

8. Crosslinked Gels as Water Absorbents in Separations (Publication 8)

A.P. Sassi, H.W. Blanch, and J.M. Prausnitz

A summary is presented of experimental and theoretical applications of hydrogels as water absorbents in separation operations. Proposed concentration schemes are described and briefly discussed. Fundamentals of gel chemistry, swelling, and selectivity are outlined. Published reports of experiments using swelling hydrogels for separations are reviewed. Theories to describe equilibrium gel swelling are presented and discussed.

9. Donnan Equilibrium. Hypernetted-Chain Study of One-Component and Multicomponent Models for Aqueous Polyelectrolyte Solutions (Publication 9)

V. Vlachy and J.M. Prausnitz

The hypernetted-chain integral equation has been applied to two polyelectrolyte models to study the Donnan equilibrium for an aqueous mixture containing large polyions and ordinary ionized salts. The first is a traditional one-component model with the polyions interacting via a screened Coulomb potential. The second is a multicomponent model, which describes the solution as an aqueous mixture of a highly asymmetric electrolyte where polyions, counterions, and co-ions are represented by charged hard spheres. The polyion-polyion distribution functions and the Donnan pressure are evaluated for a range of typical experimental conditions for aqueous solutions of globular proteins. The results show that a screened Coulomb potential model provides a good approximation if the charge on the polyions is not too high. However, there are some important differences between the results of one-component and multicomponent models for the polyion-polyion distribution function. At concentrations above 1.0 M of simple electrolyte, there is a region of interparticle distances for which the potential of mean force is attractive according to the multicomponent model; while this effect is not reproduced by the one-component model based on the screened Coulomb potential alone, it is shown correctly when we include an "osmotic" potential due to the presence of the small ions. Using the hypernetted-chain theory, a one-component model provides a successful analysis of experimental osmotic-pressure data of aqueous solutions of bovine serum albumin in 0.15 M sodium chloride for albumin concentrations up to 450 g/L.

10. Liquid-Liquid Equilibria for Saturated Aqueous Solutions of Sodium Sulfate + l-Propanol, 2-Propanol, or 2-Methylpropan-2-ol (Publication 10)

D.K. Brenner, E.W. Anderson, S. Lynn, and J.M. Prausnitz

Liquid-liquid equilibria were determined for ternary systems containing sodium sulfate, water, and a polar organic solvent. Three solvents were studied: l-propanol, 2-propanol, and 2-methylpropan-2-ol (tert-butyl alcohol). In the salt-saturated two-phase region, data were obtained in the temperature range between the lower consolute solution temperature and 80°C. In the one-phase region, the solubility of sodium sulfate was measured at 20 and 25°C at different solvent/water ratios.

11. Some Characteristics of Protein Precipitation by Salts (Publication 11)

Y.C. Shih, H.W. Blanch, and J.M. Prausnitz

The solubilities of lysozyme, α-chymotrypsin and bovine serum albumin (BSA) were studied in aqueous electrolyte solution as a function of ionic strength, pH, the chemical nature of salt, and initial protein concentration. Compositions were measured for both the supernatant phase and the precipitate phase at 25°C. Salts studied were sodium chloride, sodium sulfate, and sodium phosphate. For lysozyme, protein concentrations in supernatant and precipitate phases are independent of the initial protein concentration; solubility can be represented by the Cohn salting-out equation. Lysozyme has a minimum solubility around pH 10, close to its isoelectric point (pH 10.5). The effectiveness of the three salts studied for precipitation were in the sequence sulfate>phosphate>chloride, consistent with the Hofmeister series. However, for α-chymotrypsin and BSA, initial protein concentration affects the apparent equilibrium solubility. For these proteins, experimental results show that the compositions of the precipitate phase are also affected by the initial protein concentration. We define a distribution coefficient, k_e, to represent the equilibrium ratio of the protein concentration in the supernatant phase to that in the precipitate phase. When the salt concentration is constant, the results show that, for lysozyme, the protein concentrations in both phases are independent of the initial protein concentrations, and thus k_e is a constant. For α-chymotrypsin and BSA, their concentrations in both phases are nearly proportional to the initial protein concentrations, and therefore, for each protein, at constant salt concentration, the distribution coefficient k_e is independent of the initial protein concentration. However, for both lysozyme and α-chymotrypsin, the distribution coefficient falls with increasing salt concentration. These results indicate that care must be used in the definition of solubility. Solubility is appropriate when the precipitate phase is pure, but when it is not, the distribution coefficient better describes the phase behavior.

FY 1992 PUBLICATIONS AND REPORTS

Refereed Journals

1. C.A. Haynes, K. Tamura, H.R. Korfer, H.W. Blanch, and J.M. Prausnitz, "Thermodynamic Properties of Aqueous α-Chymotrypsin Solutions from Membrane Osmometry Measurements," J. Phys. Chem. **96**, 905 (1992).

2. J.P. Baker, D.R. Stephens, H.W. Blanch, and J.M. Prausnitz, "Swelling Equilibria for Acrylamide-Based Polyampholyte Hydrogels," Macromolecules **25**, 1955 (1992); LBL-30830.
3. A.M. Ting, S. Lynn, and J.M. Prausnitz, "Liquid-Liquid Equilibria for Aqueous Systems Containing N-N Diethylmethylamine and Sodium Chloride or Sodium Sulfate," J. Chem. Eng. Data **37**, 252 (1992); LBL-31307.
4. J.J. de Pablo, M. Bonnin, and J.M. Prausnitz, "Vapor-Liquid Equilibria for Polyatomic Fluids from Site-Site Simulations — Pure Hydrocarbons and Binary Mixtures Containing Methane," Fluid Phase Equilibria **73**, 187 (1992); LBL-31167.
5. S. Mukataka, C.A. Haynes, H.W. Blanch, and J.M. Prausnitz, "Extractive Bioconversions in Aqueous Two-Phase Systems — Enzymatic Hydrolysis of Casein Proteins," Biotech. Bioeng. **40**, 195 (1992).
6. L.Y. Chou, R.A. Siegel, H.W. Blanch, and J.M. Prausnitz, "Buffer Effects on Aqueous Swelling Kinetics of Polyelectrolyte Gels," J. Appl. Polymer Sci. **45**, 1411 (1992); LBL-31083.
7. A.P. Bunz, R. Dohrn, and J.M. Prausnitz, "High Pressure Phase Equilibria with Three-Phase Flash for Multicomponent Systems of Hydrogen for Multicomponent Systems of Hydrogen, Water and Hydrocarbons" (in German), Chemische Technik **44**, 48 (1992).
8. A.P. Sassi, H.W. Blanch, and J.M. Prausnitz, "Crosslinked Gels as Water Absorbents in Separations," in *Polymer Applications for Biotechnology. Macromolecular Separation and Identification*, D.S. Soane, Ed., Prentice Hall Polymer Science and Engineering Series, p. 244 (1992); LBL-32046.
9. V. Vlachy and J.M. Prausnitz, "Donnan Equilibrium — Hypernetted-Chain Study of One Component and Multicomponent Models for Aqueous Polyelectrolyte Solutions," J. Phys. Chem. **96**, 6465 (1992); LBL-32045.
10. D. Brenner, E.W. Anderson, S. Lynn, and J.M. Prausnitz, "Liquid-Liquid Equilibria for Saturated Aqueous Solutions of Sodium Sulfate Plus 1-Propanol, 2-Propanol, or 2-Methylpropan-2-ol," J. Chem. Eng. Data **37**, 419 (1992); LBL-31900.
11. Y.C. Shih, H.W. Blanch, and J.M. Prausnitz, "Some Characteristics of Protein Precipitation by Salts," Biotech. Bioeng. **40**, 1155 (1992); LBL-32145.

Other Publications

12. Y.C. Shih (M.S. Thesis), "Structural Aspects of Protein Solubilization in Reverse Micelles," (jointly with Prof. H.W. Blanch), December 1991.
13. A.L. Creagh (Ph.D. Thesis), "Structural and Catalytic Characteristics of Enzymes in Reverse Micelles," (jointly with Prof. H.W. Blanch), February 1992.
14. C.A. Haynes (Ph.D. Thesis), "Separation of Protein Mixtures by Extraction: Statistical-Mechanical Models of Aqueous Solutions Containing Polymers, Salts and Globular Proteins," (jointly with Prof. H.W. Blanch), February 1992.
15. J.L. George (M.S. Thesis), "Osmotic-Pressure Measurements of α-Chymotrypsin Association in Aqueous Electrolyte Solutions," (jointly with Prof. H.W. Blanch), December 1992.
16. P.M. Mathias, H.C. Klotz, and J.M. Prausnitz, "Equation of State Mixing Rules for Multicomponent Mixtures—the Problem of Invariance," Fluid Phase Equilibria **67**, 31 (1991).
17. C.A. Haynes, J. Carson, H.W. Blanch, and J.M. Prausnitz, "Electrostatic Potentials and Protein Partitioning in Aqueous 2-Phase Systems," AIChE J. **37**,1401(1991).
18. B. Smit, T. Hauschild, and J.M. Prausnitz, "Effect of a Density-Dependent Potential on the Phase Behaviour of Fluids," Molecular Phys. **77**, 1021 (1992); LBL-32415.

LBL Reports

19. A.P. Sassi, S. Beltrán, H.H. Hooper, H.W. Blanch, R.A. Siegel, and J.M. Prausnitz, "Monte Carlo Simulations of Hydrophobic Weak Polyelectrolytes: Titration Properties and pH-Induced Structural Transitions for Polymers Containing Weak Electrolytes," J. Chem. Phys. (in press); LBL-32143.
20. C. Haynes, J. Newman, H.W. Blanch, and J.M. Prausnitz, "Application of McMillan-Mayer Theory to Dilute Liquid Systems," LBL-32144.
21. S.M. Lambert, D.S. Soane, and J.M. Prausnitz, "Liquid-Liquid Equilibria in Binary Systems: Monte-Carlo Simulations for Calculating the Effect of Nonrandom Mixing," Fluid Phase Equilibria (in press); LBL-32295.
22. V. Vlachy, H.W. Blanch, and J.M. Prausnitz, "Liquid-Liquid Phase Separations in Aqueous Solutions of Globular Proteins," LBL-32414.
23. T. Hino, S.M. Lambert, D.S. Soane, and J.M. Prausnitz, "Molecular Thermodynamics for Closed-Loop Liquid-Liquid Equilibria of Binary Systems Including Polymer Solutions," submitted to AIChE J.; LBL-32707.
24. M. Kremer and J.M. Prausnitz, "Pore-Size Distribution of Cationic Polyacrylamide Hydrogels (Progress Report)," LBL-32845.
25. J.P. Baker, D.R. Stephens, H.W. Blanch, and J.M. Prausnitz, "Swelling Equilibria for Temperature-Sensitive Ampholytic Hydrogels," LBL-32956 (1992).
26. T. Hauschild and J.M. Prausnitz, "Monte Carlo Calculations for Methane and Argon over a Wide Range of Density and Temperature, Including the Two-Phase Vapor-Liquid Region," LBL-32957.

Invited Talks

27. J.M. Prausnitz, "Molecular Thermodynamics for Chemical Process Design: A Look to the Future," Aspenworld '91 Conference, Cambridge, MA, November 1991; T.W. Leland Memorial Lecture, Rice University, Houston, TX, March 1992; Chevron Lecture, Tulane University, New Orleans, LA, March 1992; Institute for Thermodynamics, Technical University of Berlin, Germany, July 1992; Linde Corporation, Dresden, Germany, July 1992.
28. A.P. Sassi, "Monte Carlo Simulations of pH-Induced Structural Transitions in Hydrophobic, Weakly-Ionizable

Polyelectrolytes," American Institute of Chemical Engineers Annual Meeting, Los Angeles, CA, November 1991.

29. J.M. Prausnitz, Dedication Speaker for New Chemical Engineering Building, University of Virginia, Charlottesville, VA, April 1992.
30. A.P. Sassi, "Sorption of Aqueous Proteins in Polyelectrolyte Hydrogels," American Chemical Society Annual Meeting, San Francisco, CA, April 1992.
31. M. Kremer, "Pore-Size Distribution of Polyelectrolyte Hydrogels," 91. Hauptversammlung der Deutschen Bunsen-Gesellschaft fur Physikalische Chemie, Vienna, Austria, May 1992.
32. S.M. Lambert, "Liquid-Liquid Equilibria in Binary Systems: Monte-Carlo Simulations for Calculating the Effect of Nonrandom Mixing," Sixth International Conference on Fluid Properties and Phase Equilibria for Chemical Process Design, Cortina, Italy, July 1992.
33. S.M. Lambert, "Correlation of Liquid-Liquid Equilibria Using Lattice Models," Koninklije Shell Laboratories, Amsterdam, The Netherlands, July 1992.
34. J.M. Prausnitz, "Phase Equilibria for Petroleum Production," Reservoir Engineering Research Institute, Palo Alto, CA, August 1992.

Work for Others

UNITED STATES OFFICE OF NAVAL RESEARCH

Normal and Superconducting Properties of High T_c Systems*

Vladimir Z. Kresin, Investigator

INTRODUCTION

This research is concerned with various aspects of superconductivity such as origin of high-T_c phenomenon of induced superconducting state, electromagnetic response, etc.

The theoretical model of induced two-gap superconductivity is directly related to spectroscopy of the high-T_c cuprates. The oxygen depletion leads to an appearance of the peculiar gapless state. Superconducting state of fullerenes is due to strong coupling to intramolecular vibrational modes.

1. Induced Superconducting State and Spectroscopy of the High T_c Oxides (Publications 1,2,3,4)

V.Z. Kresin and S.A. Wolf[†]

An induced superconducting state caused by charge transfer between intrinsically superconducting (α) and intrinsically normal (β) subsystems is studied. A most interesting case is a layered system with some layers being normal. An analysis of the general Hamiltonian describing the phenomenon allows us to evaluate T_c and the spectrum, which displays a two-gap structure. A superconducting state can be induced through different charge transfer channels (intrinsic proximity effect; inelastic two-band channel). A very important contribution comes from the "mixed" channel. Systems with various strengths of the coupling are described. The presence of magnetic impurities leads to an induced gapless superconductivity. This model is applied to high-T_c cuprates (in particular, to Y-Ba-Cu-O), as well as to conventional systems. The spectroscopy of Y-Ba-Cu-O appears to be very sensitive to the oxygen content, whereas T_c changes relatively slowly. The model is directly related to such phenomena as residual microwave losses, zero-bias anomalies, the "plateau" effect, etc.

[†]Permanent address: Naval Research Laboratory, Washington, D. C.

2. Strong Coupling in $YBa_2Cu_3O_{7-\delta}$ (Publication 6)

M. Reeves,[‡] *D. Ditmars,*[¶] *S. Wolf,*[†] *T. Vanderah,*[§] *and V. Kresin*

We report precise measurements of the relative enthalpy of polycrystalline $YBa_2Cu_3O_{7-\delta}$ at high temperatures (273 K < T < 700 K). From these data, we determine the lattice and electronic contributions to the specific heat. We find that the specific heat of the charge carriers follows the temperature dependence of a Fermi liquid with a Sommerfeld constant of 25 ± 3 mJ/mole $\cdot$ K^2. By comparing our data to measurements made at low temperatures, we determine that the electron-phonon coupling is strong in $YBa_2Cu_3O_{7-\delta}$ and adequate to account for the high-transition temperature.

[†]Permanent address: Naval Research Laboratory, Washington, D.C.
[‡]Permanent address: Department of Physics, The Catholic University, Washington, D.C.
[¶]Permanent address: National Institute of Standards and Technology, Gaithersburg, MD.
[§]Permanent address: Naval Weapons Center, China Lake, CA.

3. Microwave Properties (Publication 5)

A. Andreone,[†] *S.A. Wolf,*[‡] *and V.Z. Kresin*

The $YBa_2Cu_3O_{7-\delta}$ compound contains two conductive subsystem and as a result displays a two-gap structure. The $Cu\text{-}O_2$ planes are characterized by intrinsic pairing, whereas the superconducting state of the Cu-O chains is induced by two different charge transfer channels (intrinsic proximity effect and phonon-mediated transfer). Oxygen ordering affects the value of the induced energy gap. Such spectrum along with short coherence length leads to peculiar microwave properties of YBCO thin films. The

*This work was supported by the U.S. Office of Naval Research under Contract No. N00014-92-F0002 through an agreement with U.S. Department of Energy under Contract No. DE-AC03-76SF00098.

large residual microwave losses are explained in the framework of the two-gap model.

†Permanent address: Dipartimento di Sciences Fisiche, Universita di Napoli, Italy.
‡Permanent address: Naval Research Laboratory, Washington, D.C.

4. Superconducting State in Fullerenes (Publication 7)

V.Z. Kresin

The coupling strength λ and the characteristic phonon frequency $\langle\Omega^2\rangle^{1/2}$ in superconducting fullerenes can be determined based on general expressions for T_c and on the isotope effect and NMR experimental data. An analysis of recent data shows that the superconducting state of doped fullerenes A_3C_{60} is caused by strong electron-vibrational coupling with $\lambda_1 = 2.1$ for A = Rb and $\lambda_2 = 1.5$ for A = K and $\langle\Omega^2\rangle^{1/2} \approx 250\ cm^{-1}$.

FY 1992 PUBLICATIONS AND REPORTS

Refereed Journals

1. V.Z. Kresin and S.A. Wolf, "Induced Superconducting State and Two Gap Structure: Application to Cuprate Superconductors and Conventional Multilayers," Phys. Rev. B **46**, 6458 (1992).
2. V.Z. Kresin, S.A. Wolf, and G. Deutscher, "The Effect of Phonon Mediated Transfer and Internal Proximity Effect on the Properties of Multigap Cuprate Superconductors," Physica C **191**, 9 (1992).
3. V.Z. Kresin and S.A. Wolf, "Induced Superconductivity and Gapless State in YBaCuO," Physica C **198**, 328 (1992).
4. V.Z. Kresin and S.A. Wolf, "Charge Exchange and the "Plateau" Effect in YBCO," J. Supercon. **4**, 409 (1991).
5. A. Andreone, S.A. Wolf, and V.Z. Kresin, "Two-Gap Superconductivity and Microwave Properties of YBCO," J. Supercon. **5**, 339 (1992).

Other Publications

6. M. Reeves, D. Ditmars, S. Wolf, T. Vanderah, and V. Kresin, "Evidence for Strong Electron-Phonon Coupling from the Specific Heat of $YBa_2Cu_3O_{7-\delta}$," Phys. Rev. B (in press).
7. V.Z. Kresin, "Strength of the Coupling in Superconducting Fullerenes," Phys. Rev. B (in press).
8. V.Z. Kresin, H. Morawitz, and S.A. Wolf, "A Unified Approach to a Description of the Cuprate Superconductors: Major Normal and Superconducting Properties and the Mechanism Responsible for High T_c," in *High Temperature Superconductivity*, J. Askenazi, S. Barnes, F. Zuo, G. Vezzoli, and B. Klein, Eds. (Plenum, New York, 1992), p. 275.
9. V.Z. Kresin, S.A. Wolf, and G. Deutscher, "Correlation between Microstructure and Properties," in *High T_c Thin Films*, L. Correa, Ed. (Elsevier Science Publisher, B.V., 1992) p. 85.
10. V.Z. Kresin, "High T_c Superconductivity and Ultrasonic-Theoretical Aspects," in *Ultrasonic of High T_c and Other Unconventional Superconductors*, M. Levy, Ed. (Academic Press, Cambridge, 1992), p. 435.

Invited Talks

11. V.Z. Kresin, "Correlation between Microstructure and Properties of the High T_c Oxides," Keynote Speaker, International Conference ICMAS-91, Paris, France, October 1991.
12. V.Z. Kresin, "Induced Superconducting State," International Conference on High T_c Superconductivity, Houston, TX, February 1992.
13. V.Z. Kresin, "Theory of High T_c," Los Alamos National Laboratory, New Mexico, March 1992.
14. V.Z. Kresin, "Microwave Properties of the High T_c Oxides," International Conference on Microwave Properties, Santa Fe, NM, March 1992.
15. V.Z. Kresin, "Gapless State and Surface Resistance in Cuprates," MRS Spring Meeting, San Francisco, CA, April 1992.
16. V.Z. Kresin, "Spectroscopy of High T_c Oxides," International Conference on High T_c Superconductivity, Nyborg, Denmark, May 1992.
17. V.Z. Kresin, "Correlation between the Structure and Properties of the Cuprates," AT&T Laboratories, Murray Hill, NJ, May 1992.
18. V.Z. Kresin, "Ginzburg Criterion and High T_c," Ginzburg Symposium, NIST, Gaithersburg, MD, May 1992.
19. V.Z. Kresin, "Induced Gapless State and Properties of the High T_c Oxides," World Congress on Superconductivity, Munich, Germany, September 1992.
20. V.Z. Kresin, "Theoretical Aspects of High T_c Superconductivity," University of Geneva, Switzerland, September 1992.

Appendices

APPENDIX A

DIVISION PERSONNEL

1992 Scientific Staff

Investigators	Postdoctoral and Other Scientists	Graduate Students		Guests, Affiliates
Richard A. Andersen	B. Campion	W.W. Lukens, Jr. P. Matsunaga M.E. Smith	C.D. Sofield M. Weydert	D.J. Schwartz M.R. Smith C. Sofield
Neil Bartlett	B. Zemva	W.J. Casteel L.C. Chacon	G.M. Lucier B.-C. Shen	G.M. Lucier
Alexis T. Bell		D.B. Clarke C.S. Gittleman K. Krishna	R.M. Pittman M.J. Sandoval D.M. Wilbers	H. Abe T. Komaya D.-K. Lee I. Suzuki
Robert G. Bergman	T.Y. Meyer S.J. Yu	A.M. Baranger K.N. Bharucha M.J. Burn M.D. Butts D.A. Dobbs T.A. Hanna	M.J. Hostetler S.Y. Lee R.I. Michelman R.E. Minto R.D. Simpson	M.D. Bergman Y. Ma R.H. Schultz S.J. Yu
Eugene D. Commins		S.B. Ross		
Robert E. Connick	S. Lee			
Norman M. Edelstein	J.J. Bucher B.G. Jung D.K. Shuh			A.E. Freitag D. Piehler C. Ritter J. Sytsma A. Zalkin
Harvey A. Gould	A. Belkacem M. Klapisch			J.K. Eichler K. Momberger
Charles B. Harris	D.R. Padowitz J. Zhang	S.E. Gadd R.E. Jordan J.C. King	W.R. Merry, Jr. E.S. Peterson	S.E. Gadd J.K. Hane W.L. Jolly R.L. Lingle W.R. Merry, Jr. S.D. Miller D.M. Pennington D.J. Russell B.J. Schwartz
Harold S. Johnston				

Investigators	Postdoctoral and Other Scientists	Graduate Students		Guests, Affiliates
Vladimir Z. Kresin				A. Andreone
Andrew H. Kung	J. Xie			
Yuan T. Lee		D.W. Boo A.S. Bracker J.D. Chesko P. Chu H.F. Davis H. Hou C.A. Longfellow	T.-T. Miau J.D. Myers S.W. North L.A. Smoliar M.J.J. Vrakking J. Zhang	D.S. Anex S.-Y. Chiang H.F. Davis G.-Y. Liu C.A. Longfellow L.F. Nahon K.A. Prather M. Stemmler A. Stolow T. Suzuki
William A. Lester, Jr.		W.R. Brown E.M. Johnson	M.M. Soto	J.E. Andrews W.A. Glauser J.A. Odutola Z. Sun J.Y. Yu
Richard Marrus		B.B. Birkett		
William H. Miller	D.T. Colbert	S.M. Auerbach L.F. Gaucher	S. Keshavamurthy	J.D. Gezelter G.C. Groenenboom R. Hernandez J.J. Scherer T. Siedeman G. Stock W.H. Thompson
C. Bradley Moore	E.R. Lovejoy	R.A. Alvarez H.P. Beal S.K. Kim	C.D. Pibel R.D. Van Zee	B.M. Cheng H. Clauberg I. Garcia Moreno J.A. Harrison H. Nam J. Petty M. Rodrigues P.L. Teal
Daniel M. Neumark		C.C. Arnold D.R. Cyr	R. Metz	D.W. Arnold S.E. Bradforth R.E. Continetti D.J. Leahy D.L. Osborn
Kenneth S. Pitzer	A.M. Anderko C.S. Oakes S. Sterner			J.P. Chan J.K. Hovey
John M. Prausnitz		E.W. Anderson J.P. Baker	A.P. Sassi	A.J. Shaw V.A. Vlachy

Investigators	Postdoctoral and Other Scientists	Graduate Students		Guests, Affiliates
Michael H. Prior				F. Aumayr P. Beiersdorfer M.A. Briere J.R. Crespo Lopez-Urrutia V. Decaux D.D. Dietrich R.D. Dubois R.A. Haar D.E. Ivie H. Khemliche J.W. McDonald K. Randall D.H. Schneider L.J. Westervelt S.-D. Yao
Kenneth N. Raymond		J.K. Cammack S.J. Franklin	L.C. Uhlir D.W. Whisenhunt, Jr.	T.M. Dewey D.L. Jameson B.A. Lulay-Bryan L. Tunstad D.W. Whisenhunt, Jr. J. Xu
Richard J. Saykally		R.S. Fellers	N. Pugliano	
David A. Shirley	Z. Hussain	M.P. Blackwell Z. Huang E.A. Hudson W.R.A. Huff S.A. Kellar	L.J. Medhurst E.J. Moler B. Niu B.L. Petersen M.A. Ziegeweid	E.A. Daymo G. Kaindl T. Reich A. Schach von Wittenau P. Thalappil Y. Zheng
Andrew Streitwieser, Jr.		T. Boussie	M.C. Holmes	H. Gonzalez
David H. Templeton				L.K. Templeton
K. Peter C. Vollhardt		R. Faust M. Malaska	D.L. Mohler A.P. van Sickle	G.J. Braunlich H. Elamouri R.H. Lowack

SUPPORT STAFF

Division Administrative Staff

Division Administrator: Linda R. Maio

Administration	Personnel/Financial	Purchasing
L. Aubert	A.W. Backus	A.W. Backus
A.W. Backus	T. Lynem-Paynes	T. Lynem-Paynes
T. Lynem-Paynes	M. Graham	

Travel

S. Quarello*

Administrative/Secretarial Staff

C. Becker	J.M. Gotay	M.F. Noyd
I. Coble	I. Katsumoto	T.C. Peoples
J. Denney	E.A. Lawhead	S. Schmitt
L. English	L. Lawson	P. Southard
C. Fowler	A. McClain	K. Steele
C. Gliebe	B. Moriguchi-Iwai	P. Takahashi
N. Gonzalez	V. Narasimhan	

*Materials Sciences effective 10/01/91.

APPENDIX B

INDEX OF INVESTIGATORS*

*Boldface numbers indicate investigators' main programs.

Lawrence Berkeley Laboratory
University of California
Technical Information Department
Berkeley, California 94720